8-10-2015

Interplay of Cofilin and Capping Proteins in Branched Actin Networks and Integration of Linear and Branched Nucleation in Actin Comets

Sofya Borinskaya
University of Connecticut, sborinskaya@gmail.com

Interplay of Cofilin and Capping Proteins in Branched Actin Networks and Integration of Linear and Branched Nucleation in Actin Comets

Sofya Borinskaya, Ph.D.

University of Connecticut, 2015

Rearrangements of the actin cytoskeleton underlie many physiological processes. In my thesis work I investigated actin dynamics in broad thin protrusions (lamellipodia) at the front of migrating cells, and in locally induced dynamic actin structures (comet tails).

Cofilin is an actin regulatory protein that induces either polymerization or depolymerization in live cells. Through biochemical modeling in Virtual Cell software I examined the function of cofilin in a dynamic branched network at the tip of a lamellipodium. I found that cofilin and capping protein play synergistic roles in regulating branched actin polymerization. The model predicts that cofilin promotes actin disassembly when capping concentration is low and promotes actin assembly when capping is high and a sufficient actin monomer pool is maintained.

Nck, a SH2/SH3 adaptor protein, facilitates recruitment and increases local concentration of cytosolic effectors that induce formation of pathogenic actin comet tails. I characterized comet tails induced by experimental aggregation of Nck SH3 domains at the membrane. Experimental disruption of the balance between unbranched/branched nucleation alters the morphology and dynamics of Nck SH3 actin comets. Inhibition of linear formin-based nucleation results in formation of predominantly circular-shaped

actin structures with decreased mobility. Enhancement of branched nucleation by N-WASP overexpression similarly caused loss of the typical actin comet tail shape. The results indicate that formin-based linear actin polymerization is critical for Nck-dependent actin comet tails. Consistent with this, aggregation of an exclusively branched nucleation promoting factor (the VCA domain of N-WASP), with density and turnover similar to that of N-WASP in Nck comets, does not reconstitute dynamic elongated actin comets. The ratio of linear to dendritic actin assembly may distinguish the properties of actin structures induced by various viral and bacterial pathogens.

My thesis work uncovers two mechanisms of cooperativity in regulation of actin-based motility. First, with the use of computational modeling I elucidate the interplay between cofilin and capping proteins in regulating dynamics of branched actin networks. This finding provides a comprehensive outlook and a resolution of the conflicting *in vivo* observations about cofilin's physiological role. Second, I demonstrate a new role for the Nck adaptor protein as an integrator of signaling pathways leading to linear and branched actin polymerization in dynamic actin comet tails. Dynamic and morphological properties of actin comets depend on the balance of linear and branched actin assembly that is maintained via Nck adaptor protein.

Interplay of Cofilin and Capping Proteins in Branched Actin Networks and Integration of Linear and Branched Nucleation in Actin Comets

Sofya Borinskaya

B. S., Binghamton University, SUNY, 2004

A Dissertation

Submitted in Partial Fulfillment of the

Requirements for the Degree of Doctor of Philosophy

at the

University of Connecticut

2015

APPROVAL PAGE

Doctor of Philosophy Dissertation

Interplay of Cofilin and Capping Proteins in Branched Actin Networks and

Integration of Linear and Branched Nucleation in Actin Comets

Presented by
Sofya Borinskaya, B.S.

Major Advisor _____
Bruce J. Mayer

Major Advisor _____
Leslie M. Loew

Associate Advisor _____
Ann E. Cowan

Associate Advisor _____
William A. Mohler

Associate Advisor _____
Yi I. Wu

University of Connecticut
2015

ACKNOWLEDGMENTS

I would like to thank everyone who helped me to complete my thesis work. There are no words that can describe how grateful I am for everything you have done for me. You shaped my growth and development as a scientist, as an educator and as a person. It is not possible to personally mention everyone in this section and I will find opportunities to express my gratitude off the paper and to keep in touch in the future.

This thesis absolutely would not have been possible without my advisors Bruce Mayer and Les Loew. It is with great pleasure that I acknowledge your mentorship, advice and support. Both of you strive for the success of your students and create for them unique nurturing research environment. Thank you for sharing your excitement for scientific discovery, for respecting my choices and for all the opportunities that broadened my expertise in experimental research, computational modeling and science education.

I am grateful to all the members of my advisory committee. Ann Cowan, you are a remarkable mentor, teacher and a role model. I can not thank you enough for all the discussions, guidance and encouragement. My sincere thanks to William Mohler and Yi Wu for invaluable technical and career advice.

I consider it an honor and great privilege to work with the members of two laboratories: Mayer Lab and Loew Lab. Thank you Silas (Khong) Ng, Kazuya Machida, Joshua Jadwin, Adam Lafontaine, Sonali Ghosh, Lin Jia, Mari Ikeda and Hao Lu. I owe my deepest gratitude to former Mayer/Loew lab member, Jonathon Ditlev, who started my research project and guided my training. I am indebted to all the members of Loew Lab

for sharing their research successes and struggles during our lab meetings. Thank you for helping me improve my thesis work.

I am incredibly lucky to share the path with many brilliant and motivated graduate students in Cell Analysis and Modeling (CAM) program. Thank you Olena Marchenko, Abhijit Deb Roy, Sherry-Ann Brown, Erika Ramirez Hoyoz, Akeisha Belgrave, EunJi Kim, Rene Norman, Jing Yang, Daniel Sheehy, Ronghua Yang, Clifford Locke, Marc Rigatti and Ahmed Elmokadem.

I will miss greatly the research environment and community of the Center for Cell Analysis and Modeling. I am grateful to everyone who worked hard to make the CAM program an official Area of Concentration (AoC) of the Biomedical Science graduate program. It would have remained a dream had it not been for Raquell Holmes who led establishing of the CAM AoC. Thank you John Carson, Michael Blinov and Ji Yu for guiding the training and truly serving the interests of CAM students. My research would be impossible without the support and enthusiasm of the Virtual Cell development and support team, Jim Schaff, Ion Moraru, Frank Morgan, Edward Boyce, Jeff Dutton and Dan Vasilescu.

I am obligated to the administrative staff of the Center for Cell Analysis and Modeling and Genetics and Genome Sciences departments. Thank you Karen Zucker, Tiffany Gough, Susan Krueger, Deborah Manchak, Isolde Bates, Gail Damico and Maria Deconti.

I am beyond grateful to everyone who supported and guided my training in science education and teaching: Raquell Holmes, my research advisors, Ann Cowan, Michael Blinov and Keith Barker.

I am indebted to my family, my parents and my brother, my mother-in-law and my close and dear friends for continuous and unconditional support.

Mark David Rogov, my son, you inspire me every day with your playfulness, spontaneity and creativity. You make me the person I am. I truly cherish the title “Doctor of cells” that you granted me.

Mikhail Rogov, my dear husband, you often believe in me more than I believe in myself and that kept me on track. You have grown professionally and personally and constantly inspire me by your achievements and hard work. Thank you for your patience, understanding, caring and being there for me every moment of my graduate school experience.

This thesis is dedicated to my grandmother Rivka (Raissa) Fridman (1918-2013) who lived a life of hardship and sincere happiness, who could see the best and the worst in people and who dared to reach for the unreachable and succeeded.

TABLE OF CONTENTS

LIST OF ABBREVIATIONS

ADP	Adenosine diphosphate
ADP-Pi	Adenosine diphosphate with inorganic γ-phosphate
APC	Adenomatous polyposis coli
Arp2/3	Actin related proteins Arp 2 and Arp 3
ATP	Adenosine triphosphate
CALI	Chromophore-assisted laser inactivation
CEV	Cell-associated extracellular virus
DAD	Diaphanous autoregulatory domain
DID	Diaphanous inhibitory domain
DIP	Dia Interacting Protein
EPEC	Enteropathogenic *Escherichia coli*
EV	Extracellular virus
F-actin	Filamentous actin
FH1	Formin homology 1
FH2	Formin homology 2

FHOD1	FH1/FH2 domain-containing protein 1
FRAP	Fluorescent recovery after photobleaching
G-actin	Globular (monomeric) actin
GBD	GTPase binding domain
JMY	Junction-mediating and -regulatory protein
KD	Knock down
LIMK	LIM (Lin11, Isl-1 & Mec-3) domain kinase
mDia1	Mammalian Diaphanous 1 formin
N-WASP	Neural Wiskott-Aldrich Syndrome protein
NCKIPSD	Nck interacting protein with SH3 domain
NPF	Nucleation promoting factor
ODE	Ordinary differential equation
PDE	Partial differential equation
Pi	Inorganic γ-phosphate
PIP2	Phosphatidylinositol 4,5-bisphosphate or PtdIns(4,5)P_2
PRD	Proline-rich domain

SH2	Src homology 2
SH3	Src homology 3
SMIFH2	Small molecule inhibitor of formin homology 2 domains
SPIN90	SH3 Protein Interacting with Nck 90 kDa
SSH	Slingshot homolog
Tir	Translocated intimin receptor
TIRF	Total internal reflection fluorescence
VASP	Vasodilator-stimulated phosphoprotein
VCA	Verprolin-homology (also called WH2), cofilin-homology (central) and the acidic domains
WASH	Wiskott–Aldrich syndrome protein and SCAR homologue
WASP	Wiskott–Aldrich Syndrome protein
WH1	Wasp homology 1
WH2	Wasp homology 1
WHAMM	WASP homologue-associated protein with actin, membranes and microtubules

WIP	WASP interacting protein
WISH	WASP interacting SH3 protein

LIST OF TABLES

LIST OF FIGURES

Chapter 3

LIST OF MOVIES

1. CHAPTER I: Introduction

Attribution: The section of the thesis entitled “Detailed Biochemical Modeling of Actin Dynamics” contains a portion of a review article “Modeling Actin Dynamics” written for the Encyclopedia of Cell Biology (CELB). The section of the article entitled “Detailed Biochemical Modeling” was written by Sofya Borinskaya and edited by Leslie M. Loew. The rest of the introduction was written by Sofya Borinskaya and edited by Bruce J. Mayer and Les M. Loew.

Actin dynamics and actin-based motility

Actin is one of the most abundant and highly conserved proteins in eukaryotic cells. This 42 kDa protein is a basic building block of a wide variety of cellular structures such as lamellipodial, filopodia, stress fibers and cell cortex. *In vivo*, actin cycles between its globular (G-actin) monomeric forms and filamentous (F-actin) forms. Actin polymerization and depolymerization is referred to as actin dynamics. Polymerizing actin filaments generate a protrusive force against the cell-edge membrane. This force causes changes in cell shape and drives cell locomotion. Actin dynamics underly a multitude of physiological processes such as morphogenesis during gastrulation and embryogenesis, polarity establishment, immune response, wound healing, endocytosis, cytokinesis, cancer metastasis and invasion. Numerous accessory proteins regulate rearrangements of actin cytoskeleton and control the shape, mechanics and dynamics of different actin architectures.

Actin-based motility refers to cellular processes and mechanisms that result in movement. Actin assembly is a major force-generating component in these processes. Growing filaments can propel beads coated with actin regulatory proteins, endocytic and phagocytic vesicles in live cells, bacteria and viruses invading the host cells and various membrane protrusions in migrating and non-migrating cells.

One of the most fundamental functions of eukaryotic cells is ability to migrate (Movie 1.1). Not surprisingly, actin-based cell migration and cell motility are extensively studied phenomena in biology. It also a highly interdisciplinary field and benefits from studies in genetics, immunocytochemistry, microbial pathogenesis, biochemistry, microscopy and

computational approaches. The wealth of biochemical and live imaging data on actin polymerization attracted the interest of modelers and opened a possibility for development of informative and accurate mathematical models. Most of the first computational models of actin dynamics were phenomenological mathematical models (also called "conceptual") (Mogilner et al., 2012). Conceptual models offer a valuable qualitative insight into a specific cellular behavior (Allard and Mogilner, 2013; Barnhart et al., 2011; Herant and Dembo, 2010; Herant et al., 2003; Mogilner and Oster, 1996; Peskin et al., 1993; Rubinstein et al., 2009; Wolgemuth et al., 2011; Wolgemuth and Zajac, 2010). In order to develop a comprehensive understanding of actin-based motility it is beneficial to shift from phenomenological to detailed models of actin polymerization.

Detailed Biochemical Modeling of Actin Dynamics

Attribution: This section of the thesis entitled “Detailed Biochemical Modeling of Actin Dynamics” contains a portion of a review article “Modeling Actin Dynamics” written for the Encyclopedia of Cell Biology (CELB). The section of the article entitled “Detailed Biochemical Modeling” was written by Sofya Borinskaya and edited by Leslie M. Loew.

Actin polymerization cycle

The biochemistry underlying lamellipodial actin dynamics is extremely complex. Despite their multiple benefits, conceptual models are not meant to capture the biochemical mechanisms involved in actin cytoskeleton dynamics. Molecularly explicit mathematical models, or as we call them here, detailed biochemical models, aim to simulate the interactions of any or all of the many proteins that orchestrate spatio-temporal dynamics of actin polymerization. Such models, when combined with experimental studies, serve as invaluable tools for elucidating the functions of individual molecules or collective behaviors within a complex biochemical system. An ultimate goal of this approach may be to identify therapeutic targets and strategies. Detailed models also may offer the opportunity to address questions that are not accessible experimentally. Such ‘in silico’ biochemical simulations can generate new predictions and hypotheses to develop and direct future experimental studies. Detailed biochemical models of a complex reaction network also serve as knowledge integration platforms through which information about a physiological system can be easily shared, updated, enriched, reused, and adapted for other experimental or modeling studies. A short perspective on the benefits of detailed

models with a particular application to actin dynamics was recently published (Ditlev et al., 2013).

To begin thinking about the basic principles underlying polymerization, it would be a useful thought exercise to imagine that you have attached one link (the nucleator or seed) to a wall and then attach more links one by one at your pace (rate) to form a chain (polymer). The total assembly rate (number of links added per unit of time) for your chain is defined by your pace. Next, you might have more people who would like to engage in this activity and you provide them with the nucleator links. Let's assume they work at about the same pace as you. We are interested in the total rate of assembly (total increase in the number of links in all the chains). If you had one more person working with you, the total assembly rate would be twice your rate; if you had nine more people the total rate would increase to 10 times your rate. Alternatively, think about the situation where you don't provide other people with the nucleators, but just want them to share access to your single chain. Then everyone will be adding the links to just one chain end and the total assembly rate will not increase. This situation is analogous to polymerization of actin monomers at the barbed ends. The more available barbed ends there are in the system the higher the assembly rate will be – the polymer ends serve as 'catalysts' of the assembly process. As we noticed in the example with the chains, the assembly rate linearly depends on the number of starters (number of barbed ends in case of actin polymer). Of course, this depends on an ample abundance of links to the crew you have charged with building the chains (i.e., that the availability of G-actin is not limiting). The same is true for the disassembly rate; the more available pointed ends there are the higher the disassembly rate will be. In order to coordinate this process in space

and time the cells have an abundance of actin regulatory proteins that can control availability of filament ends, nucleation, elongation, branching, filament length, bundling, and turnover.

We will first briefly describe the major steps and components of the actin polymerization cycle. The process of actin filament treadmilling (Figure 1.1A) lies at the heart of the actin cycle. Broadly speaking, treadmilling refers to the steady-state polymerization at one end of a filament matched by an equal rate of net depolymerization at the other end; if the system is not at steady state, the filament may grow or shrink depending on which rate dominates. An individual actin monomer (G-actin) cycles through a series of biochemical events: (1) addition of ATP-bound G-actin at the barbed (growing or plus) end of F-actin, (2) hydrolysis of ATP on an F-actin subunit to generate to ADP-Pi-actin, (3) release of Pi from the ADP-Pi subunit, (4) dissociation of ADP-G-actin from the pointed (minus) end, and (5) nucleotide exchange of ADP-G-actin to recharge the monomer into the ATP-G-actin form. Profilin catalyzes the last step of ADP for ATP exchange on the actin monomer so that it may enter the next round of polymerization. Polymerization (Figure 1.1B) is stimulated by the nucleation-promoting factors (NPFs) associated with the inner side of the plasma membrane. NPFs are spatio-temporally regulated and in their active state induce branched (by activating Arp2/3 protein complex) or linear (by activating formin proteins) polymerization of actin filaments. Polymerizing filaments are proposed to push plasma membrane of motile cells by the elastic Brownian ratchet mechanism (Mogilner and Oster, 1996; Peskin et al., 1993) as discussed above. A pool of monomeric actin that is necessary for assembly at the barbed ends is maintained by the buffering activity of thymosin-β4. Capping proteins (Caps)

terminate growth of the barbed ends. Actin filaments can be destabilized by depolymerization at the pointed ends and by fragmentation into shorter filaments. There are also mechanisms that stabilize filamentous actin by protecting it from depolymerization and fragmentation.

Early Models

Early work, before the availability of much kinetic data, derived mathematical models based on the thermodynamics of polymer formation (Oosawa and Kasai, 1962). These early modeling studies resulted in discovery of the critical concentration (above which polymerization occurs in solution) of G-actin (Oosawa et al., 1959) and the treadmilling phenomenon where polymerization depends on the nucleotide state of actin monomers (Wegner, 1976). Subsequently, an increasing amount of quantitative data related to multiple aspects of actin polymerization made development and validation of detailed biochemical models possible (Ditlev et al., 2013).

Deterministic (continuous) models

(Bindschadler et al., 2004) built a first comprehensive model of the actin cycle that couples ATP-hydrolysis with actin treadmilling. This is an ODE model that predicts the complete steady-state nucleotide profile (Figure 1.2A) within the filaments and demonstrates that Pi release from ADP-Pi increases the rate of actin filament treadmilling. Essentially this is a model of actin filament assembly and disassembly from purified actin and its key regulatory proteins (Figure 1.2B): ‘explicitly’ modeled profilin

and β4-thymosin and 'implicitly' modeled barbed-end and pointed-end cappers and cofilin. A year later (Vavylonis et al., 2005) built a non-steady-state 'discrete' model using kinetic Monte-Carlo simulations based on experimental data (Fujiwara et al., 2002; Kuhn and Pollard, 2005). Eventually the model was validated and refined through experimental observations of individual actin filaments by total internal reflection fluorescence (TIRF) microscopy (Fujiwara et al., 2007). This process of model construction originating from the available experimental data, going through model modifications to fit that data, and eventually making predictions that can be verified experimentally, exemplifies how modeling and experiment synergize.

Discrete (stochastic) models

An example of a detailed discrete model that tracks individual filaments is a dendritic nucleation model by Schaus and Borisy (Schaus et al., 2007). It is a stochastic 2D computer model that allowed investigation of filament self-organization patterns at the leading edge of the lamellipodial protrusion. The model is based on the 'dendritic-nucleation/array-treadmilling' (Figure 1.1) mechanism and incorporates (1) spatially discretized G-actin diffusion, (2) Monte-Carlo filament kinetics, and (3) elastic behavior of the filament and the membrane. Branching was restricted to the region within 5.4 nm from the plasma membrane while barbed ends were protected from capping in this narrow area. Irrespective of initial filament orientation, the filaments self-organize to form a branched network with the filament orientation angle of ±35° consistent with electron microscopy observations. The system tends to increase the capping rate for the

larger angles rather than increasing the branching rates for the smaller filament orientation angles. The authors demonstrate that protection from capping in the 5.4 nm zone was critical for reproducing realistic dendritic actin patterns while branching localization was not required. Membrane flexibility did not affect pattern orientation significantly. However, filament orientation angle was very sensitive to increase in the filament bending stiffness resulting in a different angle distribution (70/0/−70°). This comprehensive discrete model brings to light the idea that experimentally observed self-organization of the dendritic network in the lamellipodium emerges from the essential dynamic properties of the network.

(Alberts and Odell, 2004) constructed a large hybrid discrete continuum model of dendritic actin nucleation to reconstitute the motility of L. monocytogenes in silico. Listeria is an intracellular rod-shaped bacteria that hijacks the actin cytoskeleton of the host cell for assembly of actin comet tails. The comet tails propel the bacteria within the cytoplasm and into the neighboring cells causing the infection to spread. The model combines biochemical and mechanistic aspects of actin-based motility of Listeria that presents the NPF ActA on its surface to activate the Arp2/3 complex in the host cell. An Arp2/3-dependent dendritic nucleation scheme (Figure 1.2C) encapsulates biochemical events of the model. Actin monomers and actin-binding proteins are described continuously with reaction-diffusion equations (characterized as protein concentrations). Interactions of continuous players with each other and with individual actin filaments (discrete components) are defined deterministically. Filaments are modeled stochastically meaning that probability (not concentration) of binding/dissociation of each individual filament is computed at each time-step. The growth of a filament depends on the state

variables that keep track of location, orientation, and biochemical state of that filament. Various forces act on the simulated bacterium including; (1) link force of ActA protein holding a filament and the bacterium together, (2) collisions of filaments with the bacterium which push them apart, (3) Brownian forces with random orientations, which act on filaments and on the bacterium. The model reproduces the gross qualitative behavior of L. monocytogenes with respect to the average speed, persistence of motion, and comet tail morphology. Additionally the simulated bacterial trajectories exhibit the small-scale saltatory (repeated runs and pauses) motion observed by experimentalists. Alberts and Odell used their model to investigate the nature of Listeria nano-saltatory motility and concluded that pauses correlated with the Brownian motion and coordinated breakage and formation of ActA links between filaments and the bacterium. The 'in silico reconstitution' allows exploration of bacterial actin-based motility mechanisms. However it was extremely computationally expensive and required 80 Linux processors to solve thousands of differential equations.

Besides Arp2/3, cells have other nucleators of actin polymerization. One class of nucleators consists of various formin proteins (Paul and Pollard, 2009; Pring et al., 2003; Pruyne et al., 2002). They induce formation of unbranched actin filaments in filopodia, polarized actin fibers, the cytokinetic ring, and stress fibers. Formins associate with the barbed ends of actin filaments and stimulate elongation while being processively attached to the growing ends. Highly conserved C- terminal FH1–FH2 domains of formin are key players in this process. A doughnut-shape dimer of FH2 domains forms a ring around the barbed end and an unstructured FH1 domain has multiple profilin-binding sites and therefore delivers profilin–actin complexes for F-actin assembly. Using available

experimental data (Kovar et al., 2006), Vavylonis built a stochastic comprehensive model (Vavylonis et al., 2006) of FH1– FH2-dependent actin polymerization. The FH1 domain recruits profilin-G-actin from the cytosol. Since FH1 has many profilin-binding sites the concentration of profilin-actin near the barbed end increases. Flexibility of the FH1 domain allows for rapid collisions between profilin and the barbed end to occur. The collision results in a transfer of profilin-actin to the barbed end if the FH2 domain is in the open state. When the FH2 domain is in the closed state, it prevents actin subunit addition. Based on this mechanism, simulated elongation rates are consistent with experimental rates for four different formins (Kovar et al., 2006). The model shows that with optimal profilin concentration, a maximal elongation rate can be higher than elongation of actin alone. However, high profilin concentration inhibits elongation because profilin outcompetes profilin-bound actin from FH1 domain.

An Open Model of Actin Dendritic Nucleation

With that historical background, we now turn to a comprehensive and extensible continuum deterministic model developed in our lab: 'An open model of actin dendritic nucleation' (henceforth referred to as the Open Model) (Ditlev et al., 2009) that is currently the most comprehensive mechanistic model of actin dynamics. The Open Model is implemented in the Virtual Cell software system (VCell) (Cowan et al., 2012; Resasco et al., 2012; Schaff et al., 1997; Slepchenko and Loew, 2010). VCell is a computational environment for modeling and simulation in biology that is designed for both experimentalists and theorists. It has a convenient GUI for formulating a model:

defining compartments and their geometries as well as molecular players and their interactions. Both deterministic and stochastic simulations for either 'compartmental' or 'spatial' models can be run in VCell. Models can include molecular reaction–diffusion–advection (flow), membrane fluxes, and can solve the corresponding 'ODEs' or 'PDEs' or stochastic equations for any cellular geometry. VCell offers a variety of data visualization tools: graphs, kymographs, images, export options to spreadsheets, images, and movies. Importantly, it is built on a database, so scientists can access public models and adapt or extend them for their own research.

The Open Model (Ditlev et al., 2009) was developed in an effort to account for the key regulatory proteins and mechanisms governing actin dynamics. It builds upon all the mechanisms simulated in the (Bindschadler et al., 2004) model and expands the latter with Arp2/3 activation by N-WASP at the membrane, Arp2/3-mediated side branching, regulation of actin dynamics by cofilin, and fragmentation and annealing of actin filaments. The molecules that are explicitly included in the model are actin, a NPF in the membrane (ex. N-WASP), Arp2/3 complex, Cap, profilin, ADF/cofilin, thymosin-β4, and various associations of actin with ATP, ADP-Pi, and ADP. Despite such a short list of molecular players the model required 60 species and 155 reactions to capture the core mechanisms driving actin dendritic nucleation. In Figure 1.3A, the blue rectangles, which overlay the corresponding regions of the reaction network, summarize the mechanisms that are explicitly defined in the Open Model. The model and the simulation results are publicly available through the Virtual Cell database. The simulations can be run on any geometry and therefore facilitate virtual experiments incorporating specifying initial molecular distributions, diffusion, and advection in realistic geometries extracted from

microscope imaging data. The Open Model actually contains many such virtual experiments, with different initial conditions, system geometries, and boundary conditions; in this sense, it is actually a collection of mathematical models all examining aspects of a common set of basic biophysical mechanisms.

The core of the Open Model is the treadmilling of actin filaments. All the events that accompany and drive this phenomenon are depicted in the cartoon in Figure 1.1A. This and many other schematic representations of actin treadmilling grossly oversimplify the actual process. Figure 1.1A shows that monomers in the ATP form add to the barbed ends and dissociate in the ADP form at the pointed ends of the filaments. The situation in vivo is more complex: monomers in all the states (ATP, ADP-Pi, and ADP) may bind to and dissociate from either barbed or pointed ends of the filaments. Suffixes T, Dpi, and D are used in the model to indicate the nucleotide state of actin 'species'. The model accurately captures complexity of the treadmilling process with the mechanisms for tracking the nucleotide state and the processes occurring at the barbed and pointed ends (barbed- and pointed-end turnover).

Some of the aspects of cytoskeletal dynamics are difficult to model explicitly. For example, tracking the nucleotide state of each monomer within the filaments could drastically increase combinatorial complexity of the model. Therefore, the nucleotide state is modeled explicitly only at the barbed and pointed ends, resulting in six variables: three states (T, DPi, and D) for each of barbed and pointed end of the filament. The states of all the actin monomers in the interior of the filaments are described implicitly by three state lumped variables FAT (F-actin in ATP form), FAD-Pi (F-actin in ADP-Pi form),

and FAD (F-actin in ADP form) (Figure 1.3B). The FAT in the filament undergoes hydrolysis (FAT-FADPi) and then inorganic phosphate dissociation (FADPi-FAD + Pi). Hydrolysis and Pi dissociation reactions are modeled explicitly and are applied to all the actin species (not only F-actin) in the reaction network.

The six variables that track the nucleotide states of barbed and pointed ends depend on the hydrolysis and phosphate (Pi) dissociation and on the association and dissociation of actin monomers in different nucleotide states. For instance, there are 18 reactions characterizing interactions of monomers with the barbed ends: three types of barbed ends reacting with G-actin in three states as well as with profilin-bound G-actin in three states. Dissociation events of monomers from the ends presented the difficulty of assigning a nucleotide state to the newly formed end (after a monomer dissociates). The monomer next to the explicitly tracked pointed end can be in any of the three nucleotide states because it was implicitly modeled (Figure 1.3B). The model assumes, therefore, that the nucleotide states at this penultimate position will have approximately the same fractional distribution of states at the ends. This assumption was applied to define dissociation rates of actin monomers from various types of barbed and pointed ends.

Actin filaments (F-actin) were shown to undergo the process of end-to-end annealing experimentally (Andrianantoandro et al., 2001; Sept et al., 1999). Similarly fragmentation of F-actin was demonstrated to be a critical mechanism underlying actin dynamical behavior (Berro et al., 2010; Schmoller et al., 2011). Annealing and fragmentation were treated as forward and reverse reactions in the Open Model reaction network (Ditlev et al., 2009). There are nine forward reactions: pointed ends in three states can anneal to the

barbed ends in three different states. The rate of annealing reaction decreases as the length of the fragment increases. Additionally annealing rate expression is scaled by a factor of $(1 - BrF)$ in order to reduce the rate by the fraction of filaments containing branches. The filaments with high BrF (branch fraction) diffuse more slowly and therefore are unlikely to undergo annealing. BrF is determined as the sum of all species where Arp2/3 is bound to FA (i.e., branches) divided by the total concentration of filaments (i.e., half the concentration of all ends).

Cofilin is an essential actin-binding protein that can stabilize as well as destabilize individual actin filaments and the actin network. We will address the overall physiological effects of cofilin on actin dynamics later during discussion of the results of the model. Kinetics and thermodynamics of cofilin–actin interaction are well characterized experimentally (Blanchoin and Pollard, 1999; Cao et al., 2006; De La Cruz, 2009; Elam et al., 2013a) and have been modeled (De La Cruz and Sept, 2010). The Open Model has a simplified mechanism of cofilin interaction and severing of actin filaments. It includes (1) acceleration of Pi release from FADPi subunits, (2) severing only when two or more neighboring FAD subunits are bound to cofilin molecules, (3) the cooperative binding phenomenon where cofilin will have higher binding affinity for the FAD subunit which has a neighboring cofilin-bound FAD.

Availability of experimental data from *in vitro* experiments provided an opportunity to validate the Open Model by running ODE simulations representing a closed well-mixed compartment. Numerous 'compartmental' (ODE) models were run for different values of total actin, Cap, cofilin, profilin, and thymosin-β4. To mimic the in vitro experimental

conditions, Arp2/3-mediated nucleation and branching were not included in these ODE simulations. Overall the results reproduced the effects of nucleotide exchange, profilin and thymosin-β4 on actin turnover, F-actin concentration, and filament length reported and simulated by (Bindschadler et al., 2004). Additionally, simulations agreed well with experimental data on the effect of Cap, fragmentation, and annealing on the average filament length. Overall, the simulations reproduced numerous experimental studies in which each of these system variables had been carefully controlled (Carlier and Pantaloni, 2007; dos Remedios et al., 2003; Pollard and Borisy, 2003; Pollard and Cooper, 1986) Running compartmental simulations not only offered an initial model validation, but the final steady state values for these calculations served as appropriate initial conditions (stable starting concentrations) for the spatial simulations with Arp2/3 activation.

One of the key VCell capabilities is to simulate cellular dynamics in space. The ultimate goal of the Open Model was to investigate the process of actin dendritic nucleation in lamellipodial protrusion. For this purpose the Open Model adopted an idealized 3D geometry of a migrating cell with a thin lamellipodium and a larger volume cell body (Figure 1.3C) to run additional virtual experiments. In spatial simulations, biochemical reactions are complemented with diffusion and flow of the molecular species. As a result Virtual Cell generates and solves a system of 'PDEs' constrained by mass conservation.

The mechanism of Arp2/3-mediated branch formation is a multiple step process. In the Open Model it was reduced to a single step to achieve computational efficiency and therefore reduce simulation time for 3D virtual experiments. Arp2/3 activation and side

branching was implemented as proposed in the modeling study by (Carlsson et al., 2004). Cytosolic Arp2/3 complex is recruited to the membrane and activated by a membrane-bound NPF (activeNWASP). Activated and membrane-localized Arp2/3 recruit two actin monomers (unbound or bound to profilin) and binds to the side of the preexisting filament. Monomer recruitment and side binding occurs in one step and results in production of a branch and a free barbed end. This is an example of one of the branching reactions:

$$ActiveArp + FAT + 2\,GAT \rightarrow PointedArpFAT + BarbedT$$

There are six nucleation reactions because FA can be in three states and GAT can also be in the GAT-Prof (profilin-bound) form.

Diffusion of all the monomeric species and actin-binding proteins was assigned a diffusion coefficient of D_{GActin} = $\mu m^2\ s^{-1}$, consistent with experimental data. Long and branched actin filaments diffuse slower than monomers, however. One of the modeling challenges was to incorporate the dependence of F-actin fragment diffusion on the filament length and branching properties of the polymer. The following equation was used to model F-actin diffusion:

$$\frac{D_{GActin}}{FilamentLength} \times (1 - BrF)$$

'FilamentLength' is the average length of actin filament. It is calculated by dividing total F-actin (which includes all nucleotide FA forms, FA species with bound cofilin or Arp2/3, and all end species) by the number of filaments, which is calculated as equal to

half the number of ends. Diffusion is also reduced (multiplication by $(1 - BrF)$) by the fraction of filaments that are branched.

The rapidly polymerizing branched actin network produces force against the plasma membrane (Figure 1.1B). This results in rearward movement of the F-actin network and also lamellipodial protrusion. The flow of the network is modeled explicitly with an advection (velocity) expression: $v_i = v_i^{max} \times BrF$. The flow is proportional to 'BranchFraction' because only actively polymerizing filaments that are connected to the dendritic network are expected to undergo the rearward movement. An experimentally determined value for $v_i^{max} = 800\ nm/min$ (Ponti et al., 2005) was employed.

To simulate actin dynamics at the leading edge of the protruding cell in 3D, the Open Model triggers the dendritic nucleation mechanism by activating NPF (ActiveNWASP) at the membrane at the leading edge (Figure 1.3C). Starting with species concentrations obtained from the steady state of corresponding compartmental simulations, Arp2/3 complex becomes activated by ActiveNWASP and stimulates branching at the front of the cell. In live cells growing branched filaments produce force by the Brownian ratchet mechanism that pushes the plasma membrane forward. Even though Virtual Cell does not model the moving membrane or force-velocity coupling, it can represent the resulting rearward motion of actin network by a combination of advection and diffusion, as discussed above. Simulation results quantitatively reproduced F-actin accumulation in the lamellipodium, velocity fields of the rearward motion of actin network, average filament length, and profilin-bound G-actin concentration (Figure 1.3D). F-actin accumulation is a hallmark of lamellipodial protrusion (Abraham et al., 1999) and was predicted accurately

by the model with a maximum concentration of 725 μM at the tip and 120 μM (depletion) in the body of the cell; the total actin (GA + FA) in the system was 200 μM. Due to rapid assembly of branched actin network in a small volume of the lamellipodial tip, profilin-bound G-actin becomes depleted (Figure 1.3D). The simulated average length of the filaments is consistent with electron microscopy measurements (Svitkina and Borisy, 1999). Filaments at the tip are much shorter (40 subunits) than in the body of the cell (400 subunits). The velocity field that characterizes rearward motion of the network also agrees with experimental observations by speckle microscopy (Ponti et al., 2005).

The Open Model highlights a few important aspects of cooperative behavior of actin regulatory proteins. The role of cofilin in regulating actin network dynamics has been a subject of debate. It was proposed to promote depolymerization and decrease in F-actin levels (Hotulainen et al., 2005; Kueh et al., 2008) as well as stimulate polymerization and cell protrusion and produce new filaments (Endo et al., 2003; Ghosh et al., 2004; Ichetovkin et al., 2002). The model offers a potential explanation of the conflicting reports. After running multiple simulations with various initial concentrations of cofilin and Cap we noticed that cofilin could either suppress or promote Arp2/3-dependent F-actin accumulation (Figure 1.3E). With low amounts of both cofilin and Cap there are enough barbed ends to produce F-actin. Increasing Cap concentration will result in a lower number of barbed ends and therefore will inhibit F-actin increase. When cofilin concentration is high and Cap is low then F-actin production is also inhibited due to small G-actin pool. Increasing capping concentration will elevate monomer concentration and therefore will result in F-actin accumulation at the tip (Figure 1.3E). These results are

consistent with the model by (Carlsson, 2006) that predicted requirement of barbed-end capping for F-actin production due to high severing activity.

Investigation of assembly and disassembly rates in the simulated 3D lamellipodium reproduces complex dynamical behavior of the dendritic actin network. Figure 1.3F reveals a sharp boundary between polymerization and depolymerization located 1 mm from the cell edge, where negative rates that indicate disassembly are color coded and positive rates are shown in white (Figure 1.3F top). The sharp assembly-disassembly transition was originally discovered with speckle microscopy studies (Ponti et al., 2004; Ponti et al., 2005). The Open Model successfully reproduces and provides an explanation for this phenomenon. The boundary is positioned right between the regions of maximum barbed (right at the tip) and pointed end concentrations (~2 μm from the edge) (Figure 1.3F bottom). Therefore the assembly-disassembly transition is very sensitive to debranching since it exposes additional pointed ends that were previously capped by the Arp2/3 complex.

Adapting An Open Model to different experimental systems

We briefly highlight two additional studies, for which the Open Model served as a starting point. These are examples of how the original model was adapted to different experimental systems and consequently to another geometric and biochemical conditions.

Fluorescent recovery after photobleaching (FRAP) and chromophore-assisted laser inactivation (CALI) microscopy techniques are used extensively to study actin dynamics. In order to interpret the experimental result of FRAP and CALI of enhanced green

fluorescent protein (eGFP)-Cap, Kapustina developed a model (Kapustina et al., 2010) where eGFP-Cap could be virtually bleached and remain active (as in FRAP) or become inactive (as in CALI) (Figure 1.4A). The model adapts all the mechanisms from the Open Model with two enhancements: modified Cap-containing reactions, to which fluorescent and nonfluorescent species were added; mechanisms involving vasodilator-stimulated phosphoprotein (VASP) bundling and uncapping activities. The results from simulated FRAP experiments allowed estimation of Cap dissociation rate which was found to be much faster than in vitro. CALI simulations of experiments in which Cap activity was locally ablated, produced results that required anti-capping activity. Thus, the model suggested that VASP exhibits cooperativity to induce the anti-capping effect, consistent with suggestions from in vitro VASP biochemistry.

A model of Nck-induced actin comet tails (Ditlev et al., 2012) expands the signaling mechanism that leads to N-WASP activation (Figure 1.4B top). Nck is an adaptor protein that normally is recruited to phosphorylated tyrosines; it recruits a number of actin regulatory molecules including N-WASP. Experimentally increasing the density of Nck molecules at the membrane results in a nonlinear response of actin polymerization. The source of the nonlinearity was discovered by testing, '*in silico*,' three different stoichiometries of Nck/N-WASP/Arp2/3 interaction and quantitatively comparing simulated and experimental actin comets. Based on this comparison, the authors proposed a 4:2:1 stoichiometry for Nck/N-WASP/Arp2/3 and a critical role of WIP (WASP inter-acting protein) in the signaling complex at the membrane. The model predictions were rigorously tested and confirmed using quantitative fluorescent microscopy. For instance

the model accurately predicts comet tail length and the number of actin molecules in the comet (Figure 1.4B bottom).

Conclusion

In this section, we first provided a brief overview of the approaches toward detailed models of actin dynamics with a focus on the core mechanisms of actin polymerization and how it is regulated to drive cell motility. The models chosen were just illustrative and not meant by any means to comprehensively review the many contributions to this field. Rather, they were meant to exemplify what might be learned from continuum versus discrete or from compartmental versus spatial models and how these various approaches can be applied to the complexity of actin biochemistry. We then focused on how the Open Model was developed, including some of the key approximations required to confront the combinatorial complexity of polymerization and its regulation; indeed, the development of such approximations, which lump multiple explicit species and reactions into a small set of tractable variables and equations, is the most creative aspect of the modeling process. Finally, we described, using the Open Model, how Virtual Experiments could be deployed to provide fresh insight into several real experimental results and could even be used to guide the design of experiments. We encourage readers of this article to access and use the Open Model by logging onto the Virtual Cell (see Section Relevant Websites) and opening the public model called ‘les: Actin Dendritic Nucleation.’

Actin nucleation and elongation

New actin filaments assemble from 'nuclei' – trimers of actin monomers. Nucleus formation is a kinetically unfavorable reaction. In live cells the nucleation step is accelerated by three families of actin nucleation factors: Arp2/3, formins and the tandem actin monomer-binding proteins.

I will first briefly describe the latter family of actin nucleators and then will introduce in detail Arp2/3 and formins that are directly related to my thesis work. Spire, cordon-bleu leiomodin families, adenomatous polyposis coli (APC) protein (Okada et al., 2010) and several bacterial nucleators (Tarp, VopF and VopL (Zahm et al., 2013)) constitute the tandem actin monomer-binding family of actin nucleators (Campellone and Welch, 2010). These nucleating proteins contain a cluster of three or more G-actin binding domains (such as WH2), which arrange G-actin into nuclei for elongation. They do not bind Arp2/3 complex and therefore are believed to nucleate unbranched filaments. Spire has the most data available about its mechanism of regulating actin dynamics (Carlier et al., 2011; Kerkhoff, 2011). The nucleating activity resides in a central region with four WH2 domains, which can nucleate actin assembly *in vitro*. Interestingly *in vivo* Spire forms a regulatory complex with formins to cooperatively promote actin nucleation (Pechlivanis et al., 2009). Spire proteins also can inhibit incorporation of profilin-actin into the barbed ends and enhance disassembly at pointed ends by severing filaments (Bosch et al., 2007).

Actin related protein 2/3 (Arp2/3)

The Arp2/3 complex is the best-characterized actin nucleator. It is a major player in the actin dendritic nucleation scheme. Arp2, Arp3 and actin monomer nucleate new filaments on the side of the pre-existing (mother) filaments at a 70° angle. Since by itself the Arp2/3 complex has very low nucleation efficiency, it requires engagement by type I nucleation promoting factors (NPFs): WASP, N-WASP, WAVE1-3, WASH, WHAMM and JMY. Type I NPFs bind actin monomers through their V (or WH2) domain and Arp2/3 through their CA domains. The C-terminal VCA domains contain different number of conserved V motifs. The N-termini of different NPFs are distinct and mediate localization, regulation of small GTPase-binding, and association with other regulators or protein complexes. A recently described competitive inhibitor of the Arp2/3 complex, Arpin, competes with VCA for binding (Dang et al., 2013). Arpin is proposed to be a 'steering factor' and control directional persistence of migration. Interestingly it is dispensable for lamellipodial protrusion.

Actin filament branch formation is not a simple linear pathway. It is a multistep process that has been extensively investigated with advanced microscopy techniques and kinetic modeling (Smith et al., 2013a; Smith et al., 2013b). According to these studies, a VCA dimer stimulates nascent branch formation (Arp2/3 bound to VCA dimer on a mother filament). However only a small fraction of nascent branches will yield daughter filaments. The rate-limiting step of branch formation is the VCA dimer release from the nascent branch.

Arp2/3 is required for lamellipodial protrusion and sensing substrate-attached migration cues (Wu et al., 2012). It is responsible for restricting assembly to the tip of the lamellipodium and contributes to treadmilling and recruitment of additional actin regulators such as capping protein, cofilin and cortactin (Koestler et al., 2013). Spatio-temporal relationships between Arp2/3-mediated nucleation, capping of barbed ends and cofilin-mediated disassembly were pointed out by (Iwasa and Mullins, 2007).

N-WASP

Neural Wiskott-Aldrich syndrome protein (N-WASP) is a ubiquitously expressed protein with a modular domain organization (Figure 1.5A). It is intrinsically autoinhibited by the interaction of the GBD region (Figure 1.5A) with the C motif of the "output" VCA domain. The autoinhibition is released by cooperative binding of PIP2 (Phosphatidylinositol 4,5-bisphosphate or PtdIns(4,5)P_2) to the Basic domain and Cdc42-GTP to the GBD (GTPase binding domain). N-WASP can also be activated by PIP2 binding to the Basic domain and Nck binding to the PRD (Proline-rich domain) (Rohatgi et al., 2001). These interactions also translocate N-WASP molecules to the membrane. N-WASP activity is stimulated by WASP interacting protein (WIP) *in vivo* (Donnelly et al., 2013). It supports N-WASP localization by interacting with the SH3 domains of Nck at the membrane and with the N-terminal WH1 domain of N-WASP. The duration of the N-WASP active state can be modulated through phosphorylation of the GBD by Src family kinases (Padrick and Rosen, 2010). Upon activation, N-WASP undergoes a conformational change so that the VCA domain can exhibit its nucleation-promoting

function. VCA is the minimal domain of N-WASP sufficient to initiate actin branching. The VCA domain of N-WASP contains two V (verprolin homology) motifs. The simultaneous binding of a G-actin monomer to the V domain (also called WH2) and the Arp2/3 complex to the CA domains gives rise to new branches on the preexisting actin filaments (Hitchcock-DeGregori, 2003), (Figure 1.5A). The class II NFP cortactin enhances Arp2/3-mediated polymerization by binding to branch junctions and accelerating VCA release (Helgeson and Nolen, 2013).

In addition to allosteric regulation, N-WASP is a subject to oligomerization in live cells. Arp2/3 activation and actin branching are greatly enhanced when two VCA molecules are available per each Arp2/3 complex (Padrick et al., 2008; Yamaguchi et al., 2000; Yamaguchi et al., 2002). Multimerization of N-WASP in cells might occur through the three tandem SH3 domains of Nck, or the BAR domain superfamily proteins that contain c-terminal SH3 domain.

N-WASP is implicated in migration and invasion of cancer cells (Escudero-Esparza et al., 2012; Jin et al., 2013; Tang et al., 2013; Yamaguchi, 2012). (Gligorijevic et al., 2012) showed that MTLn3 rat mammary adenocarcinoma cells lacking N-WASP are deficient in invadopodia formation and extracellular matrix degradation. Tumor cells in vivo require N-WASP for migration, intravasation and metastasis. Therefore (Gligorijevic et al., 2012) propose that N-WASP could be a potential anti-metastatic therapeutic target. In another study, (Yu et al., 2012) demonstrated that N-WASP mediates delivery of the matrix metalloprotease MT1-MMP to destroy extracellular matrix near the end of the invadopodium.

Nck adaptor

Nck is a 47 kDa adaptor protein comprised of one SH2 (src-homology 2) and three SH3 (src-homolgy 3) domains (Figure 1.7B and C). This modular architecture implicates Nck in assisting numerous protein-protein interactions. SH2 domains interact with phosphorylated tyrosine residues on Receptor Tyrosine Kinases and other proteins. SH3 domains bind to proline-rich segments of a variety of effector molecules (Lettau et al., 2009). Many Nck SH3 binding partners such as Abl, DIP, Cbl, WASP, N-WASP, PINCH, DOCK180, NIK, PAKs, PRK2, WIP, dynamin, synaptojanin, and NAP1BP are associated with the regulation of the actin cytoskeleton.

A major cellular function of Nck adaptors is to mediate communication of the cell surface receptors with the actin cytoskeleton (Buday et al., 2002; Li et al., 2001). This communication is required for axon pathfinding, cell migration, chemotaxis and endocytosis. Dreadlocks, the Drosophila homolog of mammalian Nck, is a key component linking the extracellular cues to axon growth cone guidance during Drosophila eye development (Rao, 2005). Enteropathogenic bacteria *Escherischia coli* (EPEC) and the virus Vaccinia invade mammalian cells by hijacking Nck and thus manipulating the host cytoskeleton (May and Machesky, 2001). In T cells, Nck is essential for the T cell receptor-induced actin rearrangements and formation of the immunological synapse (Lettau et al., 2014; Lettau et al., 2009). (Lettau et al., 2014) found that Nck binds via its SH2 domain to the phosphotyrosines on adhesion and degranulation-promoting adapter protein (ADAP) in primary human T cells. Nck and

ADAP also cooperatively mediate T cell adhesion. Based on these findings (Lettau et al., 2014) propose that ADAP/Nck complex links integrin activation with the actin cytoskeleton. The glomerular filtration barrier (GFB) in kidneys contains actin-based foot processes (pedicels), which extend from the kidney epithelial cells (podocytes). Transgenic mice with selective deletions of Nck from the podocytes have defective formation of the pedicels and a congenital nephrotic syndrome (Jones et al., 2006; New et al., 2013). In this physiological signaling pathway Nck binds phosphotyrosine residues of nephrin (necessary for proper functioning of the GFB) and consequently underlies actin rearrangements in podocytes. (New et al., 2013) demonstrated that Nck SH3 domains are important for nephrin phosphorylation. Nck interacts with the kinase Fyn and promotes Fyn activation, which results in additional nephrin phosphorylation and subsequent increase in downstream signaling to the actin network (New et al., 2013). It is not known how exactly Nck stimulates Fyn activity.

Antibody-mediated aggregation system

Our lab utilizes an antibody-mediated aggregation system that allows us to manipulate local concentrations of particular signaling molecules in live cells and then examine the effect on the actin cytoskeleton (Rivera et al., 2004). Cells are transfected with a plasmid encoding a fusion of the extracellular domain from CD16, the transmembrane domain from CD7 (both are human immunoglobulin receptors) and a fluorescent signaling molecule of interest. Antibody-mediated crosslinking in live cells is performed by consecutive application of primary mouse monoclonal antibody against CD16 and

secondary anti-mouse antibody. A schematic of aggregation of the membrane-targeted fusion proteins is diagramed in Figure 1.6. The CD16/7 clustering system allows controlling a single protein from a certain signaling pathway. Therefore the output of such cellular manipulation can be attributed solely to the protein fused to the CD16/7 construct, as opposed to most normal physiological signals, which have many molecular outputs that are activated simultaneously.

Aggregation of Nck SH3 domains, in the very first utilization of the clustering system, resulted in formation of dynamic actin comet tails (Rivera et al., 2004). Induction of localized actin polymerization in this manner required N-WASP and was Cdc42-independent. N-WASP activation downstream of the Nck SH3 clusters occurs cooperatively with PIP2 (Rivera et al., 2009). An exhaustive study of actin comets induced by Nck SH3 clustering uncovered the details of the Nck/N-WASP/Arp2/3 signaling pathway (Ditlev et al., 2012). Through the combined approach of computational modeling and quantitative microscopy (Ditlev et al., 2012) showed that actin polymerization has a nonlinear dependence on Nck SH3 density in clusters. This phenomenon is a result of 4:2:1 Nck/N-WASP/Arp2/3 stoichiometry, where two WIP molecules are required for the recruitment of two N-WASP molecules. The resulting N-WASP dimer activates one molecule of Arp2/3 complex inducing branched actin polymerization.

The CD16/7 aggregation system was used in a study of nephrin-dependent reorganization of the podocyte cytoskeleton (Jones et al., 2006). Clustering of nephrin demonstrated that

Nck is required for coupling tyrosine phosphosites on nephrin to rearrangements of the actin cytoskeleton.

Formins

Formins are large (120 – 220 kDa) multi-domain proteins present in almost all eukaryotic organisms (Figure 1.5B). They are unique in their ability to both nucleate actin filaments as well as accelerate polymer elongation. The formin-mediated elongation process is fairly well characterized while the mechanism of nucleation, which is described later in this section, is still poorly understood. Formins are characterized by the presence of the conserved formin homology domains FH1 and FH2. The FH1 domain is an unstructured polyproline domain that binds multiple profilin-actin molecules and SH3 domains. FH1-profilin interactions accelerate the elongation activity and are not important for nucleation activity (Kovar and Pollard, 2004; Romero et al., 2004). The C-terminal FH2 domain forms a "donut-shaped" antiparallel dimer that encircles the barbed end of an actin filament. It stays attached to the growing barbed end as the filament elongates in the process referred to as processive capping (Kovar and Pollard, 2004; Mizuno et al., 2011). The profilin-actin incorporation rate to the barbed end is increased by 19-fold due to this mechanism (Romero et al., 2004). The free energy required for filament elongation is proposed to arise from accelerating ATP hydrolysis associated with the profilin-actin assembly and the consequent release of profilin. The FH1 domain is thought to increase the local concentration of G-actin near the growing ends (Kovar et al., 2006). The dimeric FH2 domain shields barbed ends from capping proteins during elongation.

The FH2 domain can also nucleate filaments either by stabilizing spontaneous actin dimers and trimers (Pring et al., 2003) or by binding of one, two or three monomers to the FH2 ring (Kupi et al., 2013). It is not clear how formin nucleates actin *in vivo* because the FH2 domain has very weak binding sites for actin monomers.

Formins are maintained in an autoinhibited state by intramolecular interaction of the DAD (diaphanous autoregulatory domain) and the DID (diaphanous inhibitory domain) segments (Figure 1.5B) (Maiti et al., 2012). In the inactive state the FH2 dimer is sterically hindered from interactions with actin. Rho family GTPases (RhoA, RhoB, RhoC, and Cdc42) release the intramolecular loop by binding to the RBD (Rho-binding domain). Rho proteins are activated locally by extracellular signals and recruit formins to the membrane for remodeling of the cytoskeleton. Additional factors are proposed to be required for the full formin activation in vivo (Maiti et al., 2012; Seth et al., 2006). Association with the membrane might stabilize the active state.

Dip adaptor

The role of DIP (Dia-interacting protein) in regulating the actin cytoskeleton is uncertain. DIP has several orthologs including: NCKIPSD (Nck interacting protein with SH3 domain), SPIN90 (SH3 Protein Interacting with Nck 90 kDa) and WISH (WASP interacting SH3 protein). Mammalian SPIN90 consists of an SH3 domain, three proline-rich motifs, a serine/threonine region and a C-terminal leucine-rich region (Figure 1.5B). It induces formation of lamellipodia and ruffles in PDGF-stimulated cells (Kim et al., 2006). The C-teminus of SPIN90 was shown to directly interact with the Arp2/3 complex

and G-actin. SPIN90 also interacts with Nck (Lim et al., 2003) and co-localizes with PI(4)P5K induced actin comets. Interestingly, WISH could induce actin polymerization in N-WASP-dependent as well as in N-WASP-independent *in vitro* assay in the absence of Cdc42 (Fukuoka et al., 2001). A recent study provided evidence for direct activation of Arp2/3 by Dip1 (Wagner et al., 2013). Dip1 was proposed to induce formation the substrate filaments capped by the Arp2/3 at the pointed end.

Interactions of DIP with formins are investigated in a study by (Satoh and Tominaga, 2001). DIP was shown to bind to proline-rich domain of mDia via its SH3 domain and to Grb2 via its proline-rich region. mDia-induced stress fiber formation appeared to be affected by DIP SH3 or proline-rich domains overexpression. DIP can also regulate Rho GTPase activity via Src-induced phorphorylation (Meng et al., 2004). (Eisenmann et al., 2007) demonstrated that DIP binds to both mDia1 and mDia2. However it inhibited only mDia2 but not mDia1-mediated actin assembly and bundling *in vitro*. Moreover, DIP expression induced non-apoptotic membrane blebbing, a process involved in amoeboid cell movement. DIP/WISH is important for cell motility and adhesion as shown in MEF cells lacking DIP/WISH (Fukumi-Tominaga et al., 2009). DIP therefore regulates both the unbranched and branched actin assembly and might have a role in integrating GTPase signaling and actin nucleation pathways.

Subversion of Host Actin Cytoskeleton by Pathogens

Pathogens frequently perturb actin of the host cell as a hallmark of infection. The actin cytoskeleton promotes intracellular bacterial movement, formation of membrane protrusions and spreading into neighboring cells. *Listeria* has been used extensively as a model system to study actin dynamics via *in vivo*, *in vitro* as well as *in silico* approaches. The first detailed study of bacterial motility demonstrated an actin comet tail that sustained *Listeria* movement (Tilney and Portnoy, 1989). Bacteria and viruses with comet tails often generate protrusions of the host plasma membrane. Some protrusions are internalized by the neighboring cells, resulting in a double-membrane vacuole. Eventually the pathogen escapes from the vacuole into the cytosol.

Various pathogens utilize distinct actin-based motility mechanisms by intercepting signaling pathways to induce actin assembly at different levels (Figure 1.7A). Pathogens express effector proteins that either interact with actin or mimic regulators of actin assembly. Pathogenic effector proteins can subvert all three major classes of actin nucleators in host cells (Haglund and Welch, 2011). Such molecular mimicry of NPF activity is a conserved mechanism in pathogenesis. Therefore investigating pathogenic NPFs uncovers not only mechanisms of pathogenesis and infectivity but also normal regulation of actin polymerization in the host cells.

Vaccinia

Vaccinia is a large double-stranded DNA virus of the *Poxviridae* family of viruses. It was shown to induce formation of actin comets 20 years ago (Cudmore et al., 1995) and has

been a model system for studying signaling to the actin cytoskeleton since then. One of the two mechanisms of Vaccinia dissemination relies on actin-based motility of the extracellular virus (EV). Actin comets are critical for cell-to-cell spread of cell-associated EVs (CEVs).

An integral membrane protein A36 is required for actin tail formation. Tyrosine 112 of A36 is phosphorylated by Src and Abl family kinases that are recruited by the extracellular virus (Newsome et al., 2006). Phosphorylated tyrosine residue Y112 on the cytoplasmic domain of A36 was shown to bind Nck (Frischknecht et al., 1999) (Figure 1.7B). This interaction is essential for comet tail formation. Binding of the adaptor Grb2 to Y132 of A36 enhances formation of actin tails (Scaplehorn et al., 2002). WIP (WASP interacting protein) and N-WASP are recruited to Nck as a complex (Moreau et al., 2000) and N-WASP recruitment depends on WIP (Donnelly et al., 2013). Interaction of WIP with the second SH3 domain of Nck is essential for comet tail formation (Donnelly et al., 2013) because it is required for WIP:N-WASP complex recruitment.

In a recent study about Vaccinia actin-based motility, the formin, FHOD1, was identified as a required factor for virus dissemination (Alvarez and Agaisse, 2013). Actin tail formation and formin localization was dependent on the GBD and FH2 domains of FHOD1. Profilin and the FH1 domain of formin were required for comet tail formation. The authors of the study (Alvarez and Agaisse, 2013) also demonstrated that FHOD1 was recruited and activated by the small GTPase Rac1. It is interesting which mechanism integrates activation of both N-WASP/Arp2/3 and Rac1/FHOD1 pathways in Vaccinia actin-based motility. (Alvarez and Agaisse, 2014) suggest that Vaccinia engages a yet

unidentified Receptor Tyrosine Kinase that activates Src kinase. Src in turn phosphorylates A36 and recruits an unidentified GEF for Rac1. The former results in N-WASP activation and the latter in FHOD1 activation thereby inducing co-engagement of two signaling pathways.

EPEC

Enteropathogenic *Escherichia coli* (EPEC) is an extracellular diarrheagenic pathogen that induces attaching and effacing (A/E) lesions on the intestinal epithelium. The A/E lesions are characterized by destruction of microvilli, intimate adherence of bacteria to the apical surface of the enterocytes and accumulation of actin polymer beneath the attached bacteria. This extracellular pathogen reorganizes the actin cytoskeleton of the host cell into actin-rich pedestals at the sites of bacterial attachment. Actin pedestals are dynamic actin structures that can be up to 10 μm long and move with velocities up to 4.2 μm/min. Pedestals move along the cell surface and are proposed to facilitate colonization of the gut.

Formation of pedestals depends on the bacterial outer membrane protein intimin, which interacts with the translocated intimin receptor (Tir). Tir is injected into host cells, localized in the membrane and then interacts with intimin. This interaction results in clustering of Tir under the bacterial surface and stimulates signaling to the actin cytoskeleton (Frankel and Phillips, 2008). Tyrosine residue 474 at the C-terminus of Tir is phosphorylated by the host Src family kinase c-Fyn. The Nck adaptor that is recruited to pTyr 474 stimulates N-WASP/Arp2/3-mediated actin assembly (Figure 1.7C).

Similarly to Vaccinia, N-WASP recruitment is WIP-dependent in EPEC (Wong et al., 2012). Tir can also induce weak actin polymerization by a Nck-independent mechanism through Y454 and recruitment of the insulin receptor tyrosine kinase substrate p53 (IRSp53) (Vingadassalom et al., 2009). Another bacterial effector EspH promotes pedestal formation independently of Tir residues Y454/Y474 and Nck adaptor (Wong et al., 2012). EspH binds to the C-terminus of Tir to recruit WIP and N-WASP, which results in actin pedestal formation and elongation.

Rickettsia

Rickettsia is a small (1.6 x 0.5 μm) rod-shaped gram-negative bacterium that can be found in the nucleus and cytoplasm of infected cells. The comet tails induced by this bacterium can move with the velocity of 5-8 μm/min. *Rickettsia* expresses two different effector proteins for manipulating the actin network of the host cell – RickA and Sca2. RickA is similar to N-WASP and contains a proline-rich region and a VCA domain (Gouin et al., 2004). In vitro experiments confirm that Arp2/3 is necessary for RickA-induced formation of comet tails (Jeng et al., 2004).

(Haglund et al., 2010) discovered that *Rickettsia* also utilizes actin-based motility by formin-mediated force generation. Until then most studies of pathogenic motility focused on the exploitation of the Arp2/3 activity of the host cell. Sca2 that is expressed on the surface of the bacteria interacts directly with actin and nucleates linear filaments. Sca2 is a formin-like protein that contains four WH2 domains and two proline-rich segments (Haglund et al., 2010; Kleba et al., 2010). This bacterial protein mechanistically mimics

formins, even though it functions as a monomer and does not have autoinhibitory intramolecular interaction (Madasu et al., 2013).

Rickettsia has two distinct phases of actin-based motility. During each phase a distinct mechanism of actin nucleation is employed (Reed et al., 2014). In an early phase the bacterium relies on Arp2/3-mediated assembly initiated by RickA. In a late phase, *Rickettsia's* motility is driven by unbranched polymerization via Sca2-initiated nucleation. Sequential polarization of RickA and Sca2 plays a critical role in switching between the two phases of motility.

Listeria

Listeria is an intracytoplasmic Gram-positive pathogen that causes listeriosis. It invades non-phagocytic cells, replicates in the cytoplasm and spreads to adjacent cells by actin-based motility. Subversion of the host actin machinery manifests in the characteristic comet tails, which push the bacterium with velocities of 10-87 μm/min.

Listeria expresses a virulence factor ActA on its surface, which acts a functional mimic of N-WASP (Welch et al., 1997) and was the first identified member of the class I NPFs. ActA is a multidomain protein that binds to both Arp2/3 complex and Ena/VASP proteins. It consists of the C-terminal transmembrane (TM) segment that inserts into the bacterial membrane and the N-terminal acidic (A), central (C) and actin-binding (AB) domains; the AB domains contain two WH2 domains. The central region of ActA has 3-4 proline-rich repeats that bind Ena/VASP and profilin-actin complexes. The proline-rich motifs enhance actin assembly and are not critical for comet tail formation (Skoble et al.,

2000). The Arp2/3 complex of the host cell is necessary for *Listeria* actin assembly. The A and C domains of ActA activate the Arp2/3 complex, and the AB domains recruit actin monomers. Remarkably, the ActA protein lacks regulatory domains and therefore *Listeria* actin-based motility is largely independent of the host signaling pathways. While the serine-threonine kinase CK2 phosphorylates ActA and enhances Arp2/3-mediated bacterial motility, it is not required for ActA actitivity (Skoble et al., 2000). *Listeria* is unique in its ability to bypass the host actin regulatory pathways.

Interestingly, *Listeria*-induced actin tails are comprised of two populations of actin polymer (Sechi et al., 1997): short cross-linked filaments right at the base of the bacterium, and long parallel filaments in the remainder of the comet tail. The presence of the latter population implies involvement of formin family proteins in the actin assembly. Indeed, inhibition of the formin FH2 domain with the SMIFH2 (small molecule inhibitor of the FH2 domain) dramatically reduced the length of membrane protrusions created by *Listeria* actin comets (Fattouh et al., 2015). mDia1, mDia2 and mDia3 are localized to the protrusions and their knockdown results in decreased cell-to-cell spread of bacteria. The same study (Fattouh et al., 2015) showed that knockdown of Rho family members (Rac1, Cdc42, RhoA, RhoC, and RhoD) also affected bacterial spread into the adjacent cells. Therefore, the Rho GTPase/formin signaling pathway is involved in *Listeria*-induced protrusion formation and is critical for bacterial dissemination.

Thesis overview

Actin dynamics are characterized by constant remodeling of the actin cytoskeleton by a multitude of actin regulatory proteins. *In vivo* actin dynamics underlie the process of

actin-based motility, which can drive whole cell locomotion as well as localized structures such as actin comet tails.

Major aspects of actin polymerization and actin regulatory proteins are introduced in the beginning of the section "Detailed Biochemical Modeling of Actin Dynamics" in Chapter 1. This section also describes the 'open' model of actin dendritic nucleation (Ditlev et al., 2009) that is used as a basis for the study of cofilin activity in Chapter 2. Chapter 1 gives a detailed overview of N-WASP/Arp2/3 and formin actin nucleation mechanisms that are important for my research of actin comets in Chapter 3. At the end of Chapter 1, I highlight several examples of pathogenic subversion of actin-based motility. Until recently each pathogen was assumed to exploit a single mode of actin-based motility. However several current studies emphasize recruitment of two nucleation pathways (Arp2/3- and formin-mediated) by pathogens Vaccinia, *Rickettsia*, and *Listeria*. My main hypothesis for the project in Chapter 3 was inspired by these studies.

Chapter 2 contains an *in silico* study of the role of cofilin in regulating dendritic actin nucleation. I demonstrate yet another collaborative behavior between actin-binding proteins capping and cofilin in orchestrating the process of branched actin assembly. In Chapter 3, I present a project about the dynamics and morphology of actin comets induced by clustering Nck SH3 domains at the membrane. I propose that Nck serves as hub between the signaling pathways and fine-tunes cytoskeletal responses by maintaining a balance of linear versus branched actin assembly. Similar mechanisms might be in place during pathogen-induced actin-based motility, since Nck is hijacked by the

pathogens that rely on both linear and branched actin polymerization. In Chapter 4, I discuss the importance of these studies and propose potential future directions.

Figures

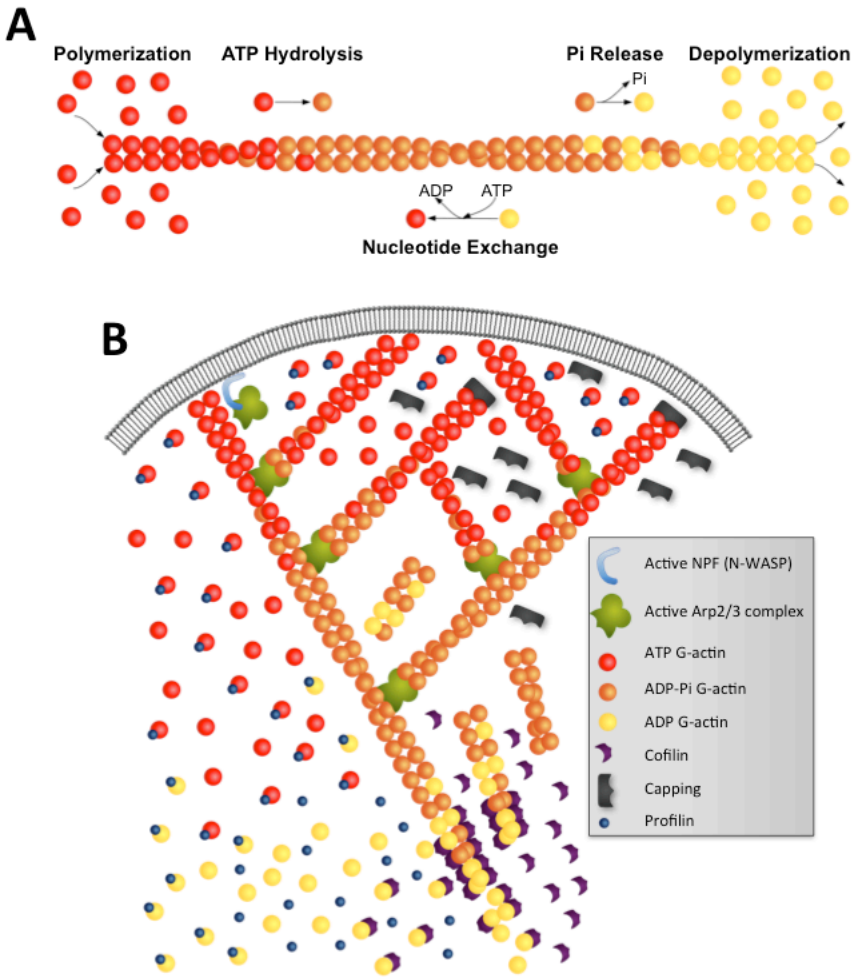
A
Polymerization
ATP Hydrolysis
Pi Release
Depolymerization
Pi
ADP
ATP
Nucleotide Exchange
B
Active NPF (N-WASP)
Active Arp2/3 complex
ATP G-actin
ADP-Pi G-actin
ADP G-actin
Cofilin
Capping
Profilin

Figure 1.1. **Schematics of actin treadmilling and dendritic nucleation mechanism.** **A.** The treadmilling process. Actin monomer undergoes repeated cycle of assembly, ATP shydrolysis, Pi dissociation, disassembly, and nucleotide exchange. **B.** Actin dendritic nucleation mechanism. The cartoon depicts several major biochemical processes underlying dendritic nucleation: N-WASP induced Arp2/3 activation and branching, filament treadmilling, cofilin-mediated severing, profilin-mediated ADP/ATP exchange on G-actin, capping of barbed ends, incorporation of ATP-G-actin at the barbed ends, and disassembly at the pointed ends. Adapted from the original cartoon from (Pollard and Borisy, 2003).

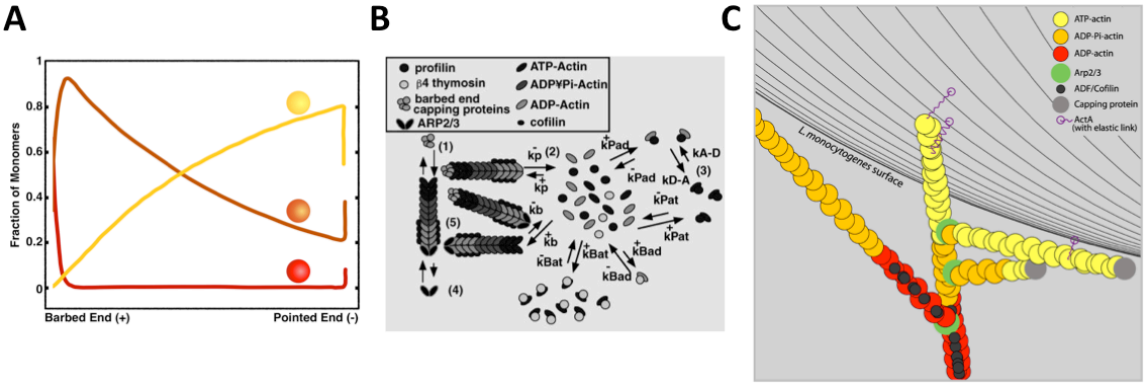
A
B
C
Fraction of Monomers
1
0.8
0.6
0.4
0.2
0
Barbed End (+)
Pointed End (-)
profilin
β4 thymosin
barbed end capping proteins
ARP2/3
ATP-Actin
ADP¥Pi-Actin
ADP-Actin
cofilin
(1)
(2)
(3)
(4)
(5)
kp
kb
kPad
kA-D
kD-A
kPat
kBat
kBad
ATP-actin
ADP-Pi-actin
ADP-actin
Arp2/3
ADF/Cofilin
Capping protein
ActA (with elastic link)
L. monocytogenes surface

Figure 1.2. Early comprehensive models.
A. Nucleotide state profile. Simulation results from (Bindschadler et al., 2004) showing fractions of ATP-bound (red curve), ADP-Pi- bound (orange curve), and ADP-bound (yellow curve) monomers along 370-subunit long (1 mm) filaments. **B.** Schematic of actin cycle. Mechanisms included in a model by (Bindschadler et al., 2004). **C.** Actin branching near bacterial surface. A simulation video frame from (Alberts and Odell, 2004) showing a branched actin filament attached (via ActA) to a surface of L. monocytogenes. Collisions of filaments with the bacterial surface produce force propelling the bacterium in the cytosol of the host cell.

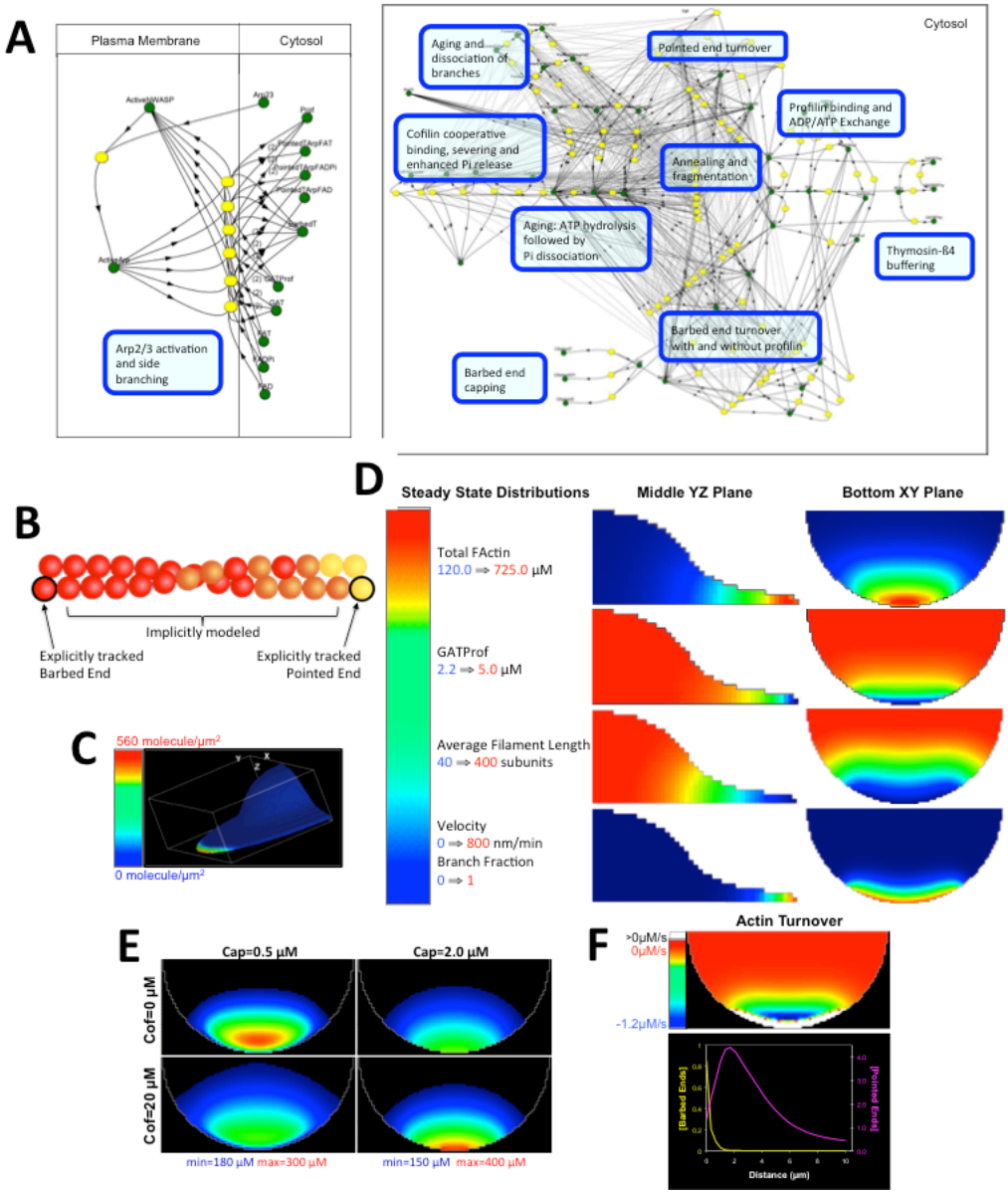
A
Plasma Membrane
Cytosol
Arp2/3 activation and side branching
Cytosol
Aging and dissociation of branches
Pointed end turnover
Profilin binding and ADP/ATP Exchange
Cofilin cooperative binding, severing and enhanced Pi release
Annealing and fragmentation
Aging: ATP hydrolysis followed by Pi dissociation
Thymosin-ß4 buffering
Barbed end turnover with and without profilin
Barbed end capping
B
Implicitly modeled
Explicitly tracked Barbed End
Explicitly tracked Pointed End
C
560 molecule/µm²
0 molecule/µm²
D
Steady State Distributions
Middle YZ Plane
Bottom XY Plane
Total FActin
120.0 ⇒ 725.0 µM
GATProf
2.2 ⇒ 5.0 µM
Average Filament Length
40 ⇒ 400 subunits
Velocity
0 ⇒ 800 nm/min
Branch Fraction
0 ⇒ 1
E
Cap=0.5 µM
Cap=2.0 µM
Cof=0 µM
Cof=20 µM
min=180 µM max=300 µM
min=150 µM max=400 µM
F
Actin Turnover
>0µM/s
0µM/s
-1.2µM/s
[Barbed Ends]
[Pointed Ends]
Distance (µm)

Figure 1.3. **An Open Model of actin dendritic nucleation (Ditlev et al., 2009).** **A.** Reaction diagram from Virtual Cell. Green circles – species. Yellow ovals – reactions/transformations. Reactions occurring at the inner side of the membrane in vivo are placed in the 'Plasma Membrane' compartment. Membrane reactions can recruit cytosolic species. Each rounded rectangle with a mechanism label points to a set of reactions involved in the indicated mechanism. **B.** Nucleotide state tracking. Nucleotide states of the barbed end (red ball outlined in black) and pointed end (yellow ball outlined in black) are explicitly modeled. The states of all the subunits in the interior of the filament are modeled implicitly (state of each subunit is unknown) by three state variables FAT, FAD-Pi, and FAD (concentrations of all the ATP-, ADP-Pi, and ADP-bound subunits respectively). The state of the newly formed pointed end (after the yellow ball outlined in black dissociates) is incorporated into the dissociation rate. **C.** Realistic 3D geometry of a protruding cell. Polymerization is triggered by ActiveNWASP (color coded) at the tip of the lamellipodium (7246 molecules). **D.** Simulation results from spatial model with Arp2/3 activation. Minimum (blue value) and maximum (red value) are provided for each variable. **E.** Interplay of cofilin and Cap. Model predictions for the total amount of F-actin under varied cofilin and capping concentrations. At low capping level increasing cofilin results in F-actin decrease. At high capping level increasing cofilin results in F-actin decrease. **F.** Sharp transition from assembly to disassembly 1 mm from the leading edge. (Upper) Simulation results (bottom xy slice) from 3D model showing assembly (white) and disassembly (color coded) rates. (Lower) Abundance of barbed and pointed ends across the lamellipodial tip.

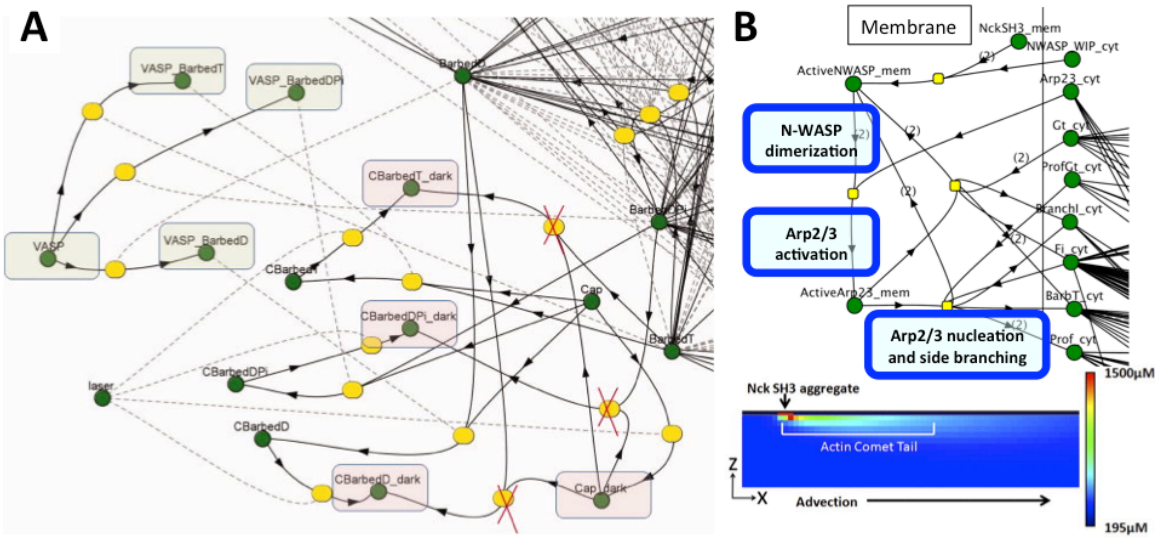
A
VASP_BarbedT
VASP_BarbedDPi
BarbedT
CBarbedT_dark
VASP
VASP_BarbedD
CBarbedT
Cap
CBarbedDPi_dark
BarbedT
CBarbedDPi
laser
CBarbedD
CBarbedD_dark
Cap_dark
B
Membrane
NckSH3_mem
NWASP_WIP_cyt
ActiveNWASP_mem
Arp23_cyt
N-WASP dimerization
Gt_cyt
ProfCt_cyt
Arp2/3 activation
BranchI_cyt
FI_cyt
ActiveArp23_mem
BarbT_cyt
Arp2/3 nucleation and side branching
Prof_cyt
1500µM
Nck SH3 aggregate
Actin Comet Tail
Z
X
Advection
195µM

Figure 1.4. Examples of models based on the Open Model.
A. CALI and FRAP of Caps. Reaction diagram of barbed-end capping mechanism from the model by (Kapustina et al., 2010). Note 'dark' Cap species in pink rectangles. In FRAP 'dark' Cap is active and able to participate in reactions. For CALI experiments the 'dark' Cap is inactive. VASP can bind each type of free barbed ends and therefore competes with Cap. **B.** N-WASP/Arp2/ 3 signaling in actin comets. (Top) Arp2/3 activation at the membrane as in the model by (Ditlev et al., 2012). Activation mechanism was modified to include Nck activation of N-WASP, WIP recruitment, and proposed 4:2:1 Nck/N-WASP/Arp2/3 stoichiometry. (Bottom) Simulation result for total F-actin in the actin comet induced by aggregation of Nck SH3 domains. Actin comets move along the membrane being propelled by polymerizing actin. Comet propulsion is modeled through the advection parameter.

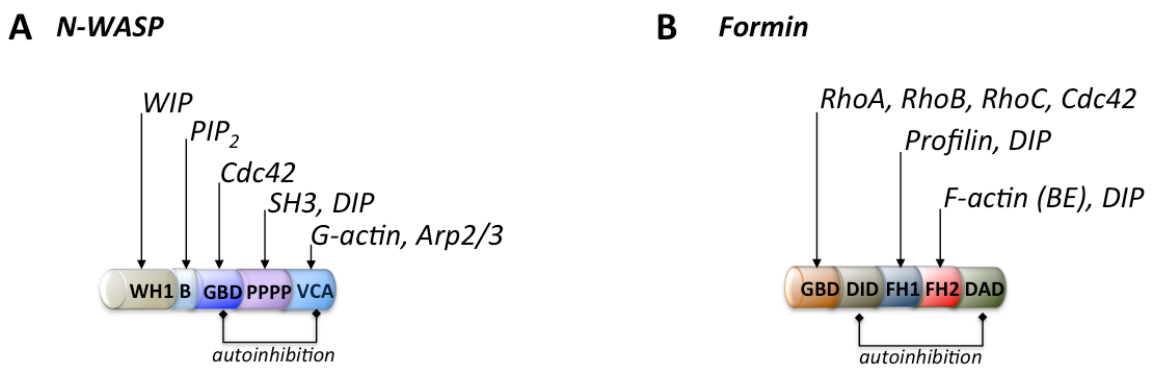
A N-WASP
WIP
PIP2
Cdc42
SH3, DIP
G-actin, Arp2/3
WH1
B
GBD
PPPP
VCA
autoinhibition
B Formin
RhoA, RhoB, RhoC, Cdc42
Profilin, DIP
F-actin (BE), DIP
GBD
DID
FH1
FH2
DAD
autoinhibition

Figure 1.5. **N-WASP and formin regulation.**
A. N-WASP is a modular protein that contains a NH2-terminal WASP homology 1 domain (WH1), followed by a basic region (B), a GTPase binding domain (GBD), a proline-rich domain (PRD), and a COOH-terminal catalytic domain (VCA). The VCA domain is composed of a WASP homology 2 domain (WH2 or V), a central region (C), and an acidic domain (A). N-WASP contains two WH2 domains. N-WASP (not shown) exist in an auto-inhibited conformation in which the VCA domain is occluded by an intramolecular interaction. The binding of WIP (WASP interacting protein) to the WH1 (WASP homology 1) domain of WASP and N-WASP maintains this inactive state. A variety of ligands synergistically activate WASP and N-WASP by disrupting the intramolecular interaction to expose the C-terminal VCA domain that binds and activates the Arp2/3 complex. The ligands include phosphatidylinositol 4,5-bisphosphate (PIP2) that binds the B domain; the Rho-GTPases Cdc42 and Rac1 that bind to the GBD; and several SH3 domain-containing proteins that interact with the central PRD. **B.** Domain organization of mouse diaphanous 1/2 (mDia1/2) that are dimeric and regulated by autoinhibition. The amino-terminal diaphanous inhibitory domain (DID) interacts with the C-terminal Dia autoregulatory domain (DAD) that mediate autoinhibition. Rho binding to the Rho-binding domain (RBD) may relieve autoinhibitory interactions. Dimerization domain (DD) and the coiled-coil (CC) domains (not shown) are located between DID and FH1 domains. The formin homology 2 (FH2) dimerizes in an anti-parallel manner to form a doughnut-shaped structure, whereas FH1 (located between the CC and FH2 domains) lacks a predicted structure but might be rope-like. mDia molecules in the dimer interact via DD and FH2 domains. Dia-interacting protein (DIP; also known as WISH and NCKIPSD) binds FH1 and FH2 of mDia1 and mDia2 (also known as DIAPH3). Profilin binds FH1 of formins.

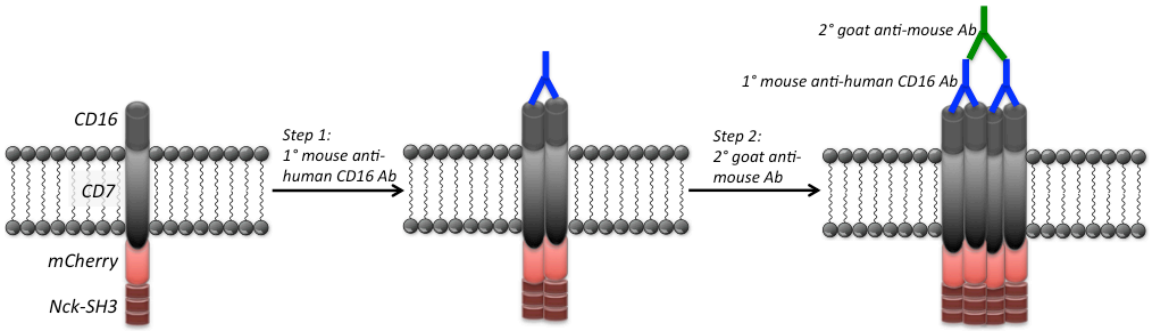
CD16
CD7
mCherry
Nck-SH3
Step 1:
1° mouse anti-
human CD16 Ab
Step 2:
2° goat anti-
mouse Ab
1° mouse anti-human CD16 Ab
2° goat anti-mouse Ab

Figure 1.6. Antibody-mediated aggregation system.
Cells expressing fusion proteins containing extracellular domain CD16, the transmembrane domain CD7 and a fluorescent signaling protein of interest are incubated sequentially with the primary monoclonal antibody against human CD16 and then with an unlabeled goat anti–mouse IgG.

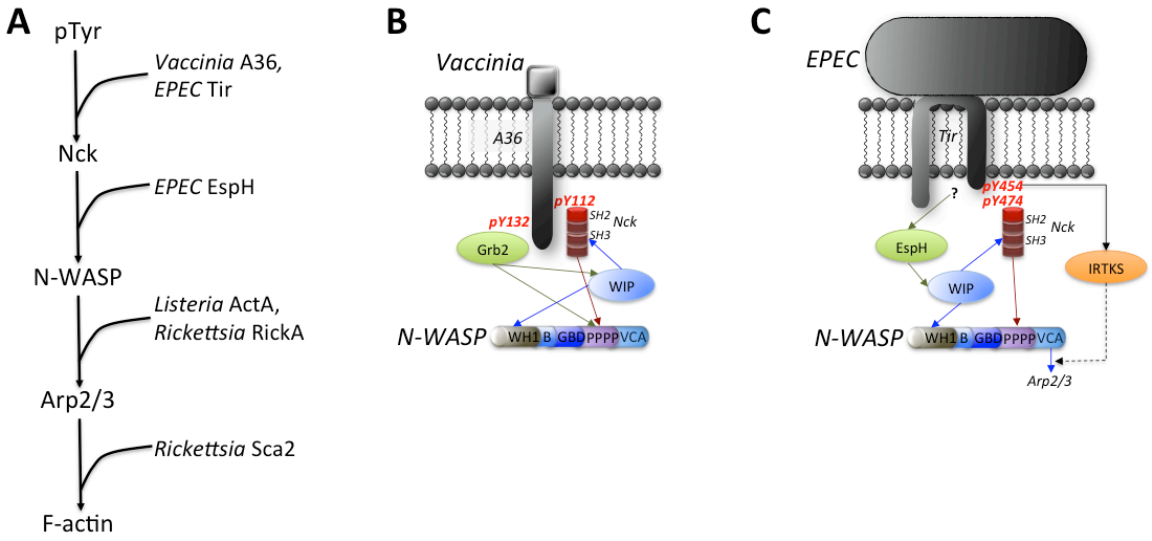
A
pTyr
Vaccinia A36,
EPEC Tir
Nck
EPEC EspH
N-WASP
Listeria ActA,
Rickettsia RickA
Arp2/3
Rickettsia Sca2
F-actin
B
Vaccinia
A36
pY112
pY132
SH2
SH3
Nck
Grb2
WIP
N-WASP
WH1
B
GBD
PPPP
VCA
C
EPEC
Tir
?
pY454
pY474
SH2
SH3
Nck
EspH
WIP
IRTKS
N-WASP
WH1
B
GBD
PPPP
VCA
Arp2/3

Figure 1.7. Signaling pathway targeted by pathogens.
A. Pathogens subvert actin assembly pathways at different levels. Vaccinia virus and EPEC express proteins (A36 and Tir) that mimic host phosphotyrosine motifs to recruit the adaptor protein Nck. EPEC produces protein EspH that recruits WIP and N-WASP. *Listeria* ActA and *Rickettsia* RickA mimic N-WASP to activate the host Arp2/3 complex. *Rickettsia* bypasses host nucleators using the formin-like protein Sca2 to interact directly with actin. **B.** Vaccinia recruits N-WASP via Nck and WIP, downstream of Src- and Abl-mediated phosphorylation of tyrosine 112 of the integral viral membrane protein A36. Grb2 recruitment is not critical, but its interaction with the proline-rich regions of WIP and N-WASP enhances actin tail formation **C.** Pedestal formation by EPEC requires N-WASP-triggered activation of Arp2/3 for actin dendritic nucleation. Clustered EPEC Tir in the cellular plasma membrane is phosphorylated at residue Y474 triggering host adaptor Nck recruitment, which binds and activates N-WASP. EPEC also generates pedestals at lower efficiency through IRTKS/IRSp53 (insulin receptor tyrosine kinase substrate p53) Nck-independent pathways (dashed black line). EspH is recruited via the C-terminus of Tir to the bacterial attachment site where the effector (directly or indirectly) promotes WIP and N-WASP recruitment independently of Nck or Y454/Y474.

Movies

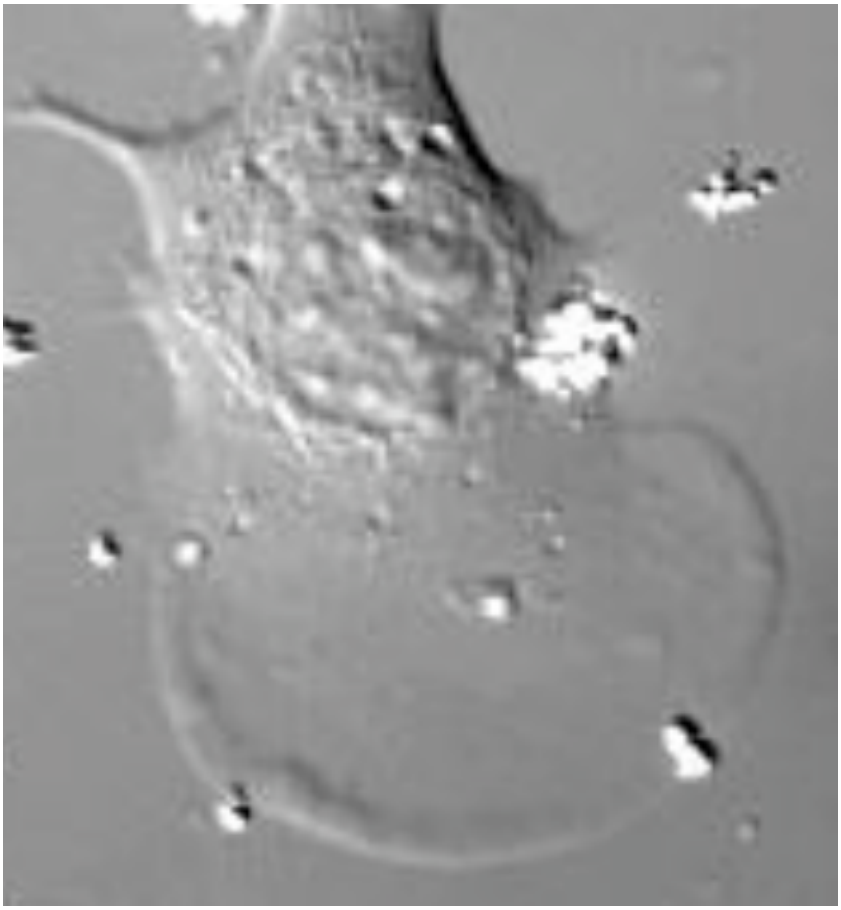

Movie 1.1. B16-F1 melanoma cell migrating on Fibronectin coated cover-glass.
Images taken every 10s, length of the movie is 10min, DIC (acknowledgement: Yi Wu).

2. CHAPTER II: Interplay of Cofilin and Capping proteins in regulation of actin dynamics in lamellipodium

Attribution: This chapter contains a draft of the manuscript by Sofya Borinskaya and Les Loew entitled “Interplay of Cofilin and Capping proteins in regulation of actin dynamics in lamellipodium”. The model was previously developed by (Ditlev et al., 2009) and simplified by Paul J. Michalski. Sofya Borinskaya is responsible for all simulation data presented in the manuscript. Manuscript was written by Sofya Borinskaya and edited by Leslie M. Loew.

Abstract

Non-muscle cofilin-1 (cofilin) is an essential actin regulatory protein that plays an important role in dynamic events at the leading edge of migrating cells. Cofilin activity is spatio-temporally regulated in cells by other actin-binding proteins, phosphorylation, pH and PIP_2 binding. The physiological function of cofilin has been a controversial subject since cofilin was shown to induce either polymerization or depolymerization according to different *in vitro* and *in vivo* studies. Here we utilize *in silico* experimentation in Virtual Cell software to investigate the function of cofilin in a dynamic branched network at the tip of a lamellipodium. We propose synergy between cofilin and capping protein in regulating Arp2/3-mediated actin polymerization. Our model predicts that cofilin promotes actin disassembly when capping protein concentration is low and promotes actin assembly when capping protein is in excess and a sufficient actin monomer pool is maintained.

Introduction

Cofilin/ADF (hereafter referred to as cofilin) plays an essential role in regulating actin dynamics in lamellipodial protrusion (Pollard and Borisy, 2003). Cofilin is a relatively small (19kDa) protein that is expressed in most eukaryotic cells. It binds to G- (monomeric) and F- (filamentous) actin and has higher affinity for ADP-bound subunits in the filaments. Cofilin enhances inorganic γ-phosphate (Pi) release from ADP-Pi subunits in the filaments, accelerates dissociation of ADP subunits from pointed ends (Blanchoin and Pollard, 1999; Suarez et al., 2011) and can inhibit nucleotide exchange on actin monomers. Furthermore, cofilin also severs actin filaments through cooperative

binding to adjacent subunits (Hayakawa et al., 2014; McGough et al., 1997) and thus generates free barbed ends (Chan et al., 2000; Ghosh et al., 2004).

Many mechanisms regulate cofilin activity with spatio-temporal precision that is critical for normal cell physiology (van Rheenen et al., 2007). Cofilin is inhibited from binding to F-actin either by interaction with $PI(4,5)P_2$ (Gorbatyuk et al., 2006) or cortactin (Oser et al., 2009) and via phosphorylation at Ser3 (Arber et al., 1998). Also tropomyosins compete with cofilin for F-actin binding and therefore prevent severing and depolymerization (DesMarais et al., 2002). Additionally, cofilin activity was shown to be stimulated by an increase in intracellular pH (Bernstein et al., 2000; Frantz et al., 2008).

Cofilin activity can promote either actin depolymerization (Hotulainen et al., 2005; Kueh et al., 2008) or polymerization (Ghosh et al., 2004; Ichetovkin et al., 2002). The *in vitro* study by (Kueh et al., 2008) demonstrates that cofilin severing activity disassembles actin filaments. Similarly cofilin and ADF knockdown studies in live cells shows that these proteins promote depolymerization and increase the pool of actin monomers (Hotulainen et al., 2005). The authors depleted cofilin and ADF levels by siRNA-induced gene silencing in NIH 3T3 and B16F1 cells. Cofilin knock-down (KD) cells migrated significantly slower and disassembly of actin filaments was diminished. G-actin/F-actin ratio was decreased in cofilin KD cells, which indicates that cofilin might regulate actin dynamics by replenishing the actin monomer pool.

On the other hand an *in vitro* study by (Ichetovkin et al., 2002) demonstrates that cofilin in synergy with Arp2/3 complex increases F-actin mass by providing additional barbed ends. In accordance with this *in vitro* sudy, (Ghosh et al., 2004) showed that cofilin

activity has similar effects in live cells. Global uncaging of constitutively active cofilin caused F-actin increase, generation of free barbed ends as well as an increase in instantaneous speed and protrusive activity of the cells. Localized photorelease of cofilin induced protrusion at the uncaging spot implicating cofilin in determining the direction of cell migration.

In this study we demonstrate through biochemical modeling how cofilin activity can induce either a decrease or an increase in F-actin content. Based on the simulation results we propose that cofilin and capping proteins exhibit synergy in regulating Arp2/3-mediated actin polymerization. When capping protein is sparse, an increase in cofilin concentration causes depolymerization. However when capping protein is in excess and can cap the newly produced barbed ends, cofilin promotes F-actin accumulation because there are enough actin monomers in the cytosol. This is yet another complex mode of regulating actin dynamics through cooperative behavior of actin regulatory proteins.

Methods

Modeling and simulations are implemented in the Virtual Cell software (http://vcell.org). We used a simplified actin dendritic nucleation model (referred to as Open Model) based on the actin dendritic nucleation model published in (Ditlev et al., 2009); simplification of the original Open Model is described in the methods section of (Ditlev et al., 2012). The reaction diagram is shown in Figure 2.1.

Cofilin biochemistry is implemented in the model according to (Blanchoin and Pollard, 1999; Cao et al., 2006) where cofilin binds cooperatively and reversibly to adjacent ADP-

F-actin subunits and also stimulates the release of Pi from ADP-Pi-F-actin. Figure 2.2 shows the reaction diagram of cofilin mechanisms and Table 2.1 lists the reactions along with the expressions and the rates. Binding cooperativity is modeled as the product of cytosolic cofilin with the F-actin-bound cofilin. Severing occurs between two neighboring cofilin-bound subunits. Two F-actin subunits next to two cofilin-bound F-actin subunits are severed via a cofilin-mediated mechanism.

Compartmental simulations (Biomodels: CofilinCapInterplay_DendriticNucleation_0 and CofilinCapInterplay_DendriticNucleation_1, application: "Steady State Turnover") without active_NWASP (i.e. in the absence of Arp2/3 activity) were run for various values of Cap (0, 0.5, … 9.5, 10 μM). For each Cap simulation, cofilin was varied from 0 to 20 μM. The total concentrations of molecular species were: [profilin] = 10 μM, [thymosin ß4] = 100 μM. Steady state compartmental results were used as initial conditions for spatial simulations, where active_NWASP locally activates Arp2/3.

The nucleation and Arp2/3-mediated branching reaction diagram is shown in Figure 2.1 and the mechanism is described in detail in (Ditlev et al., 2009). Spatial simulations (application "2D F-actin from CofCap") were run using a two-dimensional geometry of a circular half-cell with 15 μm radius shown in Figure 2.4A. N-WASP was activated at the tip of the lamellipodium as depicted on Figure 2.4B. [Arp2/3] = 1 μM and total actin concentration = 200 μM. Cytoplasmic species were assumed to have a diffusion coefficient of 5 $\mu m^2/s$; the diffusion coefficient for actin filaments is calculated as (5.0 * (1.0 - BrF) / L) $\mu m^2/s$ to account for the size and degree of branching of the polymer (Ditlev et al., 2009). The system of PDEs was solved using the finite volume solver on a

rectangular grid of 51 x 26 (geometry size is 30.4 x 15.2 μm) elements with adaptive time-steps.

Results and Discussion

We aimed to investigate the mechanism of action of cofilin protein in the lamellipodium using a kinetic modeling approach. The Open Model (Ditlev et al., 2009) is currently the most comprehensive detailed biochemical model of actin dynamics. It reproduces several complex physiological phenomena that are driven by the actin dendritic nucleation process. Therefore the Open Model served well as an *in silico* platform for our virtual experiments.

The motivation for our study was to find an explanation for the conflicting experimental results about cofilin effects on branched actin cytoskeleton dynamics (Andrianantoandro and Pollard, 2006; Ghosh et al., 2004; Hotulainen et al., 2005; Ichetovkin et al., 2002; Kiuchi et al., 2007; Kueh et al., 2008). While enzymatic activity of cofilin has been quite well characterized, its ultimate function in regulating actin dynamics and cell motility is still a subject of debate. Through its severing activity, cofilin can accelerate treadmilling and populate the pool of actin monomers (Kiuchi et al., 2007) that is necessary for polymerization. The latter is also enhanced by cofilin stimulating Pi release from ADP-Pi bound subunits. Severing also creates new barbed ends that are available for elongation. Interestingly, cofilin binds actin filaments cooperatively and its mode of action is highly dependent on concentration, pH and other actin regulatory proteins (Aggeli et al., 2014; Elam et al., 2013b).

Variability in cell types as well as in experimental approaches could potentially lead to opposing conclusions about the role of cofilin in regulating the actin cytoskeleton. Biochemical modeling allowed us to vary the concentrations of cofilin in the same *in silico* assay and observe how the branched actin network behaves at the tip of lamellipodium. We found that cofilin can in fact stimulate either actin polymerization or depolymerization in a concentration dependent manner and its role is tightly coupled to the capping of barbed ends.

Results from compartmental simulations

First we ran steady-state compartmental (ODE) simulations without activation of branched nucleation at the membrane (ActiveNWASP = 0). Total actin, profilin and thymosin were assigned physiological concentrations as defined in Methods. In cells cofilin concentration can vary significantly and reach up to 20 μM. Therefore we varied cofilin from 0 to 20 μM in the simulations. We also varied capping protein from 0 to 10 μM. In compartmental simulations, all the molecules are assumed to be uniformly distributed in space and well-mixed throughout the simulation time. The results of 441 simulations for four different variables are presented in Figure 2.3. The data are displayed as a color-coded surface where color-coding signifies how a certain variable depends on the corresponding concentration of cofilin (x-axes) and capping protein (y-axes).

We obtained initial insight on how cofilin and capping proteins might co-regulate actin polymerization. Figure 2.3A shows F-actin amount at the steady-state. In general capping activity limits, while cofilin severing increases total F-actin. Free barbed ends that are

generated by cofilin through severing the filaments (Figure 2.3B), serve as substrate for F-actin assembly. At capping protein concentrations below 1 μM, actin is almost exclusively in the F-actin form irrespective of cofilin concentration (Figure 2.3A). Consequently the G-actin pool is sparse (Figure 2.3D) because it has been converted into the filamentous form. At capping protein concentrations above 1.5 μM the total F-actin tends to be more sensitive to the amount of cofilin. Increase in capping protein concentration results in greater G-actin pool. As a result, the actin polymer amount is higher at high cofilin concentrations (when barbed ends are available) and lower at low cofilin concentrations. Both cofilin and capping proteins are critical for the turnover of the barbed ends (Figure 2.3C) and the turnover is highest at high physiological concentrations of both cofilin and capping proteins.

Results from spatial simulations

We modeled a protruding cell with a half-circle geometry (Figure 2.4A) where N-WASP was activated at the cell front (Figure 2.4B). N-WASP triggers Arp2/3-mediated nucleation and branching (Figure 2.1) beneath the plasma membrane and therefore in spatial simulations polymerization mostly occurs near the region of membrane where ActiveNWASP is mathematically constrained (Figure 2.4C). All the cytosolic species undergo diffusion and diffusion of the filamentous actin network depends on its size and amount of branching (see Methods).

Steady-state results from compartmental simulations were used as initial conditions for 441 spatial simulations with varied concentrations of cofilin and capping proteins. We

run the simulations until the system reached the steady-state after activation of the nucleation promoting factor N-WASP. Then we assessed how major variables that characterize actin dynamics in our model, depend on changes in cofilin concentration at a given capping protein concentration. The results are shown in Figure 2.5, Figure 2.6 and Figure 2.7, where color-coding of the surface plots represents an indicated variable at the leading edge of the cell (Figure 2.6A, black arrow).

Figure 2.5 demonstrates synergy of cofilin and capping activity in polymerizing actin via a dendritic nucleation mechanism. When capping protein concentration was set to 0.5 μM, the increase in cofilin caused a decrease in the total F-actin at the leading edge. Thus when capping is below ~1.5 μM, cofilin tends to inhibit Arp2/3-mediated F-actin polymerization. On the other hand, when capping concentration is higher than 1.5 μM, cofilin will stimulate actin polymerization (Figure 2.5, Cap=2.5 μM).

The effect of cofilin on F-actin is dependent on the monomer pool (Figure 2.6G) and on the available F-actin amount (Figure 2.6B). The latter is necessary for Arp2/3-mediated polymerization since branch formation occurs on the preexisting 'mother' filament. Thus when concentration of actin polymer is low (Figure 2.6B), branching is significantly decreased (Figure 2.6D). Consistently, F-actin "mother fragments" generated through severing were required for endocytic patch assembly in yeast (Chen and Pollard, 2013). Capping activity in the bulk cytoplasm supplies actin monomers (Figure 2.6G) for actin polymerization at the leading edge. Therefore cytosolic capping is heavily consumed (Figure 2.7D) by the growing actin ends when cofilin is abundant and creates an excess of barbed ends.

Without Arp2/3 nucleation and branching cofilin produces barbed ends while capping protein decreases their concentration (Figure 2.3B). Thus cofilin antagonizes capping activity in supplying free barbed ends for actin assembly. However in a branched actin network, barbed ends are also created through Arp2/3 resulting in an autocatalytic behavior; branching increases F-actin that in turn can be severed by cofilin to produce more barbed ends, which promote polymerization (Figure 2.6B and Figure 2.7A). This scenario is only possible when a sufficient monomer pool is available via capping activity. Such synergy between cofilin and capping proteins underlies the phenomenon of a dual regime of cofilin action in a dendritic actin network. Our model predicts that there is an optimal ratio of cofilin and capping proteins at which actin polymer production is maximal. The filaments are very short (Figure 2.6G) while the branching fraction (Figure 2.6D) and the turnover of the barbed ends (Figure 2.7B) are the highest at this optimal ratio of the two proteins. Cofilin overall affect on branched actin network is different below and above the optimal ratio of cofilin and capping proteins.

Conclusions

Here we propose a new synergistic mechanism by which cofilin and capping proteins regulate Arp2/3-mediated actin dynamics. Our hypothesis provides an explanation for the opposing functions of cofilin observed *in vivo*. It stimulates actin assembly when sufficient amount of capping protein is present and will promotes disassembly when there is not enough capping protein. This conclusion is consistent with the modeling result by (Carlsson, 2006) where barbed end cappers are required for maximal polymerization due

to severing activity. Consistently, capping protein is required for the formation of lamellipodial protrusion (Iwasa and Mullins, 2007) and cell migration (Sinnar et al., 2014). Also N-WASP-coated beads propel faster in the motility medium that contains capping protein (Wiesner et al., 2003). Our modeling prediction also agrees with Figure 1 of (DesMarais et al., 2005) where cofilin depolymerizes actin when monomer pool is limiting (in low capping conditions) and polymerizes actin when monomers are abundant (capping is in excess). Overall, our finding helps explain the complex physiological role of cofilin in regulating actin dynamics at the leading edge of migrating cells.

In our model, capping and cofilin severing activities are not spatially constrained. Therefore directionality is imposed only through Active_NWASP localization. Synergistic behavior of cofilin and capping protein is critical for additional 'steering' mechanisms underlying cell motility. For instance, localized cell protrusions can be produced by uncapping proteins in cooperation with the increased production of barbed ends through severing. It might serve as a fast mechanism of redirecting the Arp2/3-mediated actin network as compared to slower 'steering' through signaling pathways originating from the extracellular signals.

One of the future directions to our study is detecting cofilin and capping interplay experimentally. Multiple biochemical links exist between cofilin and capping proteins. Both can be buffered at the membrane through lipid binding and possibly have common upstream regulators (i.e. small GTPases). Additionally, capping binds tightly to CARMIL that interacts with Arp2/3 and cofilin can indirectly interact with the Arp2/3 complex. Based on these interactions alternative cofilin mechanisms will be implemented in the

model. These include but are not limited to cofilin binding to the Arp2/3 complex, cofilin inhibiting nucleotide exchange on G-actin monomers, localized inhibition of cofilin activity and concentration dependency of cofilin severing activity.

Figures

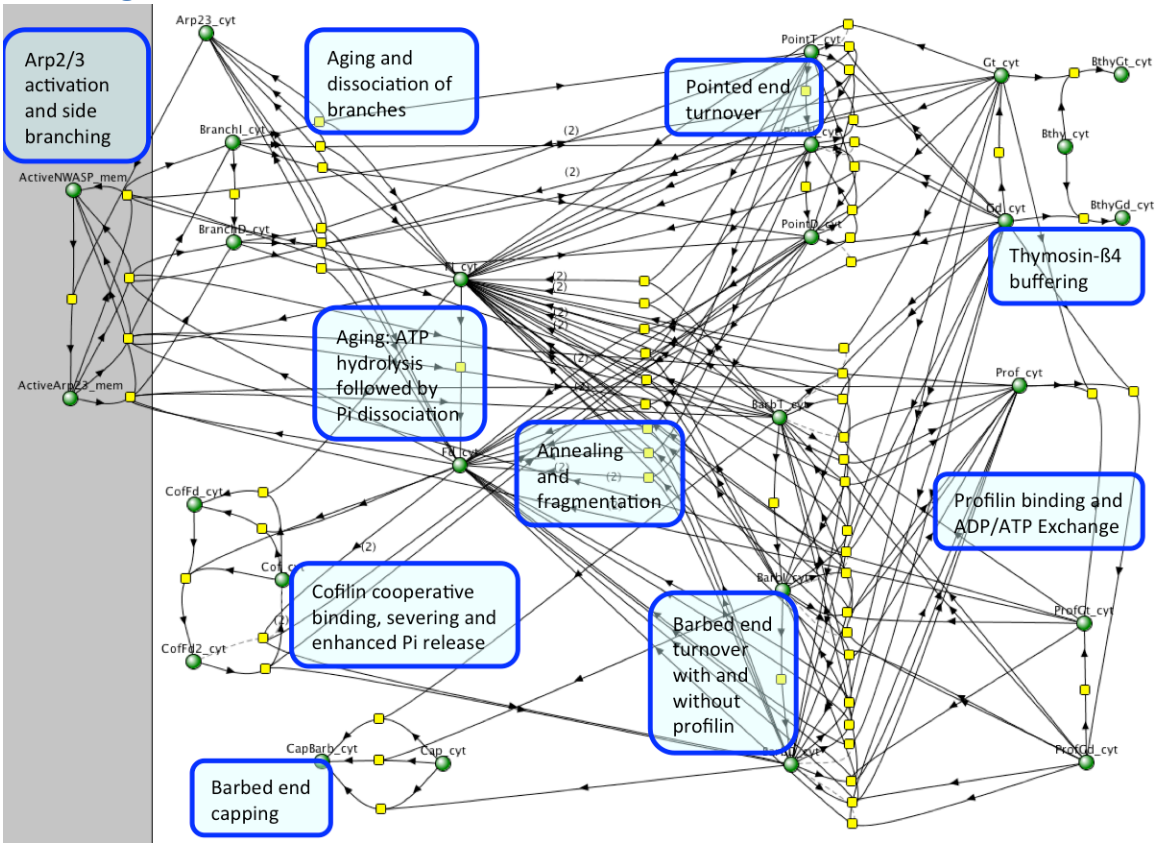
Arp2/3 activation and side branching
Aging and dissociation of branches
Pointed end turnover
Thymosin-ß4 buffering
Aging: ATP hydrolysis followed by Pi dissociation
Annealing and fragmentation
Profilin binding and ADP/ATP Exchange
Cofilin cooperative binding, severing and enhanced Pi release
Barbed end turnover with and without profilin
Barbed end capping
Arp23_cyt
BranchI_cyt
BranchD_cyt
ActiveNWASP_mem
ActiveArp23_mem
PointT_cyt
PointD_cyt
Gt_cyt
Gd_cyt
BthyGt_cyt
Bthy_cyt
BthyGd_cyt
Pi_cyt
Prof_cyt
BarbT_cyt
BarbD_cyt
ProfGt_cyt
ProfGd_cyt
CofFd_cyt
CofFd2_cyt
CapBarb_cyt
Cap_cyt

Figure 2.1. **A model of actin dendritic nucleation.**
Reaction network of "An Open Model" that is used as an *in silico* assay in this study with individual mechanisms labeled. Green circles are the species; yellow rectangles are the reaction nodes.

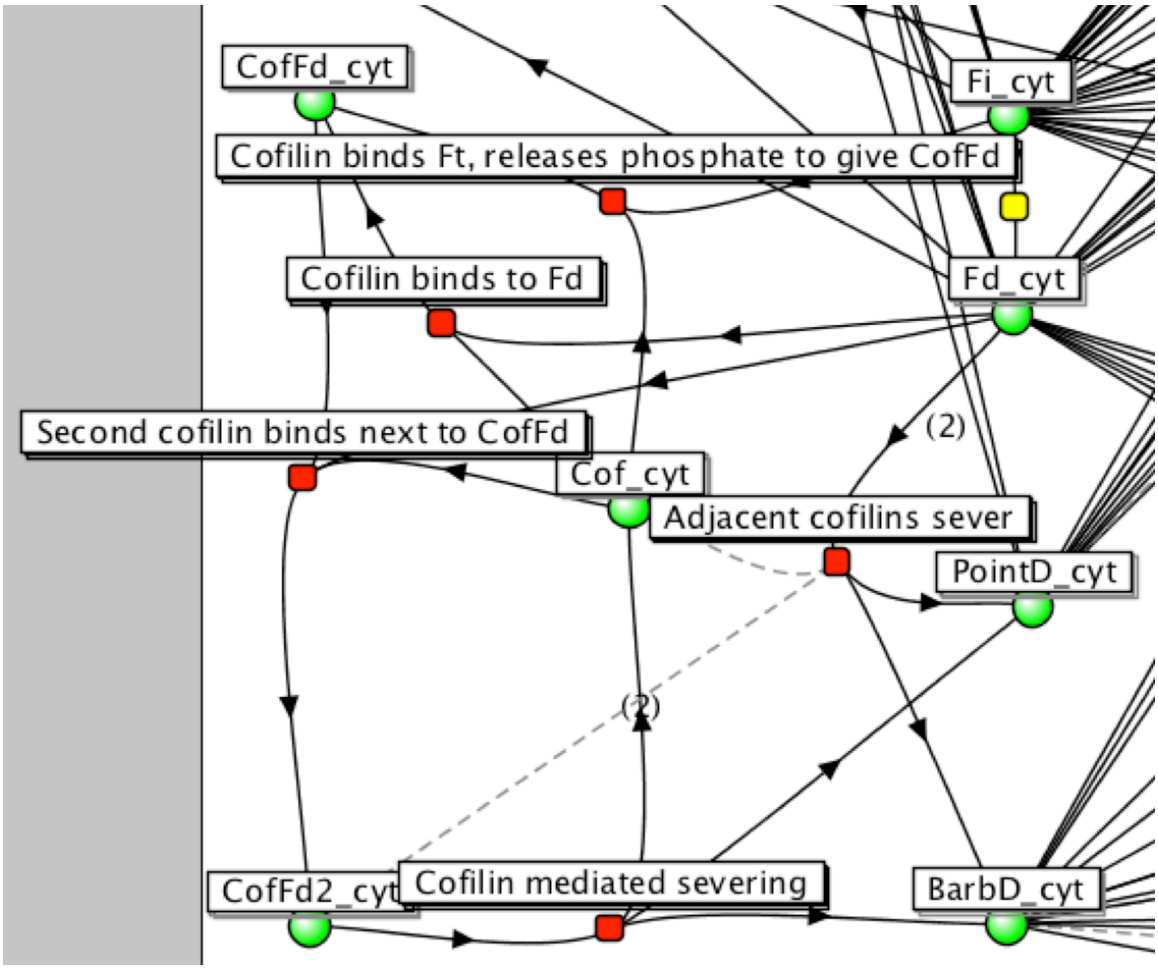
CofFd_cyt
Fi_cyt
Cofilin binds Ft, releases phosphate to give CofFd
Cofilin binds to Fd
Fd_cyt
Second cofilin binds next to CofFd
(2)
Cof_cyt
Adjacent cofilins sever
PointD_cyt
(2)
CofFd2_cyt
Cofilin mediated severing
BarbD_cyt

Figure 2.2. Cofilin mechanism in the model of actin dendritic nucleation.
A part of Virtual Cell Reaction Diagram that shows cofilin interactions. Green circles are the species; yellow and red rectangles are the reaction nodes.

Table 2.1: List of Reactions that model cofilin interactions.

Process	Cofilin binds Fi, releases phosphate to give CofFd
Reaction	Fi_Cyt + Cof_Cyt -> CofFd_cyt
Math Expression	((kon_cofI_eff * Cof_cyt * Fi_cyt) - (koff_cofI_eff * Pi * CofFd_cyt)), where kon_cofI_eff= (kon_cofI * kcof_DI / (1.0E-8 + koff_cofI + kcof_DI)) and koff_cofI_eff= (kcof_ID * koff_cofI / (1.0E-8 + koff_cofI + kcof_DI)) Pi=2,000
kon_cofI	1 $\mu M^{-1}s^{-1}$
kcof_DI	0.04 s^{-1}
koff_cofI	20 s^{-1}
kcof_ID	2.06 * 10^{-6} $\mu M^{-1}s^{-1}$

Process	Cofilin binds to Fd
Reaction	Fd_Cyt + Cof_Cyt -> CofFd_cyt
Math Expression	((kon_cofD * Cof_cyt * Fd_cyt) - (koff_cofD * CofFd_cyt))
kon_cofD	0.0085 $\mu M^{-1}s^{-1}$
koff_cofD	0.005 s^{-1}

Process	Second cofilin binds next to CofFd
Reaction	CofFd_Cyt + Cof_Cyt + Fd_Cyt -> CofFd2_cyt
Math Expression	((kon_cofD2 * Cof_cyt * CofFd_cyt * Fd_stability) - (koff_cofD * CofFd2_cyt)), where Fd_stability=(((Fd_cyt / PointedEndTotal) + (Fd_cyt * Fd_cyt * Fd_cyt / (PointedEndTotal * PointedEndTotal * PointedEndTotal))) / (1.0 + (Fd_cyt / PointedEndTotal) + (Fd_cyt * Fd_cyt * Fd_cyt / (PointedEndTotal * PointedEndTotal * PointedEndTotal))))
koff_cofD	0.005 s^{-1}

Process	Cofilin mediated severing
Reaction	CofFd2_cyt -> 2 Cof_cyt + PointD_cyt + BarbD_cyt
Math Expression	(kcut * CofFd2_cyt)
kcut	0.012 s^{-1}

Process	Adjacent cofilins sever
Reaction	2 Fd_Cyt -> PointD_cyt + BarbD_cyt
Math Expression	(kcut_eff * Cof_cyt * CofFd2_cyt * Fd_stability)
kcut	0.012 s^{-1}

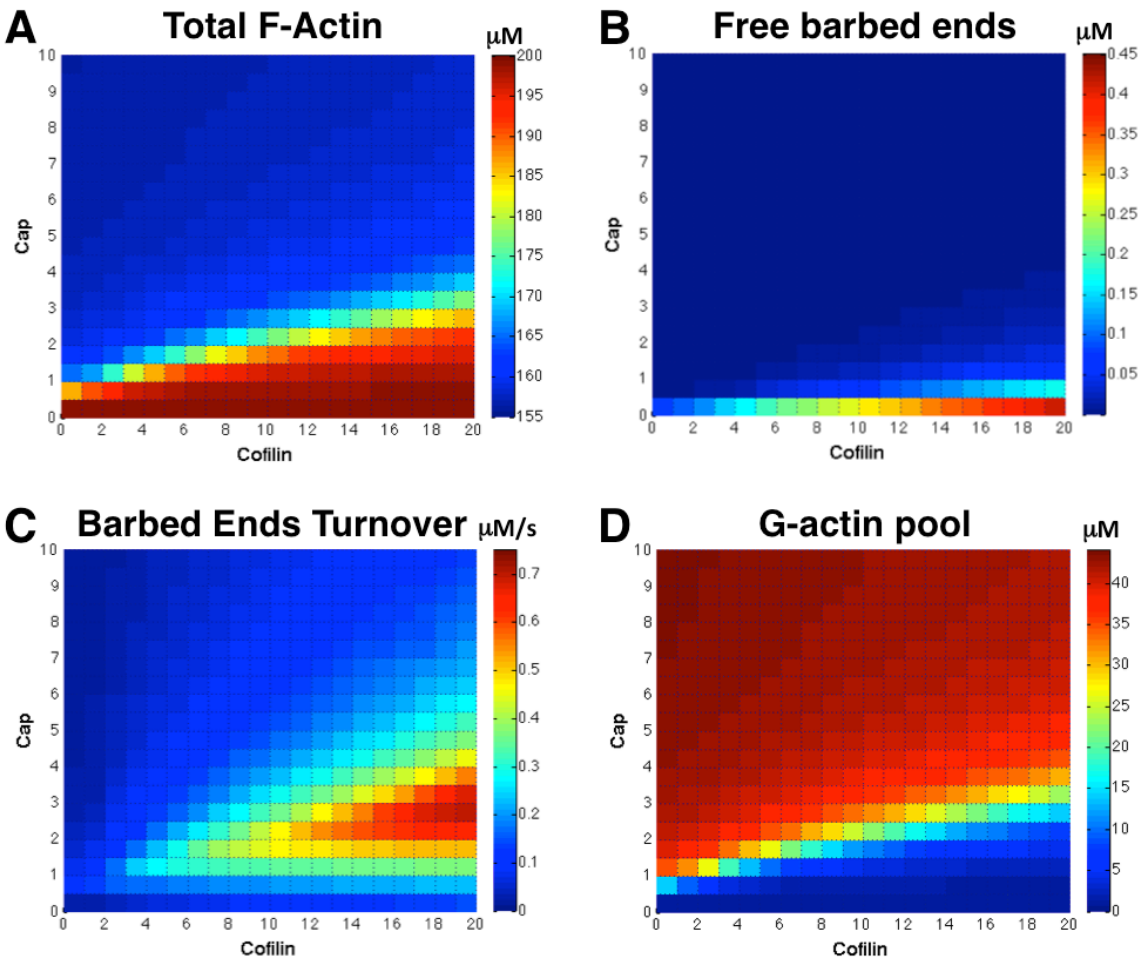
A
Total F-Actin
μM
200
195
190
185
180
175
170
165
160
155
Cap
Cofilin
B
Free barbed ends
μM
0.45
0.4
0.35
0.3
0.25
0.2
0.15
0.1
0.05
Cap
Cofilin
C
Barbed Ends Turnover μM/s
0.7
0.6
0.5
0.4
0.3
0.2
0.1
0
Cap
Cofilin
D
G-actin pool
μM
40
35
30
25
20
15
10
5
0
Cap
Cofilin

Figure 2.3. Results from the compartmental model (Arp2/3 inactive) at steady-state. **A.** Total F-actin. **B**. Free Barbed Ends. **C**. Barbed Ends Turnover. **D**. G-actin pool: includes ATP G-actin alone and ATP G-actin bound to either thymosin or profilin.

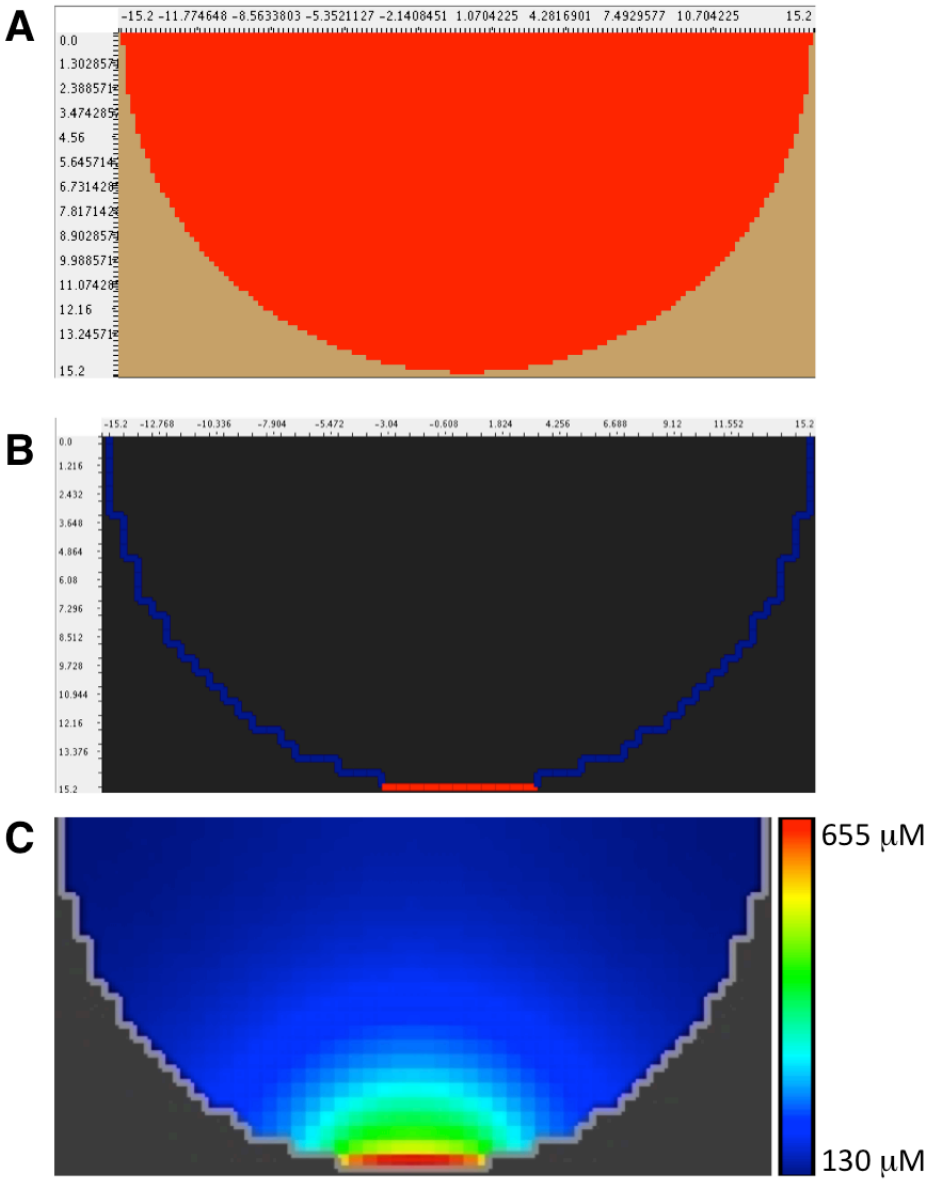
A
-15.2 -11.774648 -8.5633803 -5.3521127 -2.1408451 1.0704225 4.2816901 7.4929577 10.704225 15.2
0.0
1.302857
2.388571
3.474285
4.56
5.645714
6.731428
7.817142
8.902857
9.988571
11.07428
12.16
13.24571
15.2
B
-15.2 -12.768 -10.336 -7.904 -5.472 -3.04 -0.608 1.824 4.256 6.688 9.12 11.552 15.2
0.0
1.216
2.432
3.648
4.864
6.08
7.296
8.512
9.728
10.944
12.16
13.376
15.2
C
655 µM
130 µM

Figure 2.4. Geometry used in spatial simulations.
A. Semicircular cellular geometry that represents lamellipodial protrusion. Red – cytosolic compartment, light brown – extracellular space. Membrane is located between cytosol and EC space. **B**. N-WASP activation (500 molecules/μm^2) in the membrane compartment at the tip of lamellipodium triggers actin polymerization by activating Arp2/3. **C**. Simulation result for total F-actin from spatial model with cofilin = 10 μM, capping protein = 2 μM. Membrane is shown in light grey.

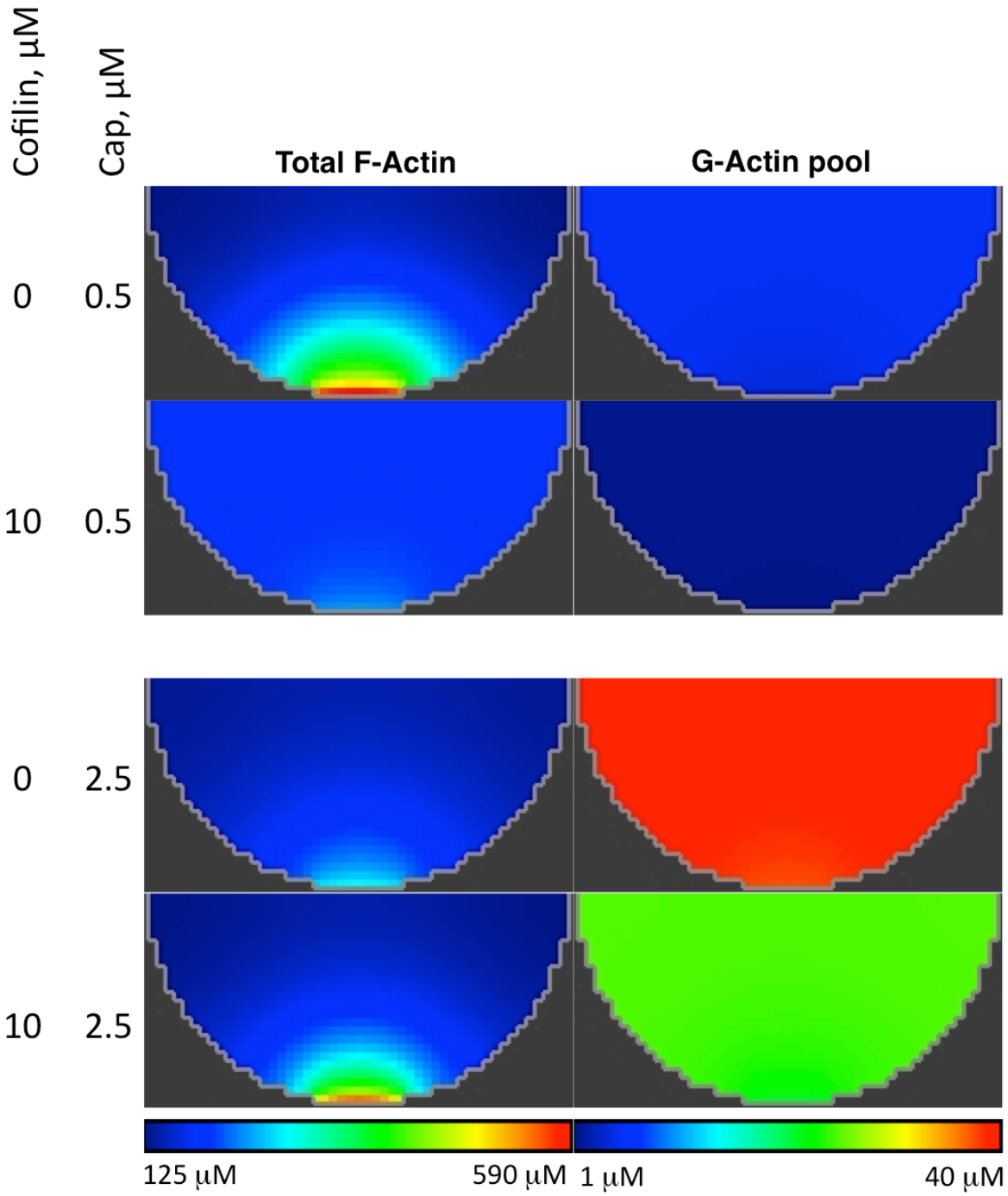
Cofilin, μM
Cap, μM
Total F-Actin
G-Actin pool
0
0.5
10
0.5
0
2.5
10
2.5
125 μM
590 μM
1 μM
40 μM

Figure 2.5. Cofilin can induce polymerization and depolymerization at the cell front (spatial simulations with Arp2/3 activation).
Total F-actin and G-actin pool dependence on the amount of cofilin and capping. Depolymerization with increase in cofilin occurs when capping concentration is low and G-actin pool is small (two top rows). Polymerization with increase in cofilin occurs when capping is in excess and G-actin pool is large (two bottom rows).

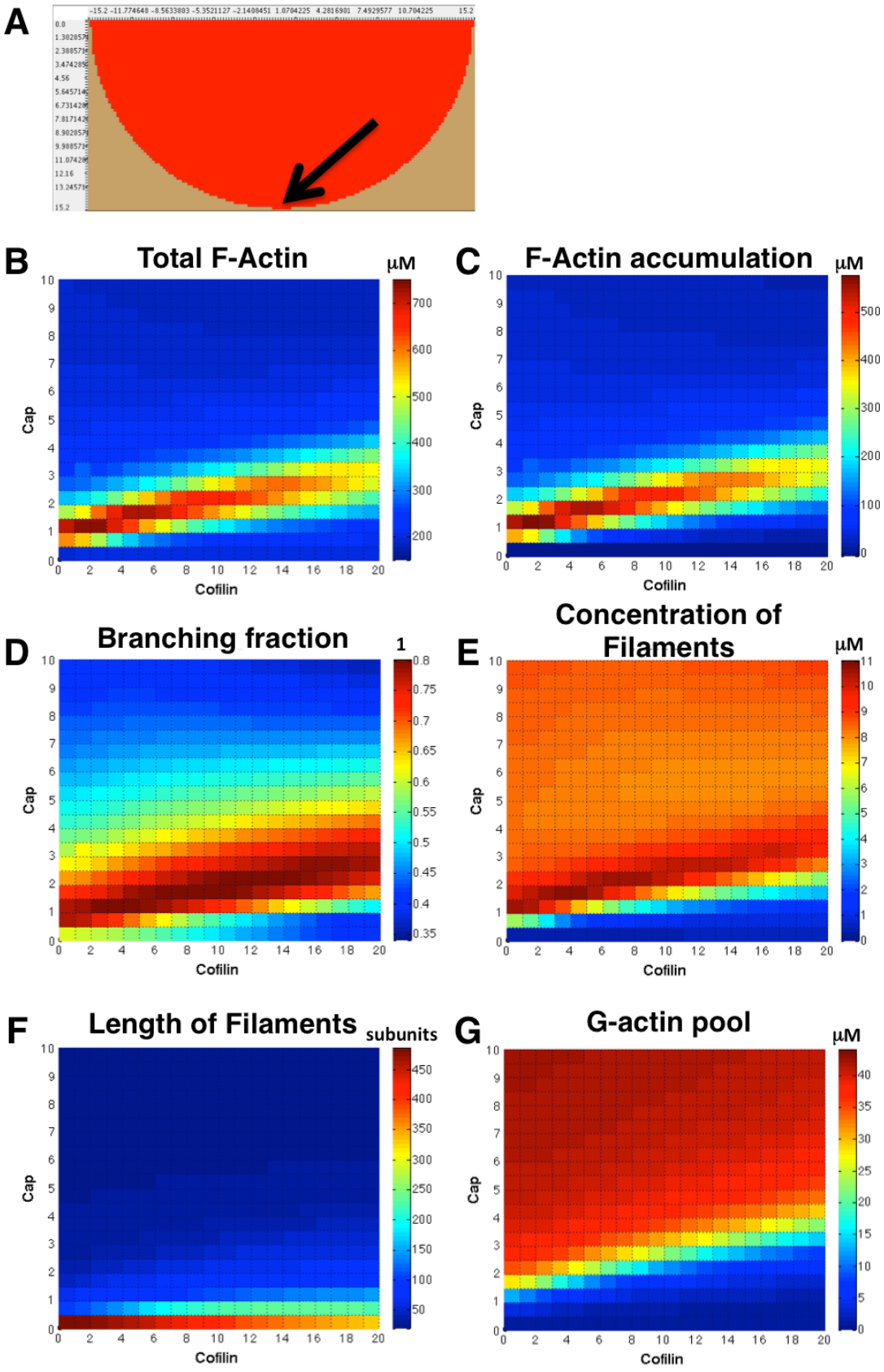
A
B
Total F-Actin
μM
Cap
Cofilin
C
F-Actin accumulation
μM
Cap
Cofilin
D
Branching fraction
1
Cap
Cofilin
E
Concentration of Filaments
μM
Cap
Cofilin
F
Length of Filaments
subunits
Cap
Cofilin
G
G-actin pool
μM
Cap
Cofilin

Figure 2.6. Actin polymerization at the cell front (spatial simulations with Arp2/3 activation).
A. Black arrow indicates a point at the lamellipodial tip, from which the data for the figures A through G was obtained. **B.** Total F-actin. **C.** F-actin accumulation. **D.** Branching Fraction. **E.** Concentration of filaments: determined as the sum of all pointed ends. **F.** Length of filaments. **G.** G-actin pool

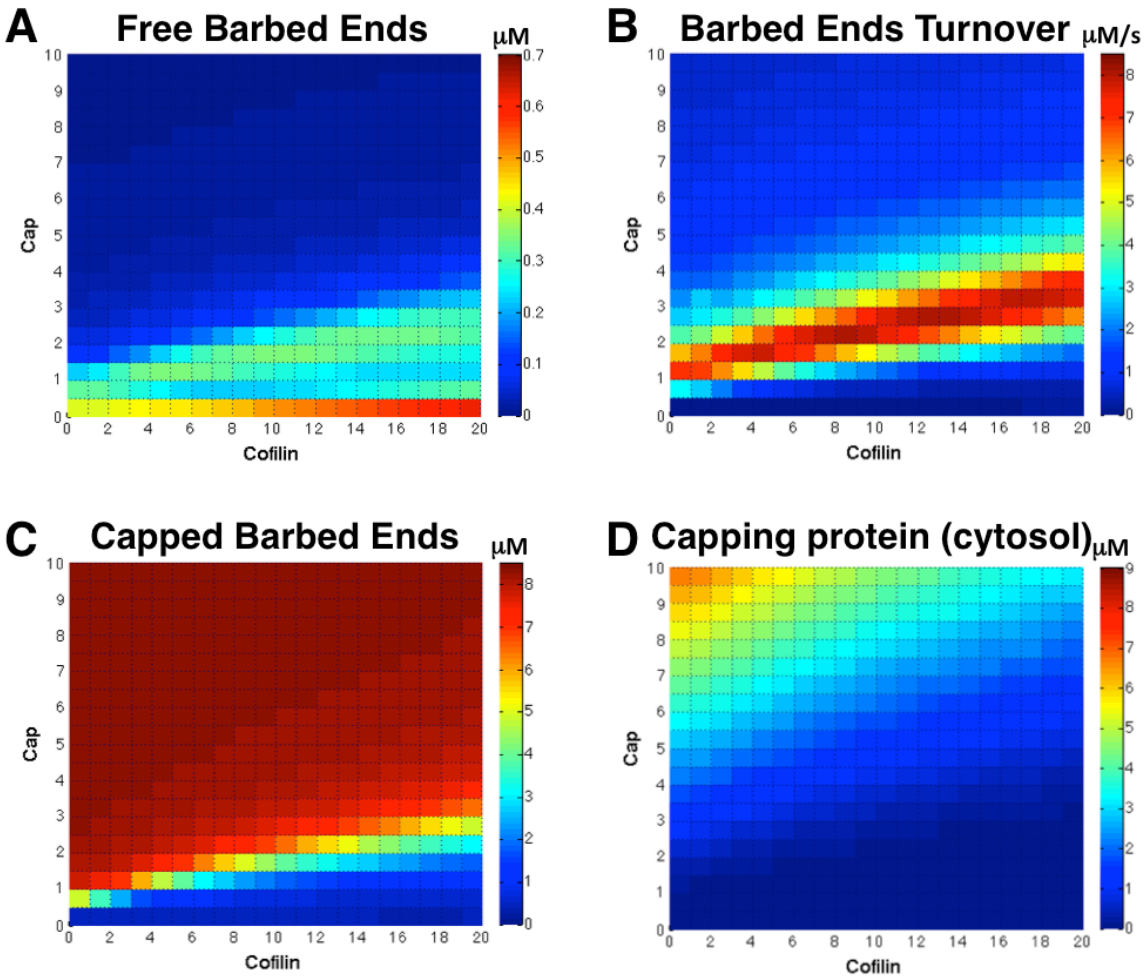
A
Free Barbed Ends
μM
B
Barbed Ends Turnover
μM/s
C
Capped Barbed Ends
μM
D
Capping protein (cytosol)
μM
Cap
Cofilin

Figure 2.7. Barbed Ends at the cell front (spatial simulations with Arp2/3 activation).
The data for the figures A through D was obtained from the same point of interest as in Figure 2.6. **A.** Free barbed ends. **B**. Barbed ends turnover. **C**. Capped barbed ends. **D**. Cytosolic capping protein.

3. CHAPTER III: Integration Of Linear And Dendritic Actin Nucleation In Nck-Induced Actin Comets

Attribution: This chapter contains th emanuscript submitted as Sofya Borinskaya, Katrina B. Velle, Kenneth G. Campellone, Arthur Talman, Diego Alvarez, Hervé Agaisse, Yi I. Wu, Leslie M. Loew, Bruce J. Mayer. Integration Of Linear And Dendritic Actin Nucleation In Nck-Induced Actin Comets. Molecular Biology of the Cell (in revision). The manuscript was written by Sofya Borinskaya and edited by Bruce J Mayer and Leslie M. Loew. Yi I. Wu provided technical advice and cDNA for designing leucine zipper protein-protein interaction interface. Arthur Talman, Diego Alvarez, Hervé Agaisse conducted experiments with Vaccinia-induced actin comets. Katrina B. Velle and Kenneth G. Campellone conducted experiments with EPEC-induced actin pedestals. All other experiments were completed by Sofya Borinskaya.

Abbreviations: NPF, nucleation promoting factor; N-WASP, neural Wiskott-Aldrich Syndrome protein; VCA, verprolin-homology, cofilin-homology and the acidic domains; Arp2/3, actin related proteins Arp 2 and Arp 3; SH2, Src homology 2; SH3, Src homology 3; mDia1, mammalian Diaphanous 1 formin; NCKIPSD, Nck interacting protein with SH3 domain; SPIN90, SH3 Protein Interacting with Nck 90 kDa; DIP, Dia Interacting Protein; WISH, WASP interacting SH3 protein.

Abstract

Nck adaptor protein plays an important role in recruiting and increasing the local concentration of cytosolic effectors that induce formation of pathogenic actin comet tails. Comet tails are dynamic elongated filamentous actin (F-actin)-rich structures that drive movement of pathogens both within the cytoplasm and from one host cell to the next. In our studies we characterize comet tails induced by experimental aggregation of Nck SH3 domains at the membrane, which are similar in their shape and dynamics to comets induced by Vaccinia virus. We show that experimental manipulation of the balance between unbranched/branched nucleation altered the morphology and dynamics of Nck SH3 actin comets. Inhibition of linear formin-based nucleation with the small molecule inhibitor SMIFH2 resulted in formation of predominantly circular-shaped actin structures with decreased mobility (actin blobs). Overexpression of the formin FH1 domain to inhibit the binding of endogenous full-length formin to the Nck SH3 membrane clusters, also resulted in slow moving actin blobs. Furthermore, enhancement of branched Arp2/3-mediated nucleation by N-WASP overexpression similarly caused loss of the typical

actin comet tail shape. These results indicate that formin-based linear actin polymerization is critical for the formation and maintenance of Nck-dependent actin comet tails. Consistent with this, aggregation of an exclusively branched nucleation promoting factor (the VCA domain of N-WASP), with density and turnover similar to that of N-WASP in Nck comets, does not reconstitute dynamic elongated actin comets. Thus the ratio of linear to dendritic nucleation activity may serve to distinguish the properties of actin structures induced by various viral and bacterial pathogens.

Introduction

Actin based cell motility is an important and well-studied physiological process. At its core is the polymerization of actin monomers into filaments (Pollard et al., 2000). Polymerization and the organization of these filaments into different cellular structures is a highly coordinated process regulated by many proteins (Disanza et al., 2005; dos Remedios et al., 2003). The force generated by growing actin barbed ends extends the plasma membrane into ruffles, lamellipodial and filopodial protrusions (Campellone and Welch, 2010). It also propels intracellular vesicles and pathogens that infect the host cell (Bhavsar et al., 2007; Stevens et al., 2006).

Polymerization of G-actin monomers into F-actin occurs in a polarized fashion. Actin monomers tend to add to the barbed (growing/plus) end of an existing filament. Formation of a primer (dimer or trimer) initiates actin filament assembly. This process, termed nucleation, is kinetically unfavorable in vitro. The Arp2/3 complex and formin family proteins are two of the three major types of actin nucleators in cells (Amann and

Pollard, 2001; Mullins et al., 1998; Pruyne et al., 2002; Sagot et al., 2002). Arp2/3 creates new actin branches at the sides of preexisting filaments. It is activated by the C-terminal VCA domain of class I nucleation promoting factors (NPFs) (Hitchcock-DeGregori, 2003; Hufner et al., 2001). The VCA domain binds G-actin and the Arp2/3 protein complex, inducing a conformational change that primes Arp2/3 for activity. Formin family proteins catalyze nucleation, increase elongation rate as well as prevent capping of the actin barbed ends (Krause and Gautreau, 2014). The highly conserved C-terminal FH1-FH2 domains of formins increase the barbed end elongation rate compared to the elongation of free barbed ends (Kovar and Pollard, 2004; Romero et al., 2004). Formins bind to SH3-containing proteins through the FH1 proline-rich domain, which also recruits profilin-actin complexes (Paul and Pollard, 2009) for addition of actin monomers onto the elongating barbed ends. The FH2 domain has a donut-shaped structure that caps and processively moves with the growing actin ends and adds actin monomers to the barbed ends of actin filaments.

Both formins and class I NPFs such as N-WASP are activated and spatio-temporally controlled through interaction with specific regulatory proteins that bind to their N-termini (Burianek and Soderling, 2013; Campellone and Welch, 2010). Many formins are autoinhibited by intramolecular interaction between their N and C termini. Activation and recruitment of formins to the membrane is mainly achieved through binding of Rho GTPases. However other factors contribute to the regulation of the activity of specific formins. SH3 domain-containing proteins such as Src family kinases (Young and Copeland, 2010) and the adaptor protein DIP (mDia interacting protein; known as SPIN90, NCKIPSD, WISH) (Eisenmann et al., 2007) interact with the proline-rich FH1

domain, suggesting that these interactions might contribute to the regulation of formin activity. Neural Wiskott-Aldrich syndrome protein (N-WASP) is a class I NPF because it contains a C-terminal catalytic VCA domain (Burianek and Soderling, 2013; Campellone and Welch, 2010). Similarly to the formins, it is maintained in the autoinhibited state in which the VCA domain is caged and therefore inactive. To stimulate N-WASP, signaling pathways target multiple cellular factors that interact with the N-terminus of N-WASP. For example, binding of the Rho family GTPase Cdc42 and phosphatidylinositol (4,5)-bisphosphate (PIP2) induces conformational changes that free the VCA domain. Another activation route that relieves N-WASP autoinhibition is the cooperative binding of PIP2 and the adaptor protein Nck (Rohatgi et al., 2001). WASP-interacting protein (WIP) binds to both Nck and N-WASP and is essential in stimulating N-WASP/Arp2/3-dependent actin polymerization (Ditlev et al., 2012; Donnelly et al., 2013).

Nck is comprised of one Src-homology 2 (SH2) and three SH3 domains. It has a pivotal role in pTyr signaling from the cell surface through N-WASP and to the actin cytoskeleton (Jones et al., 2006; Lettau et al., 2014; Lettau et al., 2009; Li et al., 2001; New et al., 2013; Rao, 2005; Stein et al., 1998). The pathogen Vaccinia virus targets the Nck adaptor of the host cell (Haglund and Welch, 2011; Hayward et al., 2006) by mimicking the host phosphotyrosine motif. Vaccinia introduces the viral A36 protein into the membrane of the infected cell. A36 undergoes tyrosine phosphorylation by Src and Abl kinases at Y112 creating a binding site for the Nck SH2 domain (Dodding and Way, 2009). By recruiting Nck, Vaccinia localizes and activates N-WASP in the host cell. This results in production of actin comet tails beneath the surface of the virus (Roberts and Smith, 2008). Other host proteins, including the adaptor Grb2, small G protein Cdc42,

and the Rho guanine-nucleotide-exchange factor (GEF) intersectin-1 have been shown to contribute to formation of Vaccinia comet tails (Humphries et al., 2014; Scaplehorn et al., 2002; Weisswange et al., 2009).

We show here that while the clustering of Nck SH3 domains at the membrane produces mostly elongated dynamic actin structures similar to those induced by Vaccinia virus (Ditlev et al., 2012; Rivera et al., 2004), the clustering of N-WASP VVCA (referred to as VCA) domains produces slow moving actin "blobs". We investigated why Nck SH3 clustering and VCA clustering results in formation of such different actin structures. First, we test if the density or turnover of the N-WASP VCA domain differentiates elongated dynamic actin assemblies from actin blobs. We show that clustering of VCA at low density, or when turnover at the membrane is allowed, does not reproduce typical actin comets. Second, we demonstrate that both branched and linear actin polymerization are necessary for the assembly of dynamic actin comet tails. Interfering with either branched or linear nucleation decreases the velocity and alteres the morphology of actin structures induced by aggregation of Nck SH3 domains. Our results suggest that the activity of linear NPFs such as formins is critical for the formation of Nck-dependent actin comets and for the maintenance of their phenotype. We propose that Nck serves as an integrator of linear and branched nucleation in the Nck-induced comet tails.

Results

Membrane clustering of Nck SH3 and VCA produces distinct actin structures

Aggregating the SH3 domains of the Nck adaptor at the membrane induces the formation of dynamic actin comet tails (Figure 3.1A) (Ditlev et al., 2012; Rivera et al., 2004; Rivera et al., 2009). Nck SH3 domains fused to a transmembrane CD7 domain and an extracellular CD16 domain were aggregated using primary anti-CD16 monoclonal antibodies and secondary anti–mouse IgG. Fluorescently labeled Nck SH3 aggregates and actin were visualized using time-lapse confocal microscopy. This assay mimics the recruitment and increased local concentration of full length Nck that occurs during biological processes such as axon growth cone guidance during *Drosophila* eye development (Rao, 2005), formation of the immunological synapse (Lettau et al., 2009), and actin rearrangements in kidney podocytes (Jones et al., 2006). Actin comet tails formed beneath multiple mCherry-tagged Nck SH3 clusters (Figure 3.1B). Nck is an activator of NWASP-Arp2/3 mediated actin assembly in mammalian cells (Kempiak et al., 2005; Rohatgi et al., 2001), so clustering and activation of N-WASP is thought to be the critical step in Nck SH3-induced actin comets. To test this, we directly aggregated mCherry-tagged N-WASP VCA domains at the membrane (Figure 3.1C). Compared to clustering of Nck SH3 domains, this bypasses WIP-dependent N-WASP recruitment and activation steps as well as signaling to the actin cytoskeleton through Nck SH3 binding proteins other than N-WASP. To our surprise, we found the actin structures induced by aggregation of Nck SH3 and VCA domains (Figure 3.1B and D) have distinctly different

distribution of morphologies (Figure 3.1G) and velocities (Figure 3.1H and Movie 3.1) in cells.

The morphology of actin particles was compared by determining a circularity parameter (scale of 0 to 1), where elongated objects such as comet tails have low values and circular-shaped objects such as blobs approach circularity values of 1 (see Methods). We quantified the percentage of particles per cell with circularity below 0.6 (elongated structures). Nck SH3 clustering produces 37% (Figure 3.1G) while VCA induced only 16% of elongated actin structures. The velocity of actin assemblies was compared by tracking actin particles over time and plotting the distribution of average velocity per cell. The population of motile ($v > 0.06$ um/sec) actin structures is much greater for Nck SH3 aggregates (23%) compared to VCA aggregates (4%) (Figure 3.1H). By these quantitative parameters, Nck SH3-induced actin structures are very similar to the comets induced by Vaccinia virus (Figure 3.1B and F). Nck SH3 and Vaccinia comets have comparable circularity (Figure 3.1G) and a subset of highly motile actin particles (Figure 3.1H, Movie 3.1).

The dramatic differences in shape and dynamic behavior of actin structures induced by clustering of Nck SH3 and VCA led us to investigate the molecular mechanisms that might underlie these differences.

Does VCA density differentiate Nck SH3- and VCA-induced actin structures?

We first explored whether the density of VCA domains in membrane clusters might explain differences between the Nck SH3 and VCA induced actin structures. Dilution of functional A36 viral protein, which stimulates N-WASP/Arp2/3-mediated actin assembly, resulted in formation of longer and faster Vaccinia actin comets (Humphries et al., 2012). The density of VCA domains in the VCA aggregates is 100% because each CD16/7-mCherry membrane protein has VCA covalently linked at the C-terminus (Figure 3.1C). The VCA density in Nck SH3 clusters is always lower than 100% (Figure 3.2A). This is because Nck SH3 domains have multiple binding partners besides N-WASP (Antoku et al., 2008; Kitamura et al., 1996; Quilliam et al., 1996; Ramesh and Geha, 2009; Schmidt and Dikic, 2005; Wunderlich et al., 1999; Zhao et al., 2000) and N-WASP can dissociate (Siton et al., 2011; Smith et al., 2013; Weisswange et al., 2009) from Nck SH3 domains after a new actin branch has been formed. Also at equilibrium only 38% of Nck molecules are predicted to be bound by N-WASP (based on estimates of Nck/N-WASP affinity and N-WASP abundance), and experimental and computational modeling data strongly suggest that the Nck:VCA stoichiometry in Nck comets is 2:1 (Ditlev et al., 2012).

To test whether VCA domain density differentiates Nck SH3- and VCA-induced actin assemblies, we experimentally lowered the density of VCA molecules in CD16/7-mCherry-VCA clusters. CD16/7-mCherry-VCA proteins were co-clustered with CD16/7 proteins lacking VCA ("Empty") (Figure 3.2B). NIH3T3 cells were transfected with different ratios of VCA and Empty constructs so that VCA expression was 100%, 60%,

37%, 15%, and 0% of the combined VCA and Empty protein amount (Figure S 3.1). CD16/7 fusion proteins were aggregated, the cells were imaged (Figure 3.2C, Movie 3.2), and actin particle morphology and velocity (Figure 3.2D and E) was analyzed. Our prediction was that membrane clusters with 60%, 37% or 15% VCA density would induce more comet-like actin structures. However at 60% and 37% VCA in the clusters, fairly typical actin blobs formed (Figure 3.1D, C). At densities below 37% VCA could still induce actin polymerization even though the actin structures appeared to be smaller. Notably, decreasing VCA density in membrane clusters did not in any case result in formation of elongated dynamic actin structures similar to those induced by Nck SH3 (Figure 3.1B) aggregation. These results are inconsistent with the hypothesis that the lower density of recruited VCA in Nck SH3 clusters is responsible for the phenotypical differences between Nck SH3- (Figure 3.1B) and VCA- (Figure 3.1D) induced actin assemblies. Comet tail morphology and dynamics cannot be reproduced solely by decreasing VCA density in membrane clusters.

Does VCA turnover differentiate Nck SH3- and VCA-induced actin structures?

In CD16/7-mCherry-Nck clusters, endogenous N-WASP protein has the ability to dissociate from the membrane aggregates and undergo turnover. After photobleaching, GFP-NWASP recovers in the head of the Vaccinia-induced comet with a half-time of 1-3s (Donnelly et al., 2013; Humphries et al., 2014; Weisswange et al., 2009). In vitro, Nck SH3 domains activate N-WASP with Kact≈80nM (Rohatgi et al., 2001), suggesting

they interact with modest affinity and thus complexes turn over relatively rapidly. By contrast, in CD16/7-mCherry-VCA clusters the C-terminal VCA domain of NWASP is covalently attached to the transmembrane protein (Figure 3.1C). As expected, mCherry fluorescence of CD16/7-mCherry-VCA clusters does not recover after being bleached (Figure S 3.2A, Movie 3.3A).

To test whether turnover of the VCA domain is critical for producing actin comets, we generated VCA membrane clusters where turnover is possible. To allow interaction between CD16/7 membrane fusion proteins and mCherry-VCA domains we utilized a coiled-coil motif interaction interface that consists of the parallel coiled-coil pair SYNZIP1:SYNZIP2 (Reinke et al., 2010). These 47aa long peptides form tight heterospecific complexes (Kd≤10nM) and display minimal self-association (Thompson et al., 2012). CD16/7 was tagged with eYFP and fused to SYNZIP1 (Figure 3.3B). SYNZIP2 was attached to the N-terminus of the mCherry-VCA (Figure 3.3B). Expression of CD16/7-eYFP-SYNZIP1 and SYNZIP2-mCherry-NWASP-VCA in NIH3T3 cells was verified by western blotting (Figure S 3.2B). We confirmed that clusters of membrane-embedded SYNZIP1 do in fact recruit cytosolic SYNZIP2-mCherry-VCA protein (Figure 3.3C). Turnover of SYNZIP2-mCherry-VCA in the clusters was shown by performing FRAP of mCherry (Figure S 3.2A, Movie 3.3A, half-time ~40s). Clusters of SYNZIP2-mCherry-VCA and actin aggregates did not form without inducing antibody-mediated aggregation of CD16/7-eYFP-SYNZIP1 (Figure S 3.2Figure S 3.2C). Clustering of CD16/7-eYFP-SYNZIP1 resulted in localized actin recruitment (Figure S 3.2C). However morphology and velocity analysis (Figure 3.3D and E) of the actin structures revealed that they do not exhibit the dynamic behavior and

morphological features of comet tails. Thus even though VCA turnover is likely to be important for comet tail behavior (Smith et al., 2013), it is not sufficient to reproduce the phenotype of elongated dynamic Nck SH3-induced actin assemblies and cannot explain the differences between VCA and Nck SH3 induced actin structures.

Inhibition of formin FH2 domain disrupts Nck SH3-induced actin comets

The actin architecture of the baculovirus comet tail was recently visualized by electron microscopy (Mueller et al., 2014). There are multiple actin branches that stem from the center axis of the comet. There are also long parallel unbranched actin filaments in the center of these comets. Additionally in the branched actin network, filament fragmentation and subsequent elongation often take place. These facts suggest that a linear elongation mechanism should be an important contributor to the structure and behavior of actin comet tails. Formins catalyze actin polymerization by adding monomers to barbed ends and thus elongate existing actin filaments. We hypothesized that formin-mediated barbed end elongation activity would be higher in the Nck SH3-induced comets than in the VCA-induced actin structures (Figure 3.4A). Nck SH3 domains can potentially recruit formin through the adaptor DIP (Eisenmann et al., 2007; Lim et al., 2001) or possibly by directly binding the proline-rich FH1 domain of formin (Figure S 3.3).

To test whether inhibition of formin-mediated actin assembly would affect Nck SH3-induced actin structures, we treated NIH3T3 cells with a small molecule inhibitor of

formin homology 2 domains (SMIFH2) (Rizvi et al., 2009). mCherry-Nck SH3 was aggregated in both SMIFH2-treated and control cells. Then cells were fixed and mCherry membrane proteins and GFP-stained actin were visualized (Figure 3.4B). SMIFH2 treatment had a dramatic effect on Nck SH3-associated actin (Figure 3.4B). The amount of elongated actin assemblies associated with Nck SH3 clusters was significantly lower in treated cells (18%) comparing to the DMSO-treated control cells (55%) (Figure 3.4C).

To observe the effect of the formin inhibitor on Nck SH3-induced actin in live cells, CD16/7-mCherry-Nck and GFP-actin expressing cells were subjected to the aggregation protocol and then imaged with every 2.5 min (Movie 3.4A). The inhibitor was added after five frames of acquisition. For control cells, DMSO was added at the same time point during the acquisition. We tracked all the Nck SH3-induced actin particles (Figure 3.4D and E) and analyzed their velocity before and after the treatment (Figure 3.4F). After addition of SMIFH2 velocity of Nck SH3 induced actin aggregates drops on average by 37% (Figure 3.4D, F) and 72% of actin aggregates moved more than two fold slower after drug treatment. The velocity of actin particles in the control cells did not change significantly (Figure 3.4E, F and Movie 3.4A). Similar decrease in velocity due to SMIFH2 treatment was observed when Nck SH3 induced actin aggregates were imaged every 30s (Movie 3.4B).

To test whether inhibition of formin-mediated actin assembly would affect Vaccinia actin comets, we inhibited FH2 domain in HeLa cells that were infected with Vaccinia virus. After treatment with the SMIFH2 inhibitor (or DMSO alone as control) the cells were fixed and then immunostained virus and phalloidin-stained actin were visualized (Figure

S 3.4A). SMIFH2 treatment had a dramatic effect on Vaccinia-associated actin structures in accord with the findings by (Alvarez and Agaisse, 2013). The amount of elongated actin assemblies associated with the virus was significantly lower in treated cells (5%) comparing to the DMSO-treated control cells (40%) (Figure S 3.4B).

These results suggest that formin-mediated barbed end assembly is important for the elongated morphology and rapid motility that are characteristic of actin comets induced by Nck SH3 aggregation.

Formin FH1 domain overexpression disrupts Nck SH3-induced actin comets

The FH1 domain of formin interacts with the actin-binding protein profilin. Recruitment of profilin-actin complexes by FH1 feeds actin monomers to the FH2 domain at the growing barbed ends (Paul and Pollard, 2008; Truong et al., 2014; Vavylonis et al., 2006). The FH1 domain is rich in poly-proline repeats and also interacts with SH3-domain-containing proteins such as DIP and Src (Young and Copeland, 2010). Therefore we decided to use the formin-FH1 domain as a competitive inhibitor of the endogenous formin activity on locally induced Nck SH3 actin structures. If formins are important for formation of actin comets, we expected that FH1 domain overexpression would have a greater impact on actin structures induced by Nck SH3 compared to those induced by VCA.

NIH3T3 cells were co-transfected with aggregatable VCA or Nck SH3, fluorescently labeled actin with or without the FH1 domain of formin mDia1. Compared to control,

overexpression of the FH1 domain (Figure S 3.5) reduced the number of actin assemblies induced by Nck SH3 aggregation that had low circularity (31% vs 47%) (Figure 3.5A and C), while the morphology of VCA-induced actin structures was not significantly affected by FH1 overexpression (11% vs 13%) (Figure 3.5B and E). Velocity analysis revealed that Nck SH3-induced structures moved more slowly (Movie 3.5A) in the cells expressing FH1 (Figure 3.5D), while the velocity of the N-WASP-VCA actin structures (Movie 3.5B) was not impacted by the presence of the FH1 domain (Figure 3.5F).

The results indicate that competitive inhibition of formin in membrane clusters strongly affected the properties of Nck SH3- but not VCA-induced actin assemblies, suggesting that formin-based polymerization distinguishes dynamic elongated actin comets from slow moving actin blobs.

N-WASP overexpression changes the morphology of Nck SH3-induced actin structures

As another approach to probe whether the balance of linear and dendritic nucleation is crucial in Nck SH3-induced actin comets, we overexpressed GFP-N-WASP in the cells with CD16/7-Nck SH3 fusion proteins (Figure 3.4A). We hypothesized that excess N-WASP would occupy more of the Nck SH3 domains in the membrane clusters at the expense of formin, resulting in a higher ratio of branched nucleation in the Nck SH3-induced actin comets. CD16/7-VCA and CD16/7-Nck expressing NIH3T3 cells with or without GFP-N-WASP were first subjected to antibody-mediated aggregation. Then the cells were fixed and stained with Texas-red phalloidin to visualize filamentous actin. As

compared to control cells (Figure 3.6A), overexpression of N-WASP had a dramatic effect on the shape of the Nck SH3-induced actin assemblies (Figure 3.6C). This effect is reflected in a decrease in the number of actin particles with low circularity (61% vs 5%) due to N-WASP overexpression (Figure 3.6D). In fact, the amount of elongated actin structures induced by Nck SH3 clustering in N-WASP overexpressing cells (5%) was as low as in the cells with VCA-induced actin blobs (7%) (Figure 3.6B and D). This result is consistent with the proposal that shifting the balance in favor of branched vs. linear nucleation affects Nck SH3-dependent actin comet tail formation and causes assembly of slow moving blob-like actin structures.

Discussion

The main goal of these studies was to understand the role of the Nck adaptor protein in determining the morphology and dynamic behavior of actin comet tails. To address this question we used antibody-mediated aggregation of proteins of interest at the membrane to induce localized actin assembly (Rivera et al., 2004); this gives us the ability to manipulate the signaling inputs leading to actin polymerization in a much more direct way than is possible in the case of pathogen-induced comets. Aggregation of Nck SH3 domains results in formation of actin comet tails (Rivera et al., 2004) similar to the Vaccinia-induced comets (Dodding and Way, 2009; Frischknecht and Way, 2001). We reasoned that if the role of Nck was to merely recruit and activate the NPF of branched nucleation N-WASP to the membrane, then it should be possible to recreate comet tails by clustering just the catalytic VCA domain of N-WASP. Surprisingly, we found that

VCA clustering caused formation of actin blob structures, which do not have comet-like morphology and dynamics. Comparing Nck comets and VCA blobs deepened our understanding of mechanisms of formation of phenotypically distinct actin structures and revealed a critical and previously unappreciated role for Nck in the assembly of actin comet tails.

We first tested whether the Nck adaptor might promote comet tail formation by regulating the density and/or the turnover of VCA domains in the membrane clusters. Clustering CD16/7-mCherry-VCA with various ratios of CD16/7-XFP (empty) transmembrane proteins allowed us to produce clusters in which VCA density could be systematically varied. We found that comet tails were not induced at lower densities of VCA. We aimed to mimic cytosolic N-WASP interaction with Nck SH3 clusters through the coiled-coil-mediated interaction of VCA with CD16/7 (Kd = 10 nM) which should fairly well simulate N-WASP – Nck binding. Nevertheless, providing VCA turnover in membrane clusters in this manner did not yield production of comet tails. Thus differences in VCA density or turnover are unlikely to explain why aggregation of Nck SH3 domains can induce actin comet tails, while aggregation of VCA alone cannot.

Another possible role of Nck SH3 is to promote linear actin nucleation in actin comet tails via recruitment and activation of formins. Accelerating barbed end elongation is a crucial mechanism supporting growth of filopodial membrane protrusions (Pellegrin and Mellor, 2005; Schirenbeck et al., 2005; Yang and Svitkina, 2011). Similar to filopodia, actin comet tails are narrow actin-rich structures pushing against the plasma membrane. Extremely long membrane protrusions can be formed in this manner. Indeed, we observe

some Nck SH3 induced comets extending away from the cell boundary up to a distance greater than the diameter of a cell. This process is in fact very important for cell-to-cell spread of Vaccinia virus (Cudmore et al., 1995; Doceul et al., 2010).

The Agaisse group showed that N-WASP and formin FHOD1 activities are both present in Vaccinia comet tails (Alvarez and Agaisse, 2013; Alvarez and Agaisse, 2014). FHOD1 depletion results in less efficient comet tail production and slower velocity of Vaccinia comets in host cells. Hence we reasoned that formin-based actin polymerization could be critical for the maintenance of comet tail shape and dynamics. By contrast, VCA-induced actin structures would be predicted to contain exclusively a branched actin network because clusters of VCA at the membrane should activate predominantly Arp2/3 molecules. Thus differences in the ability to promote linear polymerization might explain the phenotypical differences between Nck SH3 comets and VCA blobs.

We hypothesized that Nck engages and controls the balance between the linear and branched nucleation machinery, thereby determining the shape and dynamic behavior of the resulting actin structures. The branched/linear actin nucleation balance in Nck SH3-induced comets could be upset by either inhibiting formin-based nucleation, or by increasing Arp2/3-based nucleation. We first inhibited FH2-mediated elongation of actin barbed ends (Rizvi et al., 2009) which altered the morphology and decreased the mobility of Nck SH3 actin assemblies. As an alternate method for reducing unbranched actin growth, we overexpressed the proline-rich FH1 domain of the formin mDia1. We found that Nck SH3 clusters produced mostly circular-shaped slow moving actin structures when FH1 was overexpressed. These results are consistent with an important role for

linear actin nucleation in comet tail formation. To shift the balance towards branched nucleation in actin comets, we overexpressed N-WASP, which promotes branched nucleation. Under these conditions, Nck SH3-induced actin assemblies drastically changed their morphology.Experimentally shifting the unbranched/branched nucleation balance altered the morphology and dynamics of Nck SH3 actin comets. This is consistent with our idea that the integration of signaling pathways between linear and branched polymerization is critical for the comet tail phenotype.

The subversion of signaling to the Arp2/3-mediated branched actin network by pathogens has been actively studied (Haglund and Welch, 2011; Welch and Way, 2013). Although the critical role of Nck in recruiting and activating N-WASP to promote the branched nucleation has been well established in those studies, our results show that Nck performs a balancing act to also promote linear nucleation. We demonstrate that in Nck SH3-induced actin comets, the linear and dendritic polymerization machinery both contribute to the morphology and dynamic behavior of actin comets. Interestingly, it was recently reported that Rickettsia utilizes two modes of actin polymerization sequentially: Arp2/3 based for the early stage of infection, and formin-like for later comet tail motility (Haglund et al., 2010; Jermy, 2010; Reed et al., 2014). Recent studies of the F-actin composition in Listeria monocytogenes (Jasnin et al., 2013) and baculovirus (Mueller et al., 2014) comet tails suggested the presence of fairly long unbranched and bundled actin filaments.

Enteropathogenic Escherichia coli (EPEC) integrates its Tir (translocated intimin receptor) effector into the plasma membrane; Y474 of Tir is phosphorylated by host

kinases Fyn and Abl to generate a binding site for the Nck SH2 domain (Bhavsar et al., 2007; Hayward et al., 2006). By recruiting Nck, EPEC localizes and activates N-WASP in the host cell. This results in production of actin pedestals juxtaposed to the surface of the bacteria (Goosney et al., 1999). The morphology and dynamics of EPEC pedestals is similar to VCA-induced actin blobs (Movie 3.6, Figure S 3.6). Based on our results we predict that the ratio of branched to linear actin nucleation activity may distinguish slow moving actin pedestals from long dynamic comet tails, and that the formin activity in EPEC pedestals is lower (as compared to N-WASP activity) than in Vaccinia comets. Consistent with this hypothesis we did not observe a significant effect of SMIFH2 (25 μM) on the dynamics and morphology of EPEC actin pedestals (data not shown). Alternatively, the behavior of EPEC-induced actin structures may be constrained by the physical properties of the bacterium itself. EPEC has a large surface area of attachment on the membrane, since bacteria are about 2 μm long (much larger than CD16/7-induced aggregates studied here). Therefore the circularity of underlying pedestals approaches the value of 1.

In summary, our results point to a role for Nck in maintaining a tight balance between the formin-mediated linear and the Arp2/3-based branched nucleation pathways. The dynamic behavior and elongated morphology of Nck SH3-induced actin comets depend on the presence of both pathways. Manipulations that inhibit linear nucleation or enhance branched nucleation have dramatic effects on actin comets in this system. We expect that the Nck adaptor plays a similar role in integrating the branched and linear nucleation pathways in actin assemblies induced in host cells by microbial pathogens, thus determining the dynamic properties of the resulting actin structures. The dynamics and

morphology of other actin-rich structures, such as kidney podocyte foot processes and invadopodia, potentially also depend on the integration of different nucleation pathways through the Nck adaptor protein. Further studies will address the specific mechanism by which Nck engages the formin-based linear nucleation pathway.

Acknowledgements

We thank A. Cowan, S. Krueger and W. Mohler for expert advice in imaging techniques and image analysis. We are grateful to A. Cowan for critically reading and providing insightful comments on this manuscript.

This work was supported by P41GM103313 to L. M. L. and R01 CA82258 to B. J. M.

Materials and Methods

Plasmid construction

Details of constructions in the mammalian expression vector pEBB encoding fusion proteins consisting of the extracellular domain of CD16, the transmembrane domain of CD7, and HA tag have been previously described (Rivera et al., 2004). CD16/7-mCherry-Nck SH3-HA, CD16/7-Nck SH3-HA, CD16/7-HA (Empty) constructs are described in (Ditlev et al., 2012). CD16/7-mCherry-VCA-HA and CD16/7-VCA-HA were cloned by replacing Nck SH3 domains with N-WASP VVCA (rat, aa P388-D501) in CD16/7-mCherry-Nck SH3-HA and CD16/7-Nck SH3-HA respectively. CD16/7-eYFP-SynZip1 was generated by replacing HA in CD16/7-eYFP-HA with SynZip1 sequence (Reinke et al., 2010). HA-SynZip2-mCherry-VCA was generated by cloning SynZip2-mCherry-VCA (obtained by overlapping PCR; SynZip2 as in (Reinke et al., 2010)) into parental

pEBB vector containing N-terminal HA tag. mVen-FH1 construct was generated by cloning the FH1(aa S543-P747) domain of mDia1 (mouse) into pTriEx4-mVen plasmid. mVen-N-WASP (rat) construct was generated by cloning full-length N-WASP into pTriEx4-mVen plasmid. GFP-actin is described in (Gerisch and Muller-Taubenberger, 2003; Rivera et al., 2004). pmTFP1-actin was purchased from Allele Biotechnology.

Cell culture, transfections, antibody-mediated aggregation, fixation, drug treatment

Mouse NIH-3T3 cells were cultured in Dulbecco's Modified Eagle's Medium (DMEM) supplemented with 10% calf serum and 1% Pen/strep solution (Mediatech Inc.). Transient transfections were carried out using the Lipofectamine, Lipofectamine 2000 (Life Technologies) or FuGene6 (Promega Corporation) transfection reagents according to manufacturers' protocol. Antibody-mediated aggregation protocol is described in detail in (Ditlev et al., 2012; Rivera et al., 2004). Briefly - approximately 36-48 h after transfection, cells were sequentially incubated with a monoclonal antibody against human CD16 (Santa Cruz Biotechnology, Inc.) (0.75 μg/ml, 20 min, 37°C) and then with an unlabeled goat anti–mouse IgG (Thermo Fisher Scientific) (0.50 μg/ml, 30 min, 37°C); unbound antibody was removed from the cells by washing with complete medium after each antibody application, and then cells were immediately imaged using confocal microscopy or fixed for imaging at a later time. Fixation was performed with 4% paraformaldehyde in PBS, followed by mounting on glass coverslips with Aqua-Poly/Mount, Polysciences. Small molecule inhibitor of formin homology 2 (FH2) domains SMIFH2 was purchased from Tocris and dissolved in DMSO to 25 mM stock.

Cells were treated with 100 μM SMIFH2 (or same amount of DMSO for control) during antibody-mediated aggregation procedure for later fixed-cell imaging (Fig. 4B). For live-cell imaging (Movie S4), SMIFH2 (or DMSO for control) was diluted in 100 μL of imaging media and added to cells at indicated time.

Western Blotting

For Western immunoblotting, cell lysates were obtained from NIH-3T3 cells as in (Rivera et al., 2009). Protein content was determined by the Bradford Assay (Bio-Rad), and equal amounts of protein were subjected to SDS-PAGE. After transfer to nitrocellulose membranes, blots were probed with anti-GFP (Rabbit polyclonal IgG, Santa Cruz Biotechnology, Inc.) to detect CD16/7-eYFP-SynZip1, anti-dsRed (Rabbit polyclonal, Clontech) to detect HA-SynZip2-mCherry-VCA and anti-tubulin (Mouse monoclonal, Abcam) for loading control (Fig. S2B).

For the VCA density decrease experiments in Fig. 2 the amount CD16/7-mCherry-VCA DNA was 100%, 60%, 33%, 14% and 0% from the total amount of CD16/7-mCherry-VCA (VCA) and CD16/7 (Empty) DNA that was used for transfection. CD16/7 fusion proteins (CD16/7-mCherry-VCA and CD16/7) were detected with anti-CD16 antibody (Santa Cruz Biotechnology, Inc.). In cells co-expressing VCA and Empty fusion proteins (Fig. S1 – 3rd, 4th and 5th lane), the expression of VCA was estimated to be 60%, 37%, and 15% of the combined VCA and Empty expression.

To estimate overexpression of formin FH1 domain (Fig. 5, Fig. S4) the cells expressing FH1 domain were compared to the cells expressing full-length mDia1. The cells

expressing mDia1 were transfected with the same amount of DNA (mVen-mDia1) that was used for transfection of mVen-FH1 expressing cells. Both mVen-FH1 and mVen-mDia1 were detected with anti-GFP (Rabbit polyclonal IgG, Santa Cruz Biotechnology, Inc.); mVen-mDia1 was also detected with anti-mDia1. The level of FH1 domain overexpression versus the endogenous FH1 was estimated by comparing Ven-mDia1 band to the Ven-FH1 band (Fig. S4, IB: GFP).

Microscopy

18-24 h after transfection, cells were trypsinized and re-plated on either 25mm cover glass for fixation or 35-mm glass-bottomed culture dishes (MatTek or WPI) for live imaging.

Transfected cells were imaged in phenol red–free DMEM (Invitrogen) supplemented with 10% calf serum in glass-bottomed culture dishes and maintained at 37°C using a stage/objective heating (and CO2 regulation for LSM 780) system. Live-cell images were obtained using a spinning microlens confocal system (UltraView; PerkinElmer) mounted on an inverted microscope (TE2000; Nikon) equipped with a charge-coupled device camera (Orca-ER Firewire; Hamamatsu Photonics) MetaMorph (Molecular Devices) software and a 40×1.25 NA oil immersion objective; or laser scanning confocal microscope (LSM 510 Meta or LSM 780; Carl Zeiss) with a 63×1.4 NA oil immersion objective using LSM or ZEN (Carl Zeiss) software to acquire the time-lapse images. Images were collected as vertical Z-stacks of optical sections. Maximum z-projections were used for analysis. Fluorescent recovery after photobleaching (FRAP) of mCherry-

VCA (Fig. S2A, Movie S3A) was done on LSM 780, AxioObserver with C-Apochromat 40x/1.20 W Korr objective. Fluorescence from single confocal z-slice of ROI with multiple CD16/7 aggregates of was acquired; mCherry-VCA was bleached (5-10 times) after frame 3 in ROI smaller than the acquisition ROI. For FH2 inhibition experiment (Fig. 4) the cells were treated with 100µm SMIFH2 or DMSO (for control); multiple cells (using multistage acquisition mode) from each sample were imaged live every 153s. The drug (or DMSO) was added between the frames 5 and 6.

Cell culture, transfection, infection and imaging of Vaccinia comets

HeLa cells (ATCC) were grown in DMEM (Invitrogen) supplemented with 10% FBS (Gibco) at 37°C in a 5% CO2 incubator. Cells were seeded on glass coverslips, at 20% confluency, infected with vB5R-GFP vaccinia virus (Ward and Moss, 2001) at 1 pfu per cell for 1 h, then washed three times with PBS before adding fresh media. 12 h after infection cells were washed three times in PBS, fixed in 4% paraformaldehyde in PBS, permeabilized with 0.05% Triton X-100 in PBS and stained with phalloidin-AlexaFluor-568 (Life technologies) to visualize actin tails. For time-lapse video microscopy (Alvarez and Agaisse, 2013), cells were seeded on a 35 mm MatTek glass-bottom dish (MatTek Corporation) at a confluency of 30-50%. Cells were transfected with pYFP–N-WASP and actin-CFP the day prior to infection and infected with WR vaccinia virus (Ward and Moss, 2001) at 10 pfu per cell. Images were captured 10 h after infection every 12 s on a spinning disc confocal microscope (TE2000E) using a 60x Oil objective with the Volocity software (Perkin Elmer).

Cell culture, transfection, infection and imaging of Enteropathogenic E. Coli (EPEC) pedestals

NIH3T3 cells stably expressing mCherry-βactin were maintained in subconfluent monolayers in DMEM supplemented with 10% heat inactivated FCS, 1X antibiotic/antimycotic (Gibco), and 500μg/ml G418 at 37˚C + 5% CO2. Two days before infection, cells were seeded into 35mm glass-bottom plates and were induced to express mCherry-actin with 7.6 mM sodium butyrate 16 h prior to infection. EPEC cultures were grown overnight in DMEM + 100mM HEPES at 37˚C + 5% CO2 to enhance type 3 secretion. The overnight culture was diluted 1:200 into DMEM + 3.5% FBS + 20 mM HEPES for infection at an MOI of ~6. Bacteria were centrifuged onto the cells at 200 x g for 5 min to synchronize the infection. After 3 h of infection, cells were washed twice with PBS, given fresh media, and imaged 3-5 h post infection. Live imaging of mCherry fluorescence was performed using a Nikon Eclipse Ti microscope with a Plan Apoλ 100x 1.45 NA objective. Images were captured at 10 to 15 s intervals using an Andor Clara-E camera and NIS Elements software.

Image Analysis

Morphometric analysis was done in ImageJ with a custom written macro. In brief, each actin dense structure was roughly outlined manually including the surrounding area, background was subtracted, the object was thresholded (20-40%) against the local background region and was subjected to circularity measurement in ImageJ. Circularity ranges from 0 (infinitely long polygon or a line) to 1 (perfect circle) and is calculated as

$4\pi \times \frac{Area}{Perimeter^2}$. For the velocity analysis all the actin structures associated with the membrane CD16/7 clusters were tracked with the MTrackJ plugin to ImageJ (http://www.imagescience.org/meijering/software/mtrackj/). Velocity comparison graphs show the distribution (mean of 3 to 13 cells) of the average velocity per cell.

For the step size analysis (Fig. 4F) the average step size (distance between two consecutive positions of the particle) after the treatment (frames 6-20) was divided by the average step size before the treatment (frames 1-5).

Figures

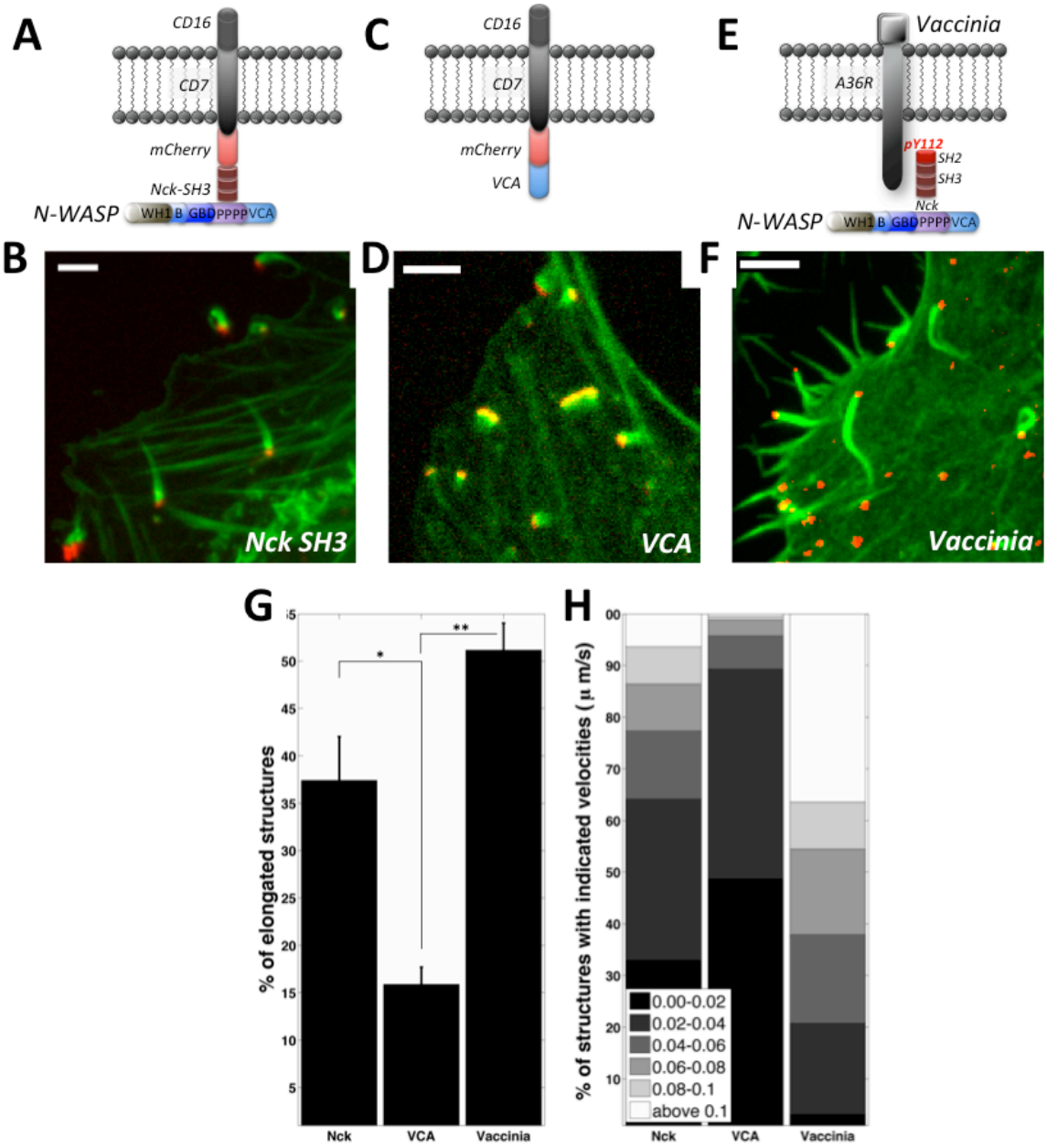
A
CD16
CD7
mCherry
Nck-SH3
N-WASP
WH1 B GBD PPPP VCA
C
CD16
CD7
mCherry
VCA
E
Vaccinia
A36R
pY112
SH2
SH3
Nck
N-WASP
WH1 B GBD PPPP VCA
B
Nck SH3
D
VCA
F
Vaccinia
G
% of elongated structures
Nck
VCA
Vaccinia
H
% of structures with indicated velocities (μ m/s)
0.00-0.02
0.02-0.04
0.04-0.06
0.06-0.08
0.08-0.1
above 0.1
Nck
VCA
Vaccinia

Figure 3.1. Membrane clustering of Nck SH3 and VCA induces formation of dissimilar actin structures.
A, C. Schematic of the CD16/7-mCherry-Nck-SH3 and CD16/7-mCherry-VCA trans-membrane fusion proteins. Both were aggregated by sequential application of primary mouse anti-CD16 and secondary anti-mouse antibodies. N-WASP recruitment to Nck SH3 required WIP (not shown in the schematic).
B. Aggregation of the Nck SH3 domains induces formation of actin comet tails. Staining: CD16/7-mCherry-Nck (red), actin (green).
D. Aggregation of the VCA domain of N-WASP induces formation of blob-like actin structures. Staining: CD16/7-mCherry-VCA (red), actin (green). Scale bars=5μm.
E. Schematic of signaling cascade to branched actin nucleation in cells infected with Vaccinia virus. Not shown in the schematic is that N-WASP recruitment requires WIP, and that A36 also recruits Grb2, which enhances comet tail formation.
F. Vaccinia-induced actin comets in HeLa cells. Staining: actin (green/Phalloidin), Vaccinia (red).
G. Morphology comparison of Nck- and VCA-induced actin structures and Vaccinia actin comet tails. The bars in the plot represent the average percentage of particles per cell with circularity below 0.6. (Nck: 3 cells, 540 aggregates; VCA: 3 cells, 336 aggregates; Vaccinia: 9 cells, 371 aggregates). Error bars are mean ± s.e.m. *$P<0.01$, **$P<0.001$.
H. Velocity comparison of Nck- and VCA-induced actin structures and Vaccinia actin comet tails. The stacked histogram plot represents the average distribution of mean velocities (μm/s). The legend indicates bin sizes (ranges of velocities) that were used to calculate the distribution. (Nck: 7 cells, 654 aggregates; VCA: 7 cells, 945 aggregates; Vaccinia: 7 cells, 125 aggregates)

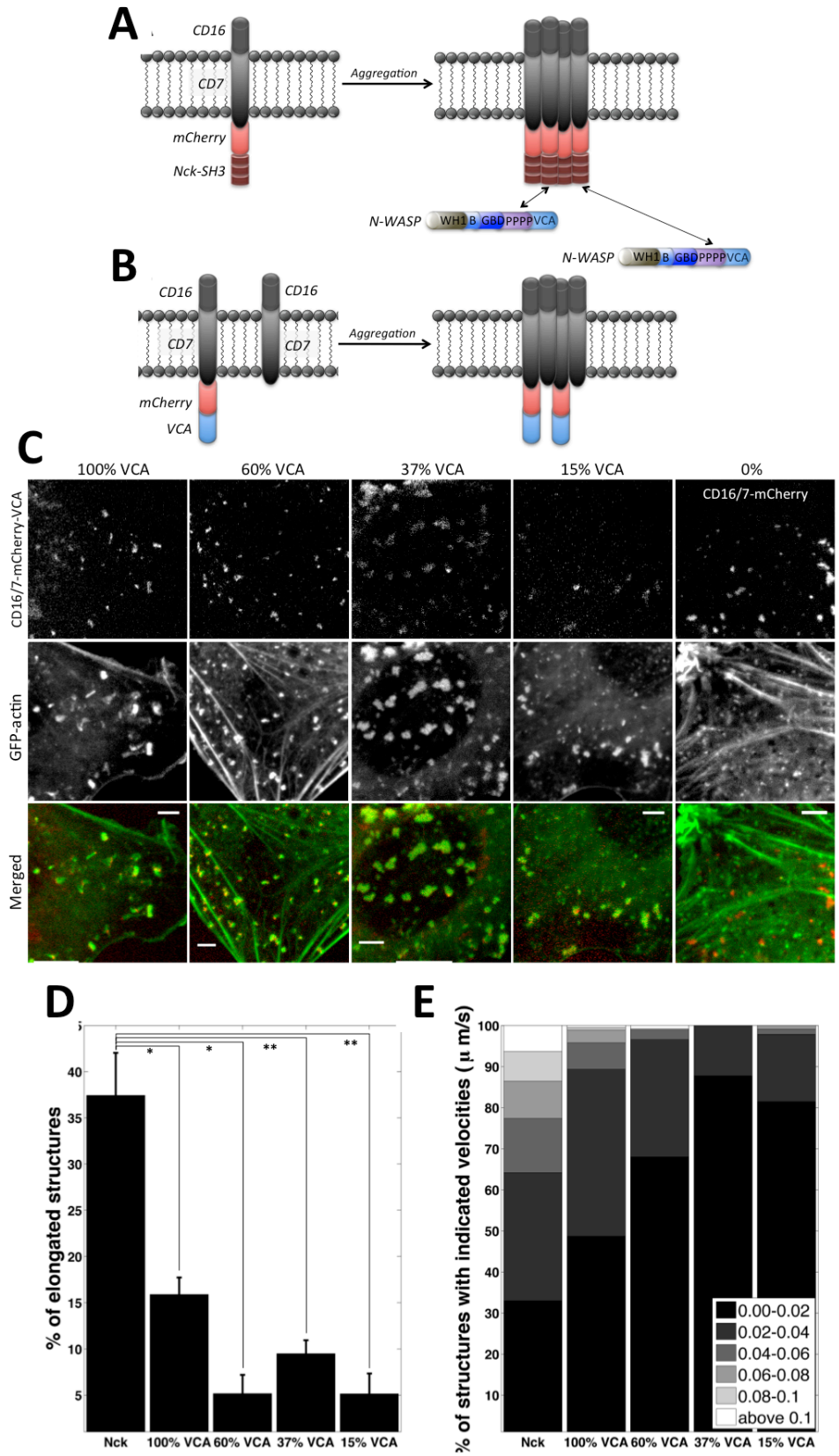
A
CD16
CD7
mCherry
Nck-SH3
Aggregation
N-WASP
WH1 B GBD PPPP VCA
B
CD16
CD7
mCherry
VCA
Aggregation
C
100% VCA
60% VCA
37% VCA
15% VCA
0%
CD16/7-mCherry
CD16/7-mCherry-VCA
GFP-actin
Merged
D
% of elongated structures
Nck
100% VCA
60% VCA
37% VCA
15% VCA
E
% of structures with indicated velocities (µ m/s)
0.00-0.02
0.02-0.04
0.04-0.06
0.06-0.08
0.08-0.1
above 0.1

Figure 3.2. Decreasing VCA density in membrane clusters is not sufficient for comet tail formation.
A. Schematic of CD16/7-mCherry-Nck aggregation and binding by endogenous N-WASP protein.
B. Schematic of CD16/7-mCherry-VCA co-aggregation with empty CD16/7 fusion proteins resulting in membrane VCA cluster of decreased density (comparable to density of VCA in Nck aggregates).
C. Aggregation of VCA diluted with Empty fusion proteins. Staining in merged images: GFP-actin (green), CD16/7-mCherry-VCA (red) in 100%, 60%, 37%, 15%, and CD16/7-mCherry (red) in 0% VCA. Scale bars=5μm.
D. Morphology comparison of Nck and VCA-induced and actin structures induced with diluted VCA clusters. (*Nck: 3 cells, 540 aggregates; 100% VCA: 3 cells, 336 aggregates; 60% VCA: 3 cells, 619 aggregates; 37% VCA: 3 cells, 425 aggregates; 15% VCA: 3 cells, 811 aggregates*). Error bars are mean ± s.e.m. *$P<0.01$, **$P<0.05$.
E. Velocity comparison of Nck and VCA-induced and actin structures induced with diluted VCA clusters. (*Nck: 7 cells, 654 aggregates; 100% VCA: 6 cells, 872 aggregates; 60% VCA: 3 cells, 597 aggregates; 37% VCA: 3 cells, 804 aggregates; 15% VCA: 3 cells, 496 aggregates.*)

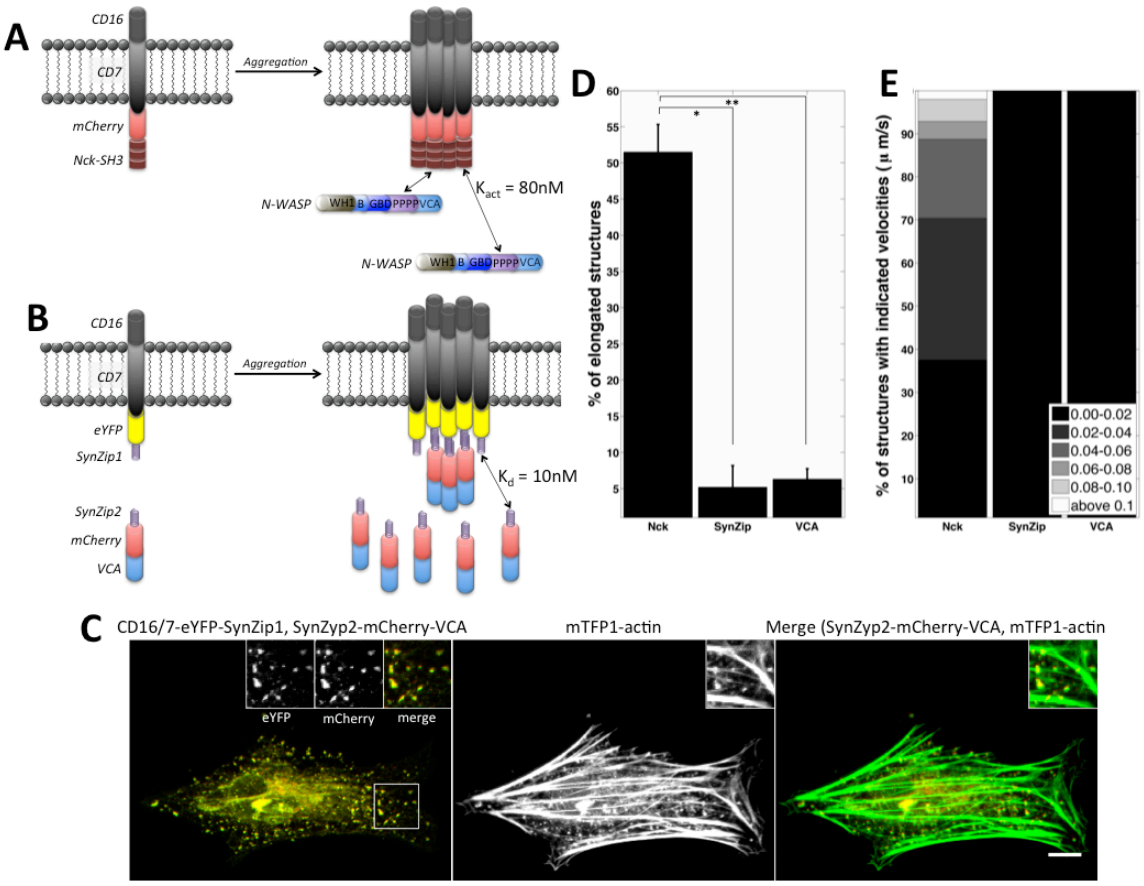
A
CD16
CD7
mCherry
Nck-SH3
Aggregation
N-WASP
WH1 B GBD PPPP VCA
K_{act} = 80nM
N-WASP
WH1 B GBD PPPP VCA
B
CD16
CD7
eYFP
SynZip1
Aggregation
K_d = 10nM
SynZip2
mCherry
VCA
D
% of elongated structures
Nck
SynZip
VCA
E
% of structures with indicated velocities (μ m/s)
0.00-0.02
0.02-0.04
0.04-0.06
0.06-0.08
0.08-0.10
above 0.1
Nck
SynZip
VCA
C
CD16/7-eYFP-SynZip1, SynZyp2-mCherry-VCA
mTFP1-actin
Merge (SynZyp2-mCherry-VCA, mTFP1-actin
eYFP
mCherry
merge

Figure 3.3. Allowing VCA turnover in membrane clusters does not result in formation of comet tails.

A. Schematic of CD16/7-mCherry-Nck aggregation and binding by endogenous N-WASP protein.

B. Schematic of VCA clusters with turnover through SynZip-mediated interaction. CD16/7-eYFP-SynZip1 aggregation results in recruitment of cytosolic SynZip2-mCherry-VCA fusion proteins.

C. Actin recruitment and shape of actin structures induced by clustering of SynZip2-mCherry-VCA through interaction with CD16/7-eYFP-SynZip1. *Leftmost* image shows merged staining of SynZip2-mCherry-VCA (red) and CD16/7-eYFP-SynZip1 (green). Insets in the leftmost image show magnified view of CD16/7-eYFP-SynZip1 (left), SynZip2-mCherry-VCA (middle) and a composite of the two (right). Image in the *middle* is actin staining alone. *Rightmost* image shows merged staining of SynZip2-mCherry-VCA (red) and mTFP1-actin (green). Scale bar=10μm.

D. Morphology analysis of actin structures induced by VCA clustered through SynZip binding. (*Nck SH3 clustering: 3 cells, 124 aggregates; VCA clustering though SynZip interaction: 8 cells, 152 aggregates; VCA clustering: 3 cells, 233 aggregates).* Error bars are mean ± s.e.m. *$P<0.001$, **$P<0.01$.

E. Velocity analysis of actin structures induced by VCA clustered through SynZip binding. (*Nck SH3 clustering: 3 cells, 121 aggregates; VCA clustering though SynZip interaction: 4 cells, 174 aggregates; VCA clustering: 246 aggregates)*

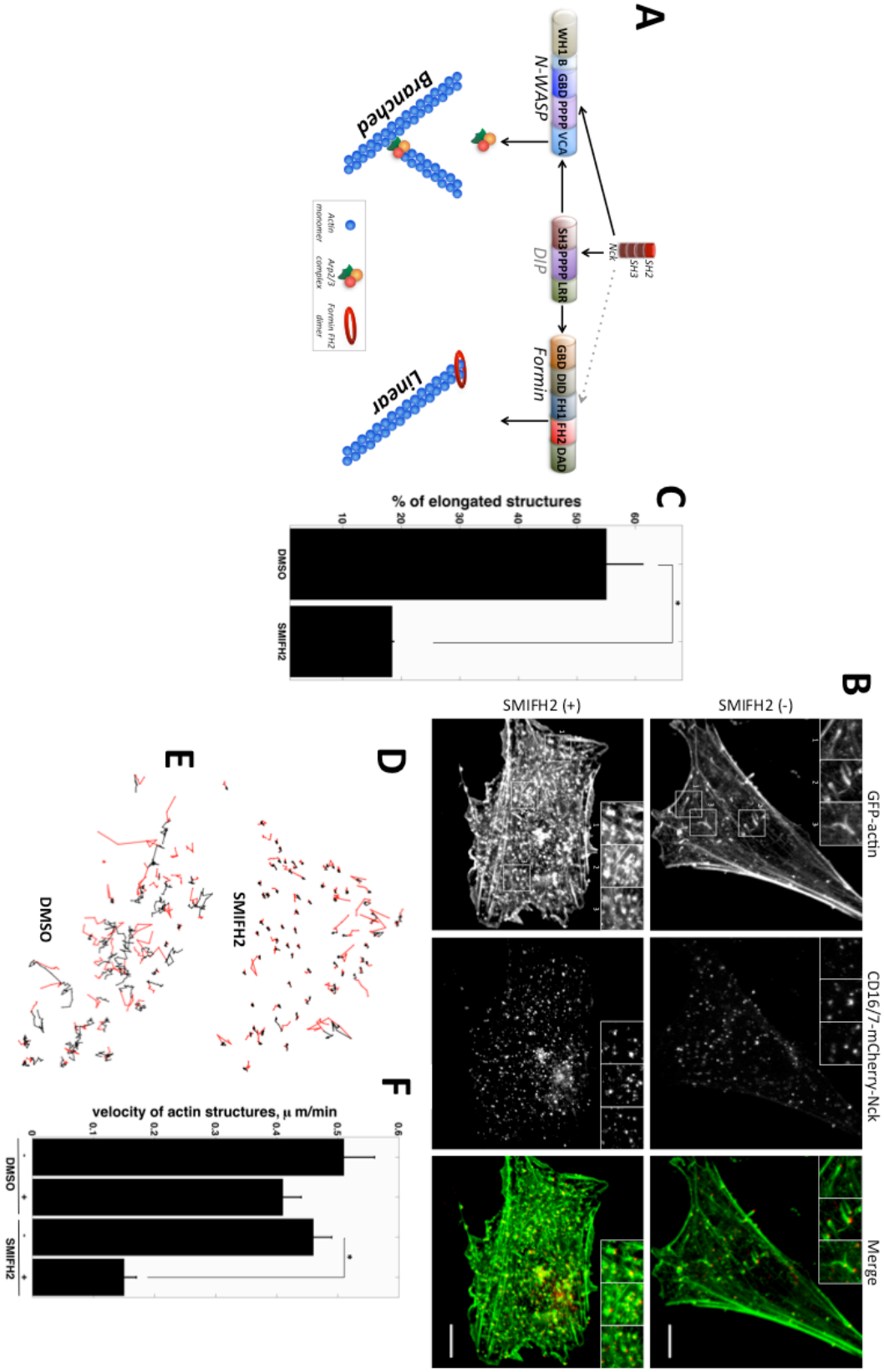
A
N-WASP
WH1 B GBD PPPP VCA
DIP
SH3 PPP LRR
Formin
GBD DID FH1 FH2 DAD
Nck
SH2
SH3
Branched
Linear
Actin monomer
Arp2/3 complex
Formin FH2 dimer
B
SMIFH2 (-)
SMIFH2 (+)
GFP-actin
CD16/7-mCherry-Nck
Merge
C
% of elongated structures
DMSO
SMIFH2
D
DMSO
SMIFH2
E
F
velocity of actin structures, μ m/min
DMSO
SMIFH2

Figure 3.4. Formin FH2 domain inhibition decreases mobility and disrupts comet tail shape of Nck SH3-induced actin structures

A. Potential role of Nck as integrator of linear and branched elongation in actin comet tails. Schematic of branched and linear elongation molecular pathways that may be initiated by Nck-SH3 clustering. Green donut-shape structure at the barbed end of unbranched filament is a dimer formed by FH2 domains of formin. Grey dotted line represents potential but not demonstrated interaction. Black dashed lines represent known interactions of DIP with Nck, N-WASP, Arp2/3 and Formin.

B. Nck SH3-induced actin aggregates in fixed DMSO-treated NIH3T3 cells (*upper panel*) or those treated with SMIFH2 inhibitor (*lower panel*). Scale bars=10μm.

C. Morphology analysis of Nck-SH3 induced actin aggregates in DMSO-treated (control) and in SMIFH2-treated fixed NIH3T3 cells. (*DMSO-treated: 3 cells, 197 aggregates; SMIFH2-treated: 3 cells, 413 aggregates).* Error bars are mean ± s.e.m. *$P<0.05$.

D, E. Tracks of Nck-SH3-induced actin structures in NIH3T3 cells treated with SMIFH2 inhibitor (D) or DMSO-treated control (E). Part of the track before treatment is colored in red; after treatment, in black. Frame rate=153 s, 20 frames.

F. Velocity of Nck SH3-induced actin aggregates before and after DMSO and SMIFH2 treatment. DMSO: V_{before}=0.51μm/min and V_{after}=0.41μm/min. SMIFH2: V_{before}=0.46μm/min and V_{after}=0.15μm/min. *(DMSO-treated: 3 cells, 92 tracks; SMIFH2-treated: 3 cells, 148 tracks).* Error bars are mean ± s.e.m. *$P<0.01$.

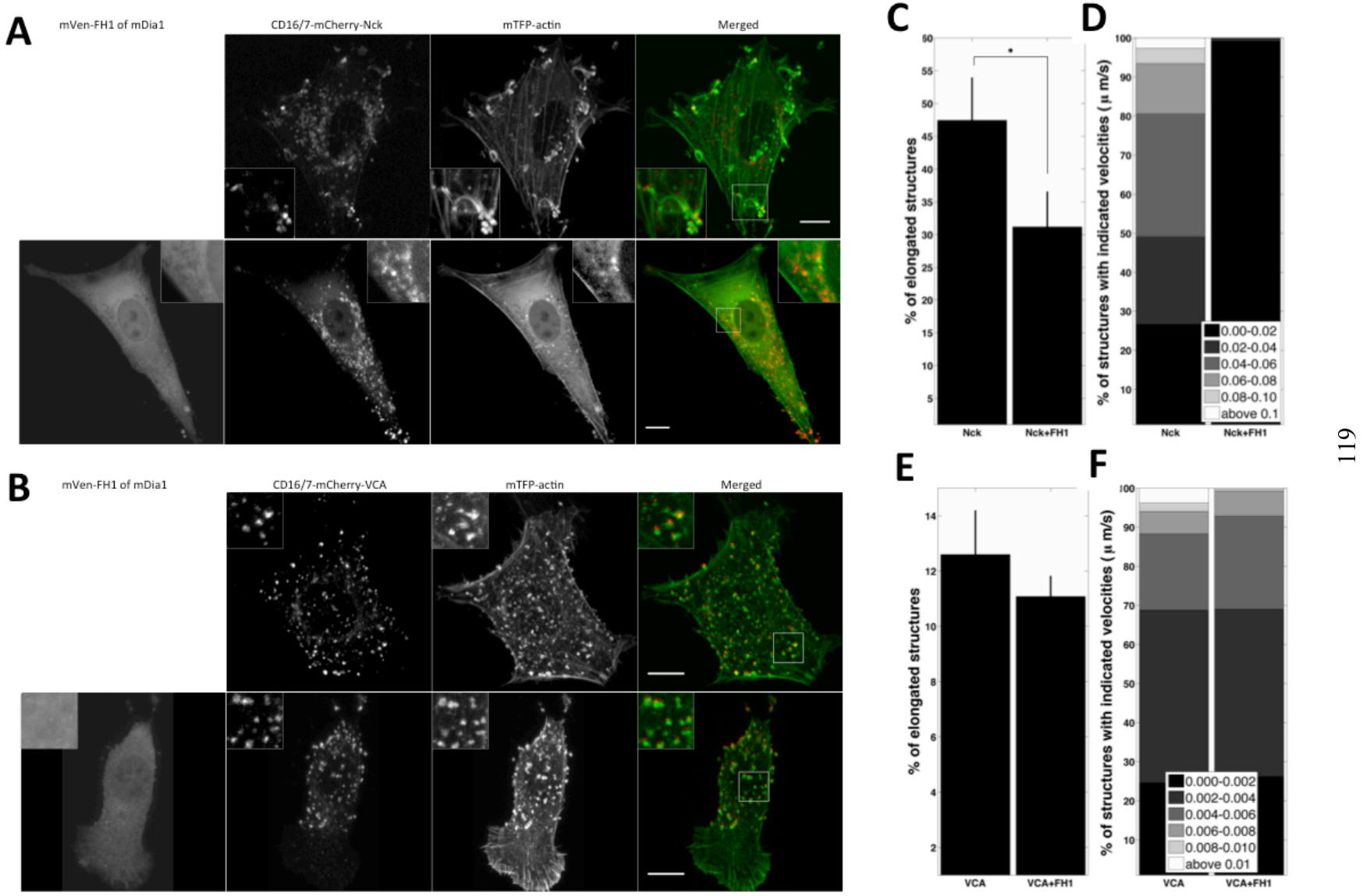
A
mVen-FH1 of mDia1
CD16/7-mCherry-Nck
mTFP-actin
Merged
B
mVen-FH1 of mDia1
CD16/7-mCherry-VCA
mTFP-actin
Merged
C
% of elongated structures
Nck
Nck+FH1
D
% of structures with indicated velocities (µ m/s)
0.00-0.02
0.02-0.04
0.04-0.06
0.06-0.08
0.08-0.10
above 0.1
Nck
Nck+FH1
E
% of elongated structures
VCA
VCA+FH1
F
% of structures with indicated velocities (µ m/s)
0.000-0.002
0.002-0.004
0.004-0.006
0.006-0.008
0.008-0.010
above 0.01
VCA
VCA+FH1

Figure 3.5. Formin FH1 domain overexpression affects the shape and dynamics of actin structures induced by Nck SH3 but not those induced by VCA clustering
A. Nck SH3-induced actin structures in cells without (*top panel*) or with (*bottom panel*) overexpression of formin FH1 domain. Merged images in both panels show the composites of CD16/7-mCherry-Nck SH3 and mTFP1-actin.
B. VCA-induced actin structures in cells without (*top panel*) or with (*bottom panel*) overexpression of formin FH1 domain (*bottom panel*). Merged images in both panels show the composites of CD16/7-mCherry-VCA and mTFP1-actin. Scale bars=10μm.
C. Morphology analysis of Nck SH3-induced actin structures in the control and in the cells overexpressing formin FH1 domain. (C*ontrol: 3 cells, 334 aggregates; FH1 overexpressing: 3 cells, 117 aggregates*). Error bars are mean ± s.e.m. **P<0.01*.
D. Velocity analysis of Nck SH3-induced actin structures in the control and in the cells overexpressing formin FH1 domain. (*Control: 3 cells, 201 aggregates; FH1 overexpressing: 4 cells, 86 aggregates.*)
E. Morphology of VCA-induced actin structures in the control and in the cells overexpressing formin FH1 domain. (C*ontrol: 3 cells, 420 aggregates; FH1 overexpressing: 3 cells, 248 aggregates*). Error bars are mean ± s.e.m.
F. Velocity of VCA-induced actin structures in the control and in the cells overexpressing formin FH1 domain. (*Control: 3 cells, 459 aggregates; FH1 overexpressing: 3 cells, 278 aggregates.*)

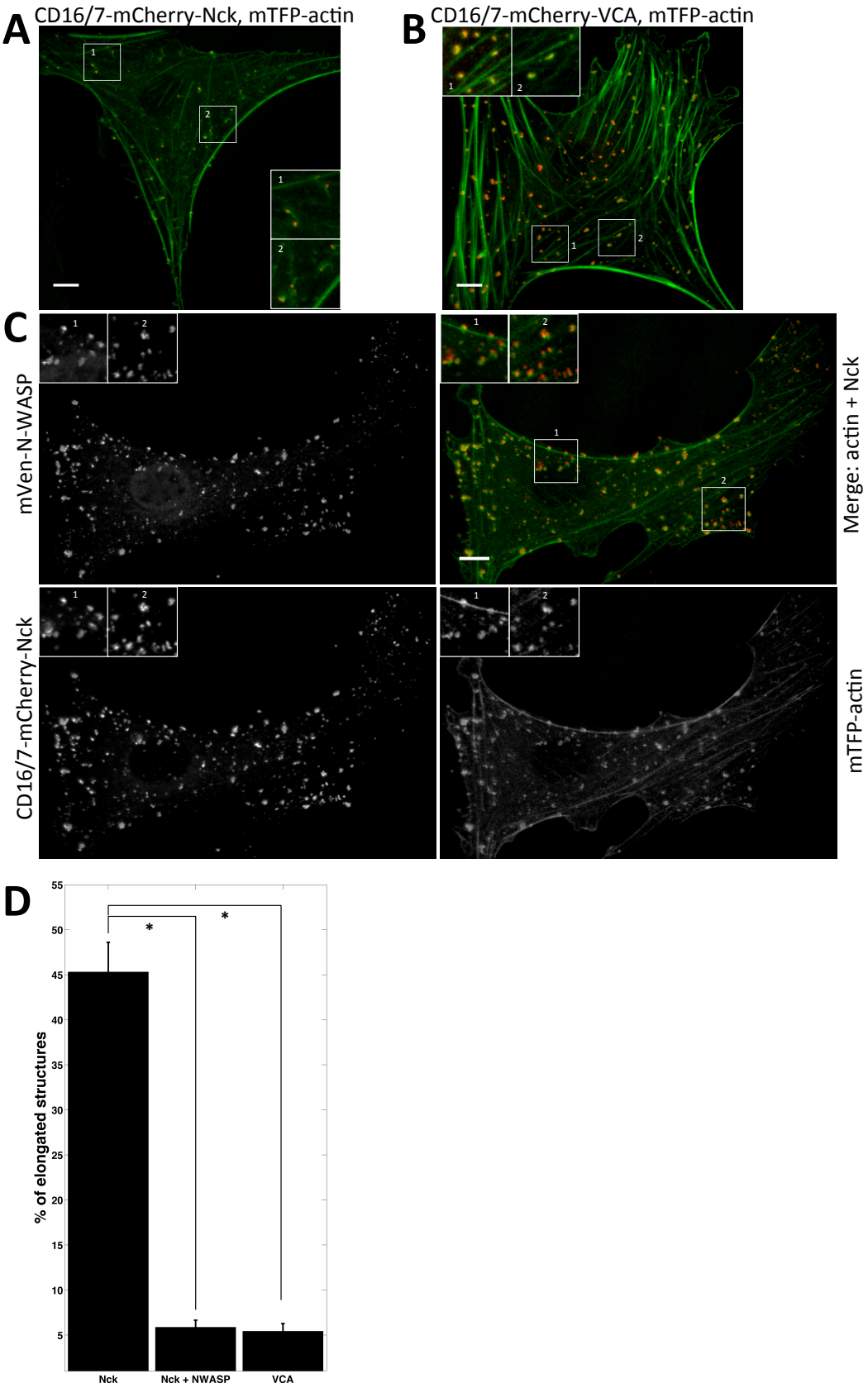
A
CD16/7-mCherry-Nck, mTFP-actin
B
CD16/7-mCherry-VCA, mTFP-actin
C
mVen-N-WASP
CD16/7-mCherry-Nck
Merge: actin + Nck
mTFP-actin
D
% of elongated structures
55
50
45
40
35
30
25
20
15
10
5
*
*
Nck
Nck + NWASP
VCA

Figure 3.6. N-WASP overexpression changes shape Nck-SH3-induced actin structures.

A-C. Actin structures induced by aggregation of Nck SH3 *(A, C)* or VCA *(B)* in NIH3T3 cells *(A, B)* or NIH3T3 cells overexpressing mVen-N-WASP *(C)*. Cells were fixed. In *(C)*, upper left image shows mVen-N-WASP, upper right image is the merge of mTFP1-actin (green) and Nck SH3 clusters (red), lower left image shows CD16/7-mCherry-Nck, and lower right image shows mTFP1-actin. Scale bars=10μm.

D. Morphology analysis of Nck SH3-induced actin structures in the control and in the cells overexpressing N-WASP. (*Nck-SH3: 3 cells, 200 aggregates; Nck-SH3 + N-WASP overexpression: 3 cells, 329 aggregates; VCA: 3 cells, 250 aggregates)*. Error bars are mean ± s.e.m. *$P<0.001$.

Supplemental Figures

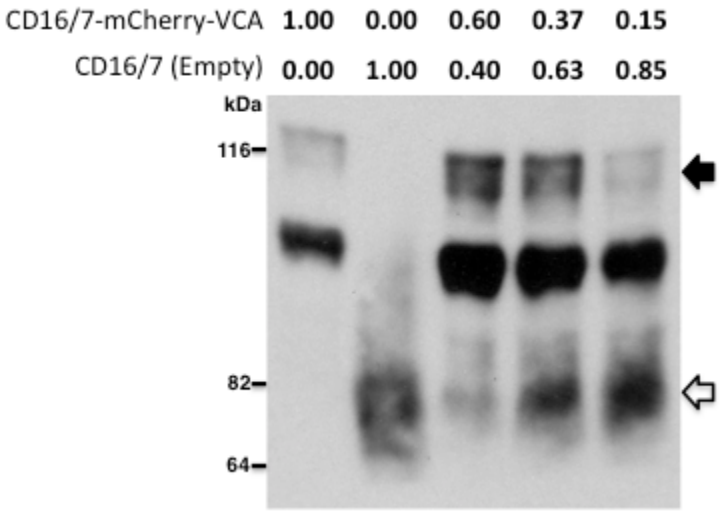

Figure S 3.1. CD16/7-mCherry-VCA and CD16/7 (Empty) fusion protein expression and co-expression in NIH-3T3 transfected cells.
A Western blot demonstrating expression (anti-CD16) of CD16/7-mCherry-VCA (black arrow) and CD16/7 (empty arrow): 100% VCA, 100% Empty, 60% VCA with 40% Empty, 37% VCA with 63% Empty, 15% VCA with 85% Empty. A double band is observed for each CD16/7 fusion protein: the top band is the full-length fusion protein; the bottom band is a cleaved fusion protein lacking the aggregatable CD16 domain.

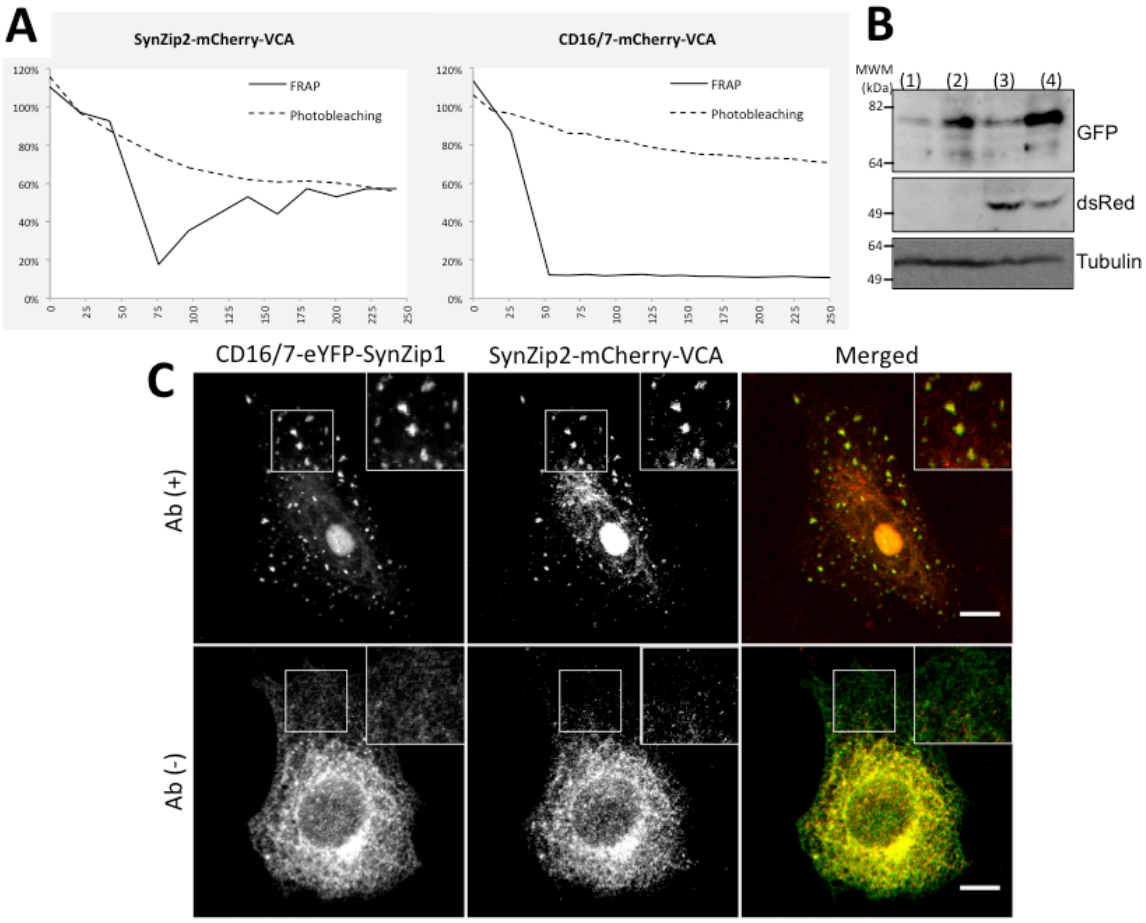
A
SynZip2-mCherry-VCA
CD16/7-mCherry-VCA
FRAP
Photobleaching
120%
100%
80%
60%
40%
20%
0%
0
25
50
75
100
125
150
175
200
225
250
B
MWM (kDa)
(1)
(2)
(3)
(4)
82
64
49
GFP
dsRed
Tubulin
C
CD16/7-eYFP-SynZip1
SynZip2-mCherry-VCA
Merged
Ab (+)
Ab (-)

Figure S 3.2. VCA turnover via SynZip binding interface in membrane clusters.
A. (*Left*) Fluorescent recovery after photobleaching (FRAP) of mCherry-VCA in CD16/7-eYFP-SynZip1 : SynZip2-mCherry-VCA clusters as compared to (*Right*) FRAP of mCherry-VCA in CD16/7-mCherry-VCA clusters. x-axis: time, seconds. y-axis: average integrated intensity of N-WASP or VCA cluster, normalized.
B. Western Blot of CD16/7-eYFP-SynZip1 (detected with anti-GFP antibody) and SynZip2-mCherry-VCA (detected with anti-dsRed antibody) expression in NIH3T3 cells. Lane (1) - wild type cells; lane (2) - cells expressing CD16/7-eYFP-SynZip1; lane (3) - cells expressing SynZip2-mCherry-VCA; lane (4) - cells co-expressing CD16/7-eYFP-SynZip1 and SynZip2-mCherry-VCA. Positions of molecular weight markers (MWM) are indicated to left.
C. Recruitment and clustering of SynZip2-mCherry-VCA after antibody-mediated aggregation of CD16/7-eYFP-SynZip1 (*top panel*). Without aggregating CD16/7-eYFP-SynZip1, SynZip2-mCherry-VCA does not cluster (*bottom panel*). Scale bars=10μm.

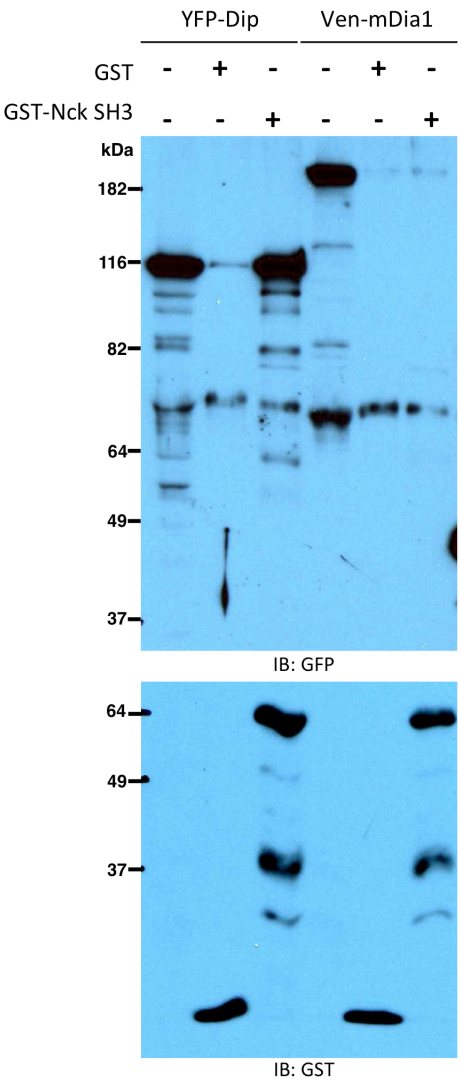
YFP-Dip
Ven-mDia1
GST - + - - + -
GST-Nck SH3 - - + - - +
kDa
182
116
82
64
49
37
IB: GFP
64
49
37
IB: GST

Figure S 3.3. Nck SH3(1-2-3) recruits the adaptor protein Dip by GST pull-down assay.
293T cells were transfected with plasmids expressing YFP-DIP and mVen-mDia1. Whole cell lysates (*WCL*) of transfected cells were incubated with either GST or GST-Nck SH3(1-2-3) purified proteins immobilized on GSH beads. *WCL* or elution fractions from the beads were immunoblotted with anti-GFP antibody to detect YFP-DIP and mVen-mDia1 and with anti-GST antibody to detect GST and GST-Nck SH3(1-2-3) proteins bound to the GSH beads.

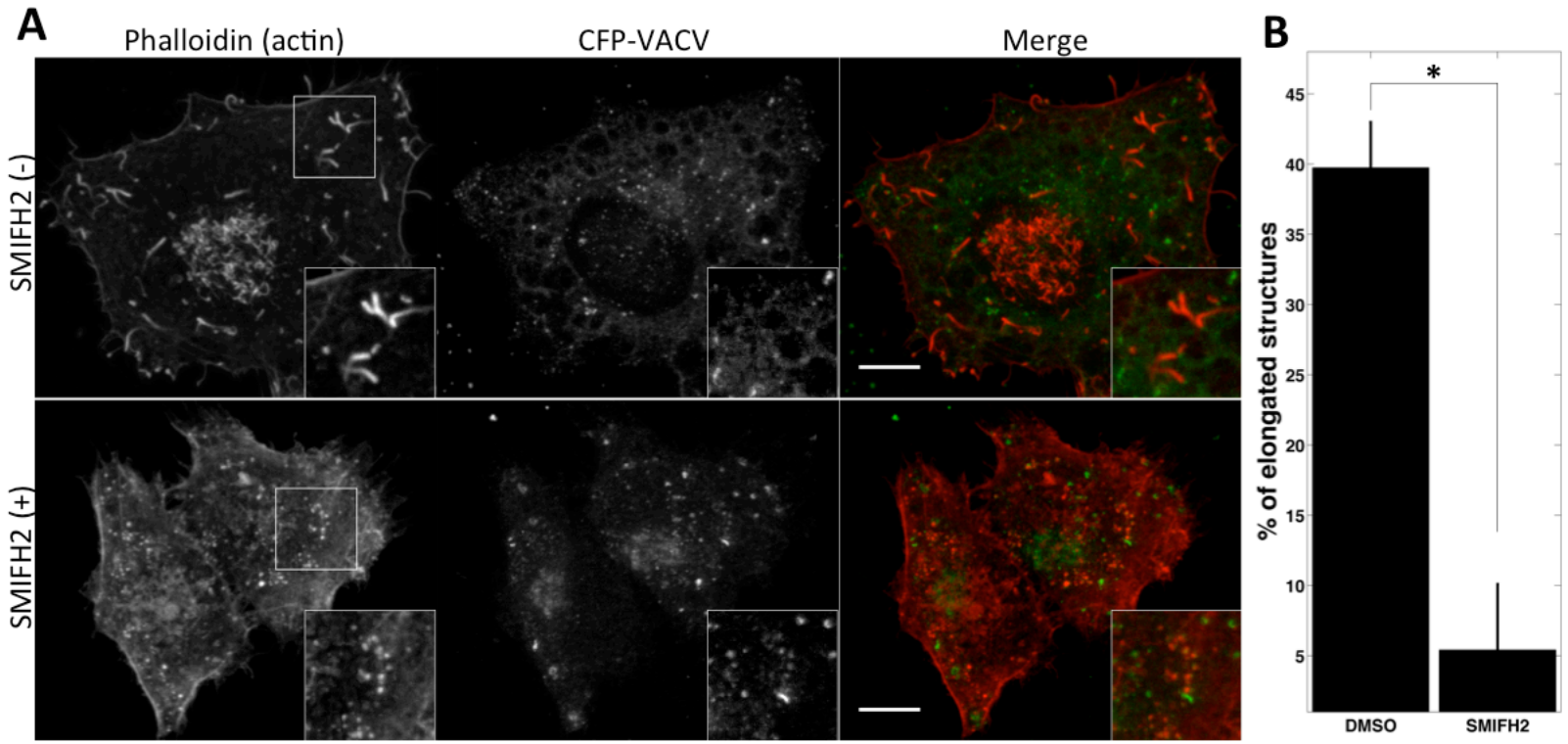
A
Phalloidin (actin)
CFP-VACV
Merge
SMIFH2 (-)
SMIFH2 (+)
B
% of elongated structures
45
40
35
30
25
20
15
10
5
*
DMSO
SMIFH2

Figure S 3.4. Formin FH2 domain inhibition disrupts comet tail shape of Vaccinia-induced actin structures.
A. Vaccinia-induced actin comets in fixed HeLa cells. Staining: actin (red/Phalloidin), Vaccinia (CFP/green). *Top panel*: control cell (DMSO). Bottom panel: cell treated with the 100μM formin inhibitor SMIFH2.
B. Morphology analysis of Vaccinia-induced actin aggregates in DMSO-treated (control) and in SMIFH2-treated fixed HeLa cells. (*DMSO-treated: 3 cells, 282 aggregates; SMIFH2-treated: 4 cells, 136 aggregates).* Error bars are mean ± s.e.m. *$P<0.005$.

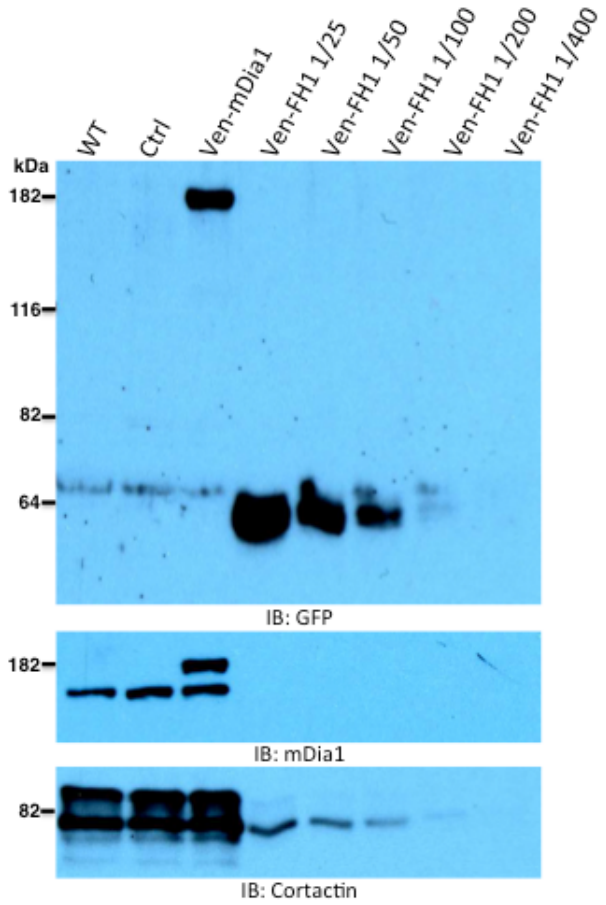
WT
Ctrl
Ven-mDia1
Ven-FH1 1/25
Ven-FH1 1/50
Ven-FH1 1/100
Ven-FH1 1/200
Ven-FH1 1/400
kDa
182
116
82
64
IB: GFP
182
IB: mDia1
82
IB: Cortactin

Figure S 3.5. Formin FH1 domain overexpression for inhibition of endogenous formin activity at membrane clusters (Fig. 5).
A Western blot demonstrating overexpression of mVenus tagged FH1 domain (anti-GFP) as compared to endogenous level of FH1 domain. *WT*: not transfected NIH-3T3 cells. *Ctrl*: cells transfected with CD16/7-mCherry-Nck SH3 and mTFP1-actin. *Ven-mDia1*: cells transfected with CD16/7-mCherry-Nck SH3, mTFP1-actin and mVenus tagged full-length mDia1 (detected with anti-GFP and anti-mDia1). *Ven-FH1* (5 lanes): cells transfected with CD16/7-mCherry-Nck SH3, mTFP1-actin and mVenus tagged FH1 domain (detected with anti-GFP); *Ven-FH1* cell lysate was diluted 1/25, 1/50, 1/100, 1/200, 1/400 times. Loading control: cortactin.

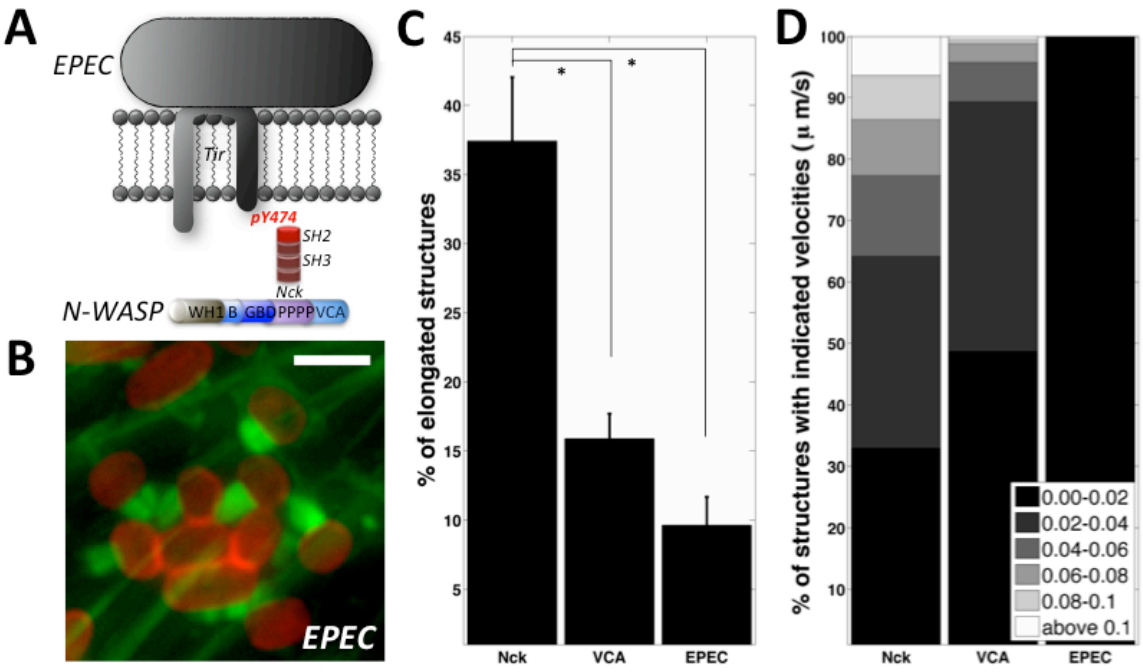
A
EPEC
Tir
pY474
SH2
SH3
Nck
N-WASP
WH1
B
GBD
PPPP
VCA
B
EPEC
C
% of elongated structures
45
40
35
30
25
20
15
10
5
*
*
Nck
VCA
EPEC
D
% of structures with indicated velocities (μ m/s)
100
90
80
70
60
50
40
30
20
10
0.00-0.02
0.02-0.04
0.04-0.06
0.06-0.08
0.08-0.1
above 0.1
Nck
VCA
EPEC

Figure S 3.6. Comparison of actin structures induced by membrane clustering of Nck SH3 and N-WASP VCA with EPEC actin pedestals.
A. Schematic of signaling cascade to branched actin nucleation in cells infected with EPEC bacteria.
B. Infection of 3T3 cells with EPEC results in formation of actin pedestals. Staining: actin is stained with phalloidin 488 (green) and EPEC is labeled with mouse anti-LPS and alexa 568 anti-mouse secondary (red). Scale bars=5μm.
C. Morphology comparison of Nck- and VCA-induced actin structures and EPEC actin pedestals. (*Nck: 3 cells, 540 aggregates; VCA: 3 cells, 336 aggregates; EPEC: 16 cells, 477 aggregates*). Error bars are mean ± s.e.m. *$P<0.01$, **$P<0.001$.
D. Velocity comparison of Nck- and VCA-induced actin structures and EPEC actin pedestals. (*Nck: 7 cells, 654 aggregates; VCA: 7 cells, 945 aggregates; EPEC: 13 cells, 405 aggregates.*)

Movies

Movie 3.1. Actin structures induced by aggregating CD16/7-mCherry-Nck and CD16/7-mCherry-VCA in NIH3T3 cells and actin comets induced by Vaccinia virus in HeLa cells.

Movie 3.2. *A*ctin structures induced by aggregation of VCA diluted with Empty CD16/7 proteins.
Movies play in the following order: 100%VCA, 60%VCA, 33%VCA, 14%VCA, 0%VCA. In 60%VCA, 33%VCA and 14%VCA samples, VCA is fluorescently tagged with mCherry (CD16/7-mCherry-VCA) and Empty protein is not tagged with a fluorescent label (CD16/7). In 0%VCA sample, Empty protein is fluorescently tagged with mCherry (CD16/7-mCherry).

Movie 3.3. FRAP experiments and actin structures induced through VCA SynZip binding interface.
Movie 3.3A. FRAP of CD16/7-mCherry-VCA in clusters and mCherry-VCA in clusters with SynZip binding interface. Scale bars=5μm.
Movie 3.3B. Movie of actin aggregates induced by NWASP-VCA undergoing turnover.

Movie 3.4. Inhibition of formin FH2 domain decreases mobility of Nck-SH3 induced actin assemblies.
Movie 3.4A. Movies and tracks of Nck-SH3 actin structures in cells treated with the 100μM formin inhibitor SMIFH2 (dissolved in DMSO) and in the non-treated control cell (DMSO alone). The treatment/mock-treatment was carried out during acquisition of sixth frame. The movies have 20 frames (every 2.5 min) and total acquisition time is about 49 min.
Movie 3.4B. Movies of Nck-SH3-induced actin structures in cells before and after the treatment with the 150μM formin inhibitor SMIFH2 (dissolved in DMSO) or with DMSO alone (control). Velocity in the SMIFH2 treated cell decreased from 0.026 μm/s to 0.01 μm/s. Velocity in the control cell did not change (remained 0.026 μm/s after the treatment with DMSO). The movies have 10 frames (every 30 s) and total acquisition time is 4.5 min.

Movie 3.5. Formin FH1 domain overexpression affects dynamics of Nck SH3- but not of the VCA-induced actin structures.
Movie 3.5A. Nck SH3-induced actin structures in the control and in the cells overexpressing FH1 domain of formin mDia1.
Movie 3.5B. VCA induced actin structures in the control and in the cells overexpressing FH1 domain of formin mDia1.

Movie 3.6. Actin pedestals induced by EPEC bacteria in NIH3T3 cells.

4. CHAPTER IV: Discussion and future directions

Discussion

In my thesis work, I studied mechanisms underlying actin-based motility in lamellipodium and in actin comet tails. Both structures rely on Arp2/3-mediated actin dynamics and signaling events that lead to activation of the Arp2/3 nucleation. Through biochemical modeling, I demonstrated a synergistic activity of cofilin and capping proteins in lamellipodium. Investigation of Nck SH3-induced actin comets revealed the presence and importance of formin-mediated actin assembly in localized actin polymerization that involves signaling via Nck adaptor protein.

In Chapter 2, I aimed to understand the basis for opposing effect of cofilin on actin assembly in different experimental studies. An open model of actin dendritic nucleation recapitulates a number of complex aspects of actin dynamics and therefore it is a validated tool for assessing cofilin mechanism of action. Biochemical modeling allowed me to systematically vary cofilin concentration and evaluate the effects on the main variables that characterize actin assembly. Concentration of capping protein was also varied in the model. I observed that an increase in cofilin promotes actin disassembly when capping protein concentration is low and therefore the pool of actin monomers is small. On the other hand cofilin stimulates actin polymerization when there is enough capping protein to maintain an abundant actin monomer pool. This phenomenon defines cooperativity of cofilin and capping proteins in the assembly of a branched actin network. There is an optimal ratio of cofilin and capping concentrations when F-actin production is maximal. Deviating from this ratio results in actin disassembly either because there are

very few barbed ends that are getting capped or because there are too many barbed ends that eventually depolymerize due to a lack of actin monomers.

In Chapter 3, I aimed to research the role of Nck adaptor protein in assembly of dynamic actin comet tails. It is known that Nck has a major role in recruitment of the branched NPF N-WASP to the membrane. Interestingly, it was not a critical aspect underlying the morphological features and dynamic behavior of actin comets. Clustering of the catalytic C-terminal VCA domain of N-WASP was not sufficient to reproduce actin comets. Ensuring appropriate density and turnover of VCA at the membrane (corresponding to that of N-WASP in Nck SH3 membrane clusters) also did not yield formation of elongated and dynamic actin structures. Nck SH3-induced actin comets have certain similarity to pathogen-induced actin comets. There are several recent findings indicating a role for formin-mediated actin assembly in formation of pathogenic actin comets. I employed two different experimental approaches to inhibit linear actin polymerization in Nck SH3-induced actin comets. In both cases morphology and dynamics of actin structures was dramatically affected. Therefore, I concluded that first – formin activity is critical for comet tail formation and second – both N-WASP/Arp2/3- and formin-mediated polymerization occurs in Nck SH3-induced actin structures. The balance between the two nucleation pathways defines morphological and dynamic properties of the localized actin structures in my experimental system. According to this hypothesis, shifting the balance towards higher branched nucleation by overexpressing N-WASP, disrupted the shape of actin comets.

My projects have provided additional insights into 1) the mechanism of cofilin activity regulation in branched actin network and 2) the role of Nck adaptor protein in converging two different actin nucleation pathways in localized actin structures. In addition, my findings give rise to a number of new questions. In the next section I define a few of these questions and propose several approaches to address them.

Future Directions

In silico investigation of cofilin's role in actin polymerization

The current model of actin dendritic nucleation would benefit from including the most recent biochemical mechanisms of regulating cofilin activity as well as effects of cofilin binding to actin filaments.

It would be useful to include in the model the three main cofilin inhibitory mechanisms: 1) inhibition through phosphorylation by LIMK (dephosphorylation by phosphatase SSH), 2) inhibition through binding to PIP2 at the membrane, 3) inhibition through biding to cortactin. In addition to binding cooperativity and enhanced Pi release, I would add several other mechanisms of cofilin association with actin filaments and modes of severing activity: 1) inhibiting nucleotide exchange on actin monomers, 2) competing with tropomyosins for F-actin binding, 3) concentration dependence of severing – at sub-stoichiometric cofilin:actin ratio severing occurs, while at saturating cofilin:actin ratio severing occurs filament stabilization occurs. Regulation of cofilin activity through manipulation of cofilin occupancy of actin filaments implies that severing activity is maximal at half-stoichiometric cofilin:actin ratio (De La Cruz, 2009). Cofilin ligands would either promote or inhibit severing depending on the initial cofilin:actin ratio. One of these ligands – tropomyosin, is known to antagonize cofilin severing activity and is worth investigating *in silico*. Binding of other actin binding proteins is strongly influenced by the presence of tropomyosins on the filaments. They protect F-actin not only from cofilin but also from Arp2/3 binding (Blanchoin et al., 2001; DesMarais et al., 2002) which may spatially restrain cofilin and Arp2/3 activity.

Cofilin activity is spatially confined in cells. For instance, in the lamellipodium of the migrating cell cofilin is inactivated 1 μm away from the leading edge. The following mechanisms of cofilin localization can be implemented in the model: 1) recruitment to the branch points (colocalization with Arp2/3 and cortactin), 2) release from the inhibitory biochemical interactions (described above) – specially release from PIP2, 3) inactivation by RhoC behind the leading edge (Bravo-Cordero et al., 2013). (Koestler et al., 2013) did not observe a direct interaction between cofilin and Arp2/3. However cofilin is thought to be present at the branch points together with a nucleation promoting factor (such as N-WASP), the Arp2/3 complex and cortactin.

It might not be at all informative to accommodate all the possible cofilin regulatory mechanisms in the model. However for the purpose of keeping the model comprehensive it will be possible to include most of the cofilin mechanisms by combining kinetically equivalent interactions or implicit modeling some of the cofilin binding partners. Due to the complexity of the cofilin activity cycle, it could be beneficial to implement cofilin physiology in a separate 'inhibitory' compartment. This will achieve two objectives: 1) validate the constructed reaction network for cofilin regulation and 2) easily position zones of cofilin inhibition for spatial confinement of cofilin activity. For instance such model implementation can then be adapted to investigate actin dynamics in invadopodia where active cofilin is restricted to the core of the structure by RhoC, which is only active outside of the invadopodium core (Bravo-Cordero et al., 2012).

Incorporation of moving boundaries in the Virtual Cell software will allow investigating how biochemical outputs affect cell migration. For example it will be interesting to

determine if cofilin/capping cooperativity also has any effect on lamellipodial protrusion velocity. Additionally it would be possible to study how spatial regulation of cofilin activity results in directed cell protrusion.

Another mechanism that would be interesting to incorporate in the model is 'filament identity establishment based on nucleation type' (Michelot and Drubin, 2011). 'Identity' is a specific conformational state of the filament that favors binding of a certain subset of actin regulators. The identity is acquired either at the nucleation step or through actin filament 'breathing' (spontaneous identity switch via Brownian motion) (Cao et al., 2006). Filaments that are nucleated by formins are targeted by tropomyosins, which in turn help maintain "linear" identity, while filaments with "branched" identity antagonize tropomyosins binding. This mechanism will be important for addressing not only regulation of cofilin severing activity, but also for a model that includes different nucleation mechanisms.

Investigating a role of cofilin and actin disassembly in Nck SH3-induced actin comets

Antibody-mediated aggregation of Nck SH3 domains can serve as *in vivo* actin-based motility assay. Various pathogens hijack signaling to actin through Nck adaptor and invoke both branched and linear actin assembly. I propose to utilize the Nck clustering experimental system to study how actin disassembly affects formation, morphology and dynamics of actin comet tails. This research is motivated by still unanswered questions in the field of pathogen motility: 'How actin-based motility is coupled to cell-to-cell

spread?' and 'How regulation of actin dynamics is affecting pathogenic actin-based motility?'

Two populations of Nck SH3 actin assemblies are observed in cells; comets that move along the membrane ('internal') and protrusions that extend away from the cell. The latter play a critical role in the spread of bacteria and viruses into the adjacent cells. However the mechanisms of formation of membrane protrusions by pathogens are poorly understood. I would first examine major characteristics of the two populations in wild type cells. The goal is to understand what is different between the comets that form a protrusion upon encountering the membrane versus the comets that keep moving along the membrane. We have an established systematic way of quantifying various features of Nck SH3 actin structures. The following outputs will be of major interest: ratio of internal to protrusive structures, velocity, actin density and morphology of both populations, length of membrane protrusions. Several experimental approaches can be employed to assess the role of actin disassembly. First, I would evaluate effects on Nck-induced actin structures due to global manipulation of cofilin in the cells: knockdown of cofilin or LIMK that inhibits cofilin, overexpression of various forms of the protein (WT, constitutively active and inactive). Then a light-activatable dimerizer system, cryptochrome 2–Cib with a constitutively active cofilin (S3A) (Hughes and Lawrence, 2014), can be used to demonstrate specificity of cofilin activity in actin comets and protrusions. In addition, activatable cofilin can be targeted to branches (fusion of CIB to Arp2/3 or cortactin) or to the whole length of filaments (fusion of CIB to tropomyosin). One plausible hypothesis is that disassembly is important for recycling of the actin network components necessary for polymerization at the head of the comet. This study

will provide insight into the cofilin function in dynamic actin tails and into the role of actin disassembly in pathogen-like membrane protrusions.

Conclusion

The field of actin dynamics benefits from the growing arsenal of microscopy tools, experimental and computational approaches and computing resources. Our understanding and knowledge continually expands with more intricate details of actin biochemistry, dynamics and signaling pathways that converge on the actin cytoskeleton. Kinetic modeling in my thesis project highlighted yet another synergistic behavior in regulation of the actin dynamics. Furthermore, revealing the presence of linear actin growth in actin comets might lead to better understanding of cooperative nature of actin nucleation pathways in other actin-based structures.

REFERENCES

Abraham, V.C., V. Krishnamurthi, D.L. Taylor, and F. Lanni. 1999. The actin-based nanomachine at the leading edge of migrating cells. *Biophys J*. 77:1721-1732.

Aggeli, D., E. Kish-Trier, M.C. Lin, B. Haarer, G. Cingolani, J.A. Cooper, S. Wilkens, and D.C. Amberg. 2014. Coordination of the filament stabilizing versus destabilizing activities of cofilin through its secondary binding site on actin. *Cytoskeleton*. 71:361-379.

Alberts, J.B., and G.M. Odell. 2004. In silico reconstitution of Listeria propulsion exhibits nano-saltation. *PLoS biology*. 2:e412.

Alvarez, D.E., and H. Agaisse. 2013. The formin FHOD1 and the small GTPase Rac1 promote vaccinia virus actin–based motility. *The Journal of Cell Biology*. 202:1075-1090.

Alvarez, D.E., and H. Agaisse. 2014. A role for the small GTPase Rac1 in vaccinia actin-based motility. *Small GTPases*. 5.

Andrianantoandro, E., L. Blanchoin, D. Sept, J.A. McCammon, and T.D. Pollard. 2001. Kinetic mechanism of end-to-end annealing of actin filaments. *Journal of molecular biology*. 312:721-730.

Andrianantoandro, E., and T.D. Pollard. 2006. Mechanism of actin filament turnover by severing and nucleation at different concentrations of ADF/cofilin. *Mol Cell*. 24:13-23.

Arber, S., F.A. Barbayannis, H. Hanser, C. Schneider, C.A. Stanyon, O. Bernard, and P. Caroni. 1998. Regulation of actin dynamics through phosphorylation of cofilin by LIM-kinase. *Nature*. 393:805-809.

Bernstein, B.W., W.B. Painter, H. Chen, L.S. Minamide, H. Abe, and J.R. Bamburg. 2000. Intracellular pH modulation of ADF/cofilin proteins. *Cell Motil Cytoskeleton*. 47:319-336.

Berro, J., V. Sirotkin, and T.D. Pollard. 2010. Mathematical modeling of endocytic actin patch kinetics in fission yeast: disassembly requires release of actin filament fragments. *Molecular biology of the cell*. 21:2905-2915.

Bindschadler, M., E.A. Osborn, C.F. Dewey, Jr., and J.L. McGrath. 2004. A mechanistic model of the actin cycle. *Biophys J*. 86:2720-2739.

Blanchoin, L., and T.D. Pollard. 1999. Mechanism of interaction of Acanthamoeba actophorin (ADF/Cofilin) with actin filaments. *J Biol Chem*. 274:15538-15546.

Blanchoin, L., T.D. Pollard, and S.E. Hitchcock-DeGregori. 2001. Inhibition of the Arp2/3 complex-nucleated actin polymerization and branch formation by tropomyosin. *Curr Biol*. 11:1300-1304.

Bosch, M., K.H. Le, B. Bugyi, J.J. Correia, L. Renault, and M.F. Carlier. 2007. Analysis of the function of Spire in actin assembly and its synergy with formin and profilin. *Mol Cell*. 28:555-568.

Bravo-Cordero, J.J., L. Hodgson, and J. Condeelis. 2012. Directed cell invasion and migration during metastasis. *Curr Opin Cell Biol*. 24:277-283.

Bravo-Cordero, J.J., V.P. Sharma, M. Roh-Johnson, X. Chen, R. Eddy, J. Condeelis, and L. Hodgson. 2013. Spatial regulation of RhoC activity defines protrusion formation in migrating cells. *J Cell Sci*. 126:3356-3369.

Buday, L., L. Wunderlich, and P. TamÃ¡s. 2002. The Nck family of adapter proteins: Regulators of actin cytoskeleton. *Cellular Signalling*. 14:723-731.

Campellone, K.G., and M.D. Welch. 2010. A nucleator arms race: cellular control of actin assembly. *Nat Rev Mol Cell Biol*. 11:237-251.

Cao, W., J.P. Goodarzi, and E.M. De La Cruz. 2006. Energetics and Kinetics of Cooperative Cofilin–Actin Filament Interactions. *Journal of Molecular Biology*. 361:257-267.

Carlier, M.-F., C. Husson, L. Renault, and D. Didry. 2011. Chapter Two - Control of Actin Assembly by the WH2 Domains and Their Multifunctional Tandem Repeats in Spire and Cordon-Bleu. *In* International Review of Cell and Molecular Biology. Vol. Volume 290. W.J. Kwang, editor. Academic Press. 55-85.

Carlier, M.F., and D. Pantaloni. 2007. Control of actin assembly dynamics in cell motility. *The Journal of biological chemistry*. 282:23005-23009.

Carlsson, A.E. 2006. Stimulation of actin polymerization by filament severing. *Biophys J*. 90:413-422.

Carlsson, A.E., M.A. Wear, and J.A. Cooper. 2004. End versus side branching by Arp2/3 complex. *Biophys J*. 86:1074-1081.

Chan, A.Y., M. Bailly, N. Zebda, J.E. Segall, and J.S. Condeelis. 2000. Role of cofilin in epidermal growth factor-stimulated actin polymerization and lamellipod protrusion. *J Cell Biol*. 148:531-542.

Chen, Q., and T.D. Pollard. 2013. Actin filament severing by cofilin dismantles actin patches and produces mother filaments for new patches. *Curr Biol*. 23:1154-1162.

Cowan, A.E., Moraru, II, J.C. Schaff, B.M. Slepchenko, and L.M. Loew. 2012. Spatial modeling of cell signaling networks. *Methods in cell biology*. 110:195-221.

Cudmore, S., P. Cossart, G. Griffiths, and M. Way. 1995. Actin-based motility of vaccinia virus. *Nature*. 378:636-638.

Dang, I., R. Gorelik, C. Sousa-Blin, E. Derivery, C. Guerin, J. Linkner, M. Nemethova, J.G. Dumortier, F.A. Giger, T.A. Chipysheva, V.D. Ermilova, S. Vacher, V. Campanacci, I. Herrada, A.G. Planson, S. Fetics, V. Henriot, V. David, K. Oguievetskaia, G. Lakisic, F. Pierre, A. Steffen, A. Boyreau, N. Peyrieras, K. Rottner, S. Zinn-Justin, J. Cherfils, I. Bieche, A.Y. Alexandrova, N.B. David, J.V.

Small, J. Faix, L. Blanchoin, and A. Gautreau. 2013. Inhibitory signalling to the Arp2/3 complex steers cell migration. *Nature*. 503:281-284.

De La Cruz, E.M. 2009. How cofilin severs an actin filament. *Biophysical reviews*. 1:51-59.

De La Cruz, E.M., and D. Sept. 2010. The Kinetics of Cooperative Cofilin Binding Reveals Two States of the Cofilin-Actin Filament. *Biophysical Journal*. 98:1893-1901.

DesMarais, V., M. Ghosh, R. Eddy, and J. Condeelis. 2005. Cofilin takes the lead. *J Cell Sci*. 118:19-26.

DesMarais, V., I. Ichetovkin, J. Condeelis, and S.E. Hitchcock-DeGregori. 2002. Spatial regulation of actin dynamics: a tropomyosin-free, actin-rich compartment at the leading edge. *J Cell Sci*. 115:4649-4660.

Ditlev, Jonathon A., Bruce J. Mayer, and Leslie M. Loew. 2013. There is More Than One Way to Model an Elephant. Experiment-Driven Modeling of the Actin Cytoskeleton. *Biophysical Journal*. 104:520-532.

Ditlev, J.A., P.J. Michalski, G. Huber, G.M. Rivera, W.A. Mohler, L.M. Loew, and B.J. Mayer. 2012. Stoichiometry of Nck-dependent actin polymerization in living cells. *J Cell Biol*. 197:643-658.

Ditlev, J.A., N.M. Vacanti, I.L. Novak, and L.M. Loew. 2009. An Open Model of Actin Dendritic Nucleation. *Biophysical Journal*. 96:3529-3542.

Donnelly, S.K., I. Weisswange, M. Zettl, and M. Way. 2013. WIP provides an essential link between Nck and N-WASP during Arp2/3-dependent actin polymerization. *Curr Biol*. 23:999-1006.

dos Remedios, C.G., D. Chhabra, M. Kekic, I.V. Dedova, M. Tsubakihara, D.A. Berry, and N.J. Nosworthy. 2003. Actin binding proteins: regulation of cytoskeletal microfilaments. *Physiological reviews*. 83:433-473.

Eisenmann, K.M., E.S. Harris, S.M. Kitchen, H.A. Holman, H.N. Higgs, and A.S. Alberts. 2007. Dia-interacting protein modulates formin-mediated actin assembly at the cell cortex. *Curr Biol*. 17:579-591.

Elam, W.A., H. Kang, and E.M. De La Cruz. 2013a. Biophysics of actin filament severing by cofilin. *FEBS Letters*. 587:1215-1219.

Elam, W.A., H. Kang, and E.M. De La Cruz. 2013b. Competitive displacement of cofilin can promote actin filament severing. *Biochem Biophys Res Commun*. 438:728-731.

Endo, M., K. Ohashi, Y. Sasaki, Y. Goshima, R. Niwa, T. Uemura, and K. Mizuno. 2003. Control of growth cone motility and morphology by LIM kinase and Slingshot via phosphorylation and dephosphorylation of cofilin. *The Journal of neuroscience : the official journal of the Society for Neuroscience*. 23:2527-2537.

Escudero-Esparza, A., W.G. Jiang, and T.A. Martin. 2012. Claudin-5 is involved in breast cancer cell motility through the N-WASP and ROCK signalling pathways. *Journal of experimental & clinical cancer research : CR*. 31:43.

Fattouh, R., H. Kwon, M.A. Czuczman, J.W. Copeland, L. Pelletier, M.E. Quinlan, A.M. Muise, D.E. Higgins, and J.H. Brumell. 2015. The Diaphanous-Related Formins Promote Protrusion Formation and Cell-to-Cell Spread of Listeria monocytogenes. *Journal of Infectious Diseases*. 211:1185-1195.

Frankel, G., and A.D. Phillips. 2008. Attaching effacing Escherichia coli and paradigms of Tir-triggered actin polymerization: getting off the pedestal. *Cell Microbiol*. 10:549-556.

Frantz, C., G. Barreiro, L. Dominguez, X. Chen, R. Eddy, J. Condeelis, M.J. Kelly, M.P. Jacobson, and D.L. Barber. 2008. Cofilin is a pH sensor for actin free barbed end formation: role of phosphoinositide binding. *J Cell Biol*. 183:865-879.

Frischknecht, F., V. Moreau, S. Rottger, S. Gonfloni, I. Reckmann, G. Superti-Furga, and M. Way. 1999. Actin-based motility of vaccinia virus mimics receptor tyrosine kinase signalling. *Nature*. 401:926-929.

Fujiwara, I., S. Takahashi, H. Tadakuma, T. Funatsu, and S.i. Ishiwata. 2002. Microscopic analysis of polymerization dynamics with individual actin filaments. *Nat Cell Biol*. 4:666-673.

Fujiwara, I., D. Vavylonis, and T.D. Pollard. 2007. Polymerization kinetics of ADP- and ADP-Pi-actin determined by fluorescence microscopy. *Proc Natl Acad Sci U S A*. 104:8827-8832.

Fukumi-Tominaga, T., Y. Mori, A. Matsuura, K. Kaneko, M. Matsui, M. Ogata, and M. Tominaga. 2009. DIP/WISH-deficient mice reveal Dia- and N-WASP-interacting protein as a regulator of cytoskeletal dynamics in embryonic fibroblasts. *Genes to cells : devoted to molecular & cellular mechanisms*. 14:1197-1207.

Fukuoka, M., S. Suetsugu, H. Miki, K. Fukami, T. Endo, and T. Takenawa. 2001. A novel neural Wiskott-Aldrich syndrome protein (N-WASP) binding protein, WISH, induces Arp2/3 complex activation independent of Cdc42. *J Cell Biol*. 152:471-482.

Ghosh, M., X. Song, G. Mouneimne, M. Sidani, D.S. Lawrence, and J.S. Condeelis. 2004. Cofilin promotes actin polymerization and defines the direction of cell motility. *Science*. 304:743-746.

Gligorijevic, B., J. Wyckoff, H. Yamaguchi, Y. Wang, E.T. Roussos, and J. Condeelis. 2012. N-WASP-mediated invadopodium formation is involved in intravasation and lung metastasis of mammary tumors. *Journal of cell science*. 125:724-734.

Gorbatyuk, V.Y., N.J. Nosworthy, S.A. Robson, N.P. Bains, M.W. Maciejewski, C.G. Dos Remedios, and G.F. King. 2006. Mapping the phosphoinositide-binding site on chick cofilin explains how PIP2 regulates the cofilin-actin interaction. *Mol Cell*. 24:511-522.

Gouin, E., C. Egile, P. Dehoux, V. Villiers, J. Adams, F. Gertler, R. Li, and P. Cossart. 2004. The RickA protein of Rickettsia conorii activates the Arp2/3 complex. *Nature*. 427:457-461.

Haglund, C.M., J.E. Choe, C.T. Skau, D.R. Kovar, and M.D. Welch. 2010. Rickettsia Sca2 is a bacterial formin-like mediator of actin-based motility. *Nature cell biology*. 12:1057-1063.

Haglund, C.M., and M.D. Welch. 2011. Pathogens and polymers: Microbe-host interactions illuminate the cytoskeleton. *The Journal of Cell Biology*. 195:7-17.

Hayakawa, K., S. Sakakibara, M. Sokabe, and H. Tatsumi. 2014. Single-molecule imaging and kinetic analysis of cooperative cofilin-actin filament interactions. *Proc Natl Acad Sci U S A*. 111:9810-9815.

Helgeson, L.A., and B.J. Nolen. 2013. Mechanism of synergistic activation of Arp2/3 complex by cortactin and N-WASP. *eLife*. 2:e00884.

Hitchcock-DeGregori, S.E. 2003. Now, swing your partner! 3D-domain switching of WASP activates Arp2/3 complex. *Nat Struct Biol*. 10:583-584.

Hotulainen, P., E. Paunola, M.K. Vartiainen, and P. Lappalainen. 2005. Actin-depolymerizing factor and cofilin-1 play overlapping roles in promoting rapid F-actin depolymerization in mammalian nonmuscle cells. *Mol Biol Cell*. 16:649-664.

Hughes, R.M., and D.S. Lawrence. 2014. Optogenetic engineering: light-directed cell motility. *Angewandte Chemie*. 53:10904-10907.

Ichetovkin, I., W. Grant, and J. Condeelis. 2002. Cofilin produces newly polymerized actin filaments that are preferred for dendritic nucleation by the Arp2/3 complex. *Curr Biol*. 12:79-84.

Iwasa, J.H., and R.D. Mullins. 2007. Spatial and temporal relationships between actin-filament nucleation, capping, and disassembly. *Curr Biol*. 17:395-406.

Jeng, R.L., E.D. Goley, J.A. D'Alessio, O.Y. Chaga, T.M. Svitkina, G.G. Borisy, R.A. Heinzen, and M.D. Welch. 2004. A Rickettsia WASP-like protein activates the Arp2/3 complex and mediates actin-based motility. *Cell Microbiol*. 6:761-769.

Jin, K.M., M. Lu, F.F. Liu, J. Gu, X.J. Du, and B.C. Xing. 2013. N-WASP is highly expressed in hepatocellular carcinoma and associated with poor prognosis. *Surgery*. 153:518-525.

Jones, N., I.M. Blasutig, V. Eremina, J.M. Ruston, F. Bladt, H. Li, H. Huang, L. Larose, S.S. Li, T. Takano, S.E. Quaggin, and T. Pawson. 2006. Nck adaptor proteins link nephrin to the actin cytoskeleton of kidney podocytes. *Nature*. 440:818-823.

Kapustina, M., E. Vitriol, T.C. Elston, L.M. Loew, and K. Jacobson. 2010. Modeling capping protein FRAP and CALI experiments reveals in vivo regulation of actin dynamics. *Cytoskeleton*. 67:519-534.

Kempiak, S.J., H. Yamaguchi, C. Sarmiento, M. Sidani, M. Ghosh, R.J. Eddy, V. Desmarais, M. Way, J. Condeelis, and J.E. Segall. 2005. A neural Wiskott-

Aldrich Syndrome protein-mediated pathway for localized activation of actin polymerization that is regulated by cortactin. *J Biol Chem*. 280:5836-5842.

Kerkhoff, E. 2011. Actin dynamics at intracellular membranes: The Spir/formin nucleator complex. *European Journal of Cell Biology*. 90:922-925.

Kim, D.J., S.H. Kim, C.S. Lim, K.Y. Choi, C.S. Park, B.H. Sung, M.G. Yeo, S. Chang, J.K. Kim, and W.K. Song. 2006. Interaction of SPIN90 with the Arp2/3 complex mediates lamellipodia and actin comet tail formation. *J Biol Chem*. 281:617-625.

Kiuchi, T., K. Ohashi, S. Kurita, and K. Mizuno. 2007. Cofilin promotes stimulus-induced lamellipodium formation by generating an abundant supply of actin monomers. *J Cell Biol*. 177:465-476.

Kleba, B., T.R. Clark, E.I. Lutter, D.W. Ellison, and T. Hackstadt. 2010. Disruption of the Rickettsia rickettsii Sca2 autotransporter inhibits actin-based motility. *Infection and immunity*. 78:2240-2247.

Koestler, S.A., A. Steffen, M. Nemethova, M. Winterhoff, N. Luo, J.M. Holleboom, J. Krupp, S. Jacob, M. Vinzenz, F. Schur, K. Schluter, P.W. Gunning, C. Winkler, C. Schmeiser, J. Faix, T.E. Stradal, J.V. Small, and K. Rottner. 2013. Arp2/3 complex is essential for actin network treadmilling as well as for targeting of capping protein and cofilin. *Mol Biol Cell*.

Kovar, D.R., E.S. Harris, R. Mahaffy, H.N. Higgs, and T.D. Pollard. 2006. Control of the assembly of ATP- and ADP-actin by formins and profilin. *Cell*. 124:423-435.

Kovar, D.R., and T.D. Pollard. 2004. Insertional assembly of actin filament barbed ends in association with formins produces piconewton forces. *Proc Natl Acad Sci U S A*. 101:14725-14730.

Kueh, H.Y., G.T. Charras, T.J. Mitchison, and W.M. Brieher. 2008. Actin disassembly by cofilin, coronin, and Aip1 occurs in bursts and is inhibited by barbed-end cappers. *J Cell Biol*. 182:341-353.

Kuhn, J.R., and T.D. Pollard. 2005. Real-Time Measurements of Actin Filament Polymerization by Total Internal Reflection Fluorescence Microscopy. *Biophysical Journal*. 88:1387-1402.

Kupi, T., P. Grof, M. Nyitrai, and J. Belagyi. 2013. Interaction of formin FH2 with skeletal muscle actin. EPR and DSC studies. *European biophysics journal : EBJ*. 42:757-765.

Lettau, M., S. Kliche, D. Kabelitz, and O. Janssen. 2014. The adapter proteins ADAP and Nck cooperate in T cell adhesion. *Molecular Immunology*. 60:72-79.

Lettau, M., J. Pieper, and O. Janssen. 2009. Nck adapter proteins: functional versatility in T cells. *Cell Commun Signal*. 7:1.

Li, W., J. Fan, and D.T. Woodley. 2001. Nck/Dock: An adapter between cell surface receptors and the actin cytoskeleton. *Oncogene*. 20:6403-6417.

Lim, C.S., S.H. Kim, J.G. Jung, J.K. Kim, and W.K. Song. 2003. Regulation of SPIN90 phosphorylation and interaction with Nck by ERK and cell adhesion. *J Biol Chem*. 278:52116-52123.

Madasu, Y., C. Suarez, D.J. Kast, D.R. Kovar, and R. Dominguez. 2013. Rickettsia Sca2 has evolved formin-like activity through a different molecular mechanism. *Proc Natl Acad Sci U S A*. 110:E2677-2686.

Maiti, S., A. Michelot, C. Gould, L. Blanchoin, O. Sokolova, and B.L. Goode. 2012. Structure and activity of full-length formin mDia1. *Cytoskeleton*. 69:393-405.

May, R.C., and L.M. Machesky. 2001. Plagiarism and pathogenesis: common themes in actin remodeling. *Developmental cell*. 1:317-318.

McGough, A., B. Pope, W. Chiu, and A. Weeds. 1997. Cofilin changes the twist of F-actin: implications for actin filament dynamics and cellular function. *J Cell Biol*. 138:771-781.

Meng, W., M. Numazaki, K. Takeuchi, Y. Uchibori, Y. Ando-Akatsuka, M. Tominaga, and T. Tominaga. 2004. DIP (mDia interacting protein) is a key molecule regulating Rho and Rac in a Src-dependent manner. *The EMBO journal*. 23:760-771.

Michelot, A., and D.G. Drubin. 2011. Building distinct actin filament networks in a common cytoplasm. *Curr Biol*. 21:R560-569.

Mizuno, H., C. Higashida, Y. Yuan, T. Ishizaki, S. Narumiya, and N. Watanabe. 2011. Rotational movement of the formin mDia1 along the double helical strand of an actin filament. *Science*. 331:80-83.

Mogilner, A., and G. Oster. 1996. Cell motility driven by actin polymerization. *Biophys J*. 71:3030-3045.

Moreau, V., F. Frischknecht, I. Reckmann, R. Vincentelli, G. Rabut, D. Stewart, and M. Way. 2000. A complex of N-WASP and WIP integrates signalling cascades that lead to actin polymerization. *Nature cell biology*. 2:441-448.

New, L.A., A. Keyvani Chahi, and N. Jones. 2013. Direct regulation of nephrin tyrosine phosphorylation by Nck adaptor proteins. *J Biol Chem*. 288:1500-1510.

Newsome, T.P., I. Weisswange, F. Frischknecht, and M. Way. 2006. Abl collaborates with Src family kinases to stimulate actin-based motility of vaccinia virus. *Cell Microbiol*. 8:233-241.

Okada, K., F. Bartolini, A.M. Deaconescu, J.B. Moseley, Z. Dogic, N. Grigorieff, G.G. Gundersen, and B.L. Goode. 2010. Adenomatous polyposis coli protein nucleates actin assembly and synergizes with the formin mDia1. *J Cell Biol*. 189:1087-1096.

Oosawa, F., S. Asakura, K. Hotta, N. Imai, and T. Ooi. 1959. G-F transformation of actin as a fibrous condensation. *Journal of Polymer Science*. 37:323-336.

Oosawa, F., and M. Kasai. 1962. A theory of linear and helical aggregations of macromolecules. *Journal of molecular biology*. 4:10-21.

Oser, M., H. Yamaguchi, C.C. Mader, J.J. Bravo-Cordero, M. Arias, X. Chen, V. Desmarais, J. van Rheenen, A.J. Koleske, and J. Condeelis. 2009. Cortactin regulates cofilin and N-WASp activities to control the stages of invadopodium assembly and maturation. *J Cell Biol*. 186:571-587.

Padrick, S.B., H.C. Cheng, A.M. Ismail, S.C. Panchal, L.K. Doolittle, S. Kim, B.M. Skehan, J. Umetani, C.A. Brautigam, J.M. Leong, and M.K. Rosen. 2008. Hierarchical regulation of WASP/WAVE proteins. *Mol Cell*. 32:426-438.

Padrick, S.B., and M.K. Rosen. 2010. Physical mechanisms of signal integration by WASP family proteins. *Annual review of biochemistry*. 79:707-735.

Paul, A.S., and T.D. Pollard. 2009. Review of the mechanism of processive actin filament elongation by formins. *Cell motility and the cytoskeleton*. 66:606-617.

Pechlivanis, M., A. Samol, and E. Kerkhoff. 2009. Identification of a short spir interaction sequence at the C-terminal end of formin subgroup proteins. *Journal of Biological Chemistry*. 284:25324-25333.

Peskin, C.S., G.M. Odell, and G.F. Oster. 1993. Cellular motions and thermal fluctuations: the Brownian ratchet. *Biophys J*. 65:316-324.

Pollard, T.D., and G.G. Borisy. 2003. Cellular motility driven by assembly and disassembly of actin filaments. *Cell*. 112:453-465.

Pollard, T.D., and J.A. Cooper. 1986. Actin and actin-binding proteins. A critical evaluation of mechanisms and functions. *Annual review of biochemistry*. 55:987-1035.

Ponti, A., M. Machacek, S.L. Gupton, C.M. Waterman-Storer, and G. Danuser. 2004. Two distinct actin networks drive the protrusion of migrating cells. *Science*. 305:1782-1786.

Ponti, A., A. Matov, M. Adams, S. Gupton, C.M. Waterman-Storer, and G. Danuser. 2005. Periodic patterns of actin turnover in lamellipodia and lamellae of migrating epithelial cells analyzed by quantitative Fluorescent Speckle Microscopy. *Biophys J*. 89:3456-3469.

Pring, M., M. Evangelista, C. Boone, C. Yang, and S.H. Zigmond. 2003. Mechanism of formin-induced nucleation of actin filaments. *Biochemistry*. 42:486-496.

Pruyne, D., M. Evangelista, C. Yang, E. Bi, S. Zigmond, A. Bretscher, and C. Boone. 2002. Role of formins in actin assembly: nucleation and barbed-end association. *Science*. 297:612-615.

Rao, Y. 2005. Dissecting Nck/Dock signaling pathways in Drosophila visual system. *Int J Biol Sci*. 1:80-86.

Reed, Shawna C.O., Rebecca L. Lamason, Viviana I. Risca, E. Abernathy, and Matthew D. Welch. 2014. Rickettsia Actin-Based Motility Occurs in Distinct Phases Mediated by Different Actin Nucleators. *Current Biology*. 24:98-103.

Resasco, D.C., F. Gao, F. Morgan, I.L. Novak, J.C. Schaff, and B.M. Slepchenko. 2012. Virtual Cell: computational tools for modeling in cell biology. *Wiley interdisciplinary reviews. Systems biology and medicine*. 4:129-140.

Rivera, G.M., C.A. Briceno, F. Takeshima, S.B. Snapper, and B.J. Mayer. 2004. Inducible clustering of membrane-targeted SH3 domains of the adaptor protein Nck triggers localized actin polymerization. *Curr Biol*. 14:11-22.

Rivera, G.M., D. Vasilescu, V. Papayannopoulos, W.A. Lim, and B.J. Mayer. 2009. A reciprocal interdependence between Nck and PI(4,5)P(2) promotes localized N-WASp-mediated actin polymerization in living cells. *Mol Cell*. 36:525-535.

Rohatgi, R., P. Nollau, H.Y. Ho, M.W. Kirschner, and B.J. Mayer. 2001. Nck and phosphatidylinositol 4,5-bisphosphate synergistically activate actin polymerization through the N-WASP-Arp2/3 pathway. *J Biol Chem*. 276:26448-26452.

Romero, S., C. Le Clainche, D. Didry, C. Egile, D. Pantaloni, and M.-F. Carlier. 2004. Formin Is a Processive Motor that Requires Profilin to Accelerate Actin Assembly and Associated ATP Hydrolysis. *Cell*. 119:419-429.

Satoh, S., and T. Tominaga. 2001. mDia-interacting protein acts downstream of Rho-mDia and modifies Src activation and stress fiber formation. *J Biol Chem*. 276:39290-39294.

Scaplehorn, N., A. Holmström, V. Moreau, F. Frischknecht, I. Reckmann, and M. Way. 2002. Grb2 and Nck Act Cooperatively to Promote Actin-Based Motility of Vaccinia Virus. *Current Biology*. 12:740-745.

Schaff, J., C.C. Fink, B. Slepchenko, J.H. Carson, and L.M. Loew. 1997. A general computational framework for modeling cellular structure and function. *Biophys J*. 73:1135-1146.

Schaus, T.E., E.W. Taylor, and G.G. Borisy. 2007. Self-organization of actin filament orientation in the dendritic-nucleation/array-treadmilling model. *Proc Natl Acad Sci U S A*. 104:7086-7091.

Schmoller, K.M., T. Niedermayer, C. Zensen, C. Wurm, and A.R. Bausch. 2011. Fragmentation is crucial for the steady-state dynamics of actin filaments. *Biophys J*. 101:803-808.

Sechi, A.S., J. Wehland, and J.V. Small. 1997. The isolated comet tail pseudopodium of Listeria monocytogenes: a tail of two actin filament populations, long and axial and short and random. *J Cell Biol*. 137:155-167.

Sept, D., J. Xu, T.D. Pollard, and J.A. McCammon. 1999. Annealing accounts for the length of actin filaments formed by spontaneous polymerization. *Biophys J*. 77:2911-2919.

Seth, A., C. Otomo, and M.K. Rosen. 2006. Autoinhibition regulates cellular localization and actin assembly activity of the diaphanous-related formins FRLalpha and mDia1. *J Cell Biol*. 174:701-713.

Sinnar, S.A., S. Antoku, J.M. Saffin, J.A. Cooper, and S. Halpain. 2014. Capping protein is essential for cell migration in vivo and for filopodial morphology and dynamics. *Mol Biol Cell*. 25:2152-2160.

Skoble, J., D.A. Portnoy, and M.D. Welch. 2000. Three regions within ActA promote Arp2/3 complex-mediated actin nucleation and Listeria monocytogenes motility. *J Cell Biol*. 150:527-538.

Slepchenko, B.M., and L.M. Loew. 2010. Use of virtual cell in studies of cellular dynamics. *Int Rev Cell Mol Biol*. 283:1-56.

Smith, B.A., K. Daugherty-Clarke, B.L. Goode, and J. Gelles. 2013a. Pathway of actin filament branch formation by Arp2/3 complex revealed by single-molecule imaging. *Proc Natl Acad Sci U S A*. 110:1285-1290.

Smith, B.A., S.B. Padrick, L.K. Doolittle, K. Daugherty-Clarke, I.R. Correa, Jr., M.Q. Xu, B.L. Goode, M.K. Rosen, and J. Gelles. 2013b. Three-color single molecule imaging shows WASP detachment from Arp2/3 complex triggers actin filament branch formation. *eLife*. 2:e01008.

Suarez, C., J. Roland, R. Boujemaa-Paterski, H. Kang, B.R. McCullough, A.C. Reymann, C. GuÃ©rin, J.L. Martiel, E.M. De La Cruz, and L. Blanchoin. 2011. Cofilin tunes the nucleotide state of actin filaments and severs at bare and decorated segment boundaries. *Current Biology*. 21:862-868.

Svitkina, T.M., and G.G. Borisy. 1999. Arp2/3 complex and actin depolymerizing factor/cofilin in dendritic organization and treadmilling of actin filament array in lamellipodia. *The Journal of cell biology*. 145:1009-1026.

Tang, Z., L.M. Araysi, and H.M. Fathallah-Shaykh. 2013. c-Src and neural Wiskott-Aldrich syndrome protein (N-WASP) promote low oxygen-induced accelerated brain invasion by gliomas. *PloS one*. 8:e75436.

Tilney, L.G., and D.A. Portnoy. 1989. Actin filaments and the growth, movement, and spread of the intracellular bacterial parasite, Listeria monocytogenes. *J Cell Biol*. 109:1597-1608.

van Rheenen, J., X. Song, W. van Roosmalen, M. Cammer, X. Chen, V. Desmarais, S.C. Yip, J.M. Backer, R.J. Eddy, and J.S. Condeelis. 2007. EGF-induced PIP2 hydrolysis releases and activates cofilin locally in carcinoma cells. *J Cell Biol*. 179:1247-1259.

Vavylonis, D., D.R. Kovar, B. O'Shaughnessy, and T.D. Pollard. 2006. Model of formin-associated actin filament elongation. *Mol Cell*. 21:455-466.

Vavylonis, D., Q. Yang, and B. O'Shaughnessy. 2005. Actin polymerization kinetics, cap structure, and fluctuations. *Proceedings of the National Academy of Sciences of the United States of America*. 102:8543-8548.

Vingadassalom, D., A. Kazlauskas, B. Skehan, H.C. Cheng, L. Magoun, D. Robbins, M.K. Rosen, K. Saksela, and J.M. Leong. 2009. Insulin receptor tyrosine kinase substrate links the E. coli O157:H7 actin assembly effectors Tir and EspF(U) during pedestal formation. *Proc Natl Acad Sci U S A*. 106:6754-6759.

Wagner, A.R., Q. Luan, S.L. Liu, and B.J. Nolen. 2013. Dip1 defines a class of Arp2/3 complex activators that function without preformed actin filaments. *Curr Biol*. 23:1990-1998.

Wegner, A. 1976. Head to tail polymerization of actin. *Journal of molecular biology*. 108:139-150.

Welch, M.D., A. Iwamatsu, and T.J. Mitchison. 1997. Actin polymerization is induced by Arp2/3 protein complex at the surface of Listeria monocytogenes. *Nature*. 385:265-269.

Wiesner, S., E. Helfer, D. Didry, G. Ducouret, F. Lafuma, M.F. Carlier, and D. Pantaloni. 2003. A biomimetic motility assay provides insight into the mechanism of actin-based motility. *J Cell Biol*. 160:387-398.

Wong, A.R., B. Raymond, J.W. Collins, V.F. Crepin, and G. Frankel. 2012. The enteropathogenic E. coli effector EspH promotes actin pedestal formation and elongation via WASP-interacting protein (WIP). *Cell Microbiol*. 14:1051-1070.

Wu, C., S.B. Asokan, M.E. Berginski, E.M. Haynes, N.E. Sharpless, J.D. Griffith, S.M. Gomez, and J.E. Bear. 2012. Arp2/3 is critical for lamellipodia and response to extracellular matrix cues but is dispensable for chemotaxis. *Cell*. 148:973-987.

Yamaguchi, H. 2012. [Molecular mechanisms of invadopodium formation by cancer cells]. *Seikagaku. The Journal of Japanese Biochemical Society*. 84:35-38.

Yamaguchi, H., H. Miki, S. Suetsugu, L. Ma, M.W. Kirschner, and T. Takenawa. 2000. Two tandem verprolin homology domains are necessary for a strong activation of Arp2/3 complex-induced actin polymerization and induction of microspike formation by N-WASP. *Proc Natl Acad Sci U S A*. 97:12631-12636.

Yamaguchi, H., H. Miki, and T. Takenawa. 2002. Two verprolin homology domains increase the Arp2/3 complex-mediated actin polymerization activities of N-WASP and WAVE1 C-terminal regions. *Biochem Biophys Res Commun*. 297:214-219.

Yu, X., T. Zech, L. McDonald, E.G. Gonzalez, A. Li, I. Macpherson, J.P. Schwarz, H. Spence, K. Futo, P. Timpson, C. Nixon, Y. Ma, I.M. Anton, B. Visegrady, R.H. Insall, K. Oien, K. Blyth, J.C. Norman, and L.M. Machesky. 2012. N-WASP coordinates the delivery and F-actin-mediated capture of MT1-MMP at invasive pseudopods. *J Cell Biol*. 199:527-544.

Zahm, Jacob A., Shae B. Padrick, Z. Chen, Chi W. Pak, Ali A. Yunus, L. Henry, Diana R. Tomchick, Z. Chen, and Michael K. Rosen. 2013. The Bacterial Effector VopL Organizes Actin into Filament-like Structures. *Cell*. 155:423-434.